

## QCD\*

*P. Z. Skands*

Theoretical Physics, CERN, Geneva, Switzerland

and

School of Physics & Astronomy, Monash University, Clayton, Australia

### Abstract

These lecture notes are directed at a level suitable for graduate students in High Energy Physics. They are intended to give an introduction to the theory and phenomenology of quantum chromodynamics (QCD), focusing on collider-physics applications. The aim is to bring the reader to a level where informed decisions can be made concerning different approaches and their uncertainties. The material is divided into five main areas: (1) fundamentals, (2) fixed-order perturbative QCD, (3) Monte Carlo event generators and parton showers, (4) Matching at Leading and Next-to-Leading Order, and (5) Soft QCD physics.

### Keywords

Lectures; quantum chromodynamics; gauge theory; jet: fragmentation; Monte Carlo; PYTHIA.

### Useful complementary references

List of additional general study/reference material:

- basic quantum field theory: Ref. [1],
- textbooks on QCD: Refs. [2, 3],
- jets and jet algorithms: Ref. [4],
- general-purpose event generators: Ref. [5],
- the string model: Ref. [6],
- step-by-step PYTHIA tutorial: see ‘worksheet’ available on the PYTHIA homepage,
- Monte Carlo methods and random numbers: Refs. [7, 8].

## 1 Introduction

When probed at very short wavelengths, quantum chromodynamics (QCD) is essentially a theory of free ‘partons’—quarks and gluons—which only scatter off one another through relatively small quantum corrections that can be systematically calculated. At longer wavelengths, of the order of the size of the proton  $\sim 1 \text{ fm} = 10^{-15} \text{ m}$ . However, we see strongly bound towers of hadron resonances emerge, with string-like potentials building up if we try to separate their partonic constituents. Due to our inability to perform analytic calculations in strongly coupled field theories, QCD is, therefore, still only partially solved. Nonetheless, all its features, across all distance scales, are believed to be encoded in a single one-line formula of alluring simplicity: the Lagrangian<sup>1</sup> of QCD.

---

\*Originally based on lectures given at ESHEP 2010 (Raseborg, Finland) and subsequently updated for TASI 2012 (Boulder, Colorado) and AEPSHEP 2014 (Puri, India).

<sup>1</sup>Throughout these notes we let it be implicit that ‘Lagrangian’ really refers to Lagrangian density,  $\mathcal{L}$ , the four-dimensional space–time integral of which is the action.

The consequence for collider physics is that some parts of QCD can be calculated in terms of the fundamental parameters of the Lagrangian, whereas others must be expressed through models or functions whose effective parameters are not a priori calculable, but which can be constrained by fits to data. However, even in the absence of a perturbative expansion, there are still several strong theorems which hold, and which can be used to give relations between seemingly different processes. (This is, e.g., the reason it makes sense to constrain parton-distribution functions (PDFs) in ep collisions and then re-use the same ones for pp collisions.) Thus, in the sections dealing with phenomenological models, we shall emphasize that the loss of a factorized perturbative expansion is not equivalent to a total loss of predictivity.

An alternative approach would be to give up on calculating QCD and use leptons instead. Formally, this amounts to summing inclusively over strong-interaction phenomena, when such are present. While such a strategy might succeed in replacing what we do know about QCD by ‘unity’, even the most adamant chromophobe must acknowledge a few basic facts of collider physics for the next decade(s). (1) At the Large Hadron Collider (LHC), the initial states are hadrons, and hence, at the very least, well-understood and precise PDFs will be required. (2) High precision will mandate calculations to higher orders in perturbation theory, which, in turn, will involve more QCD. (3) The requirement of lepton *isolation* makes the very definition of a lepton depend implicitly on QCD. (4) The rate of jets that are misreconstructed as leptons in the experiment depends explicitly on QCD. (5) Finally, although many new-physics signals *do* give observable signals in the lepton sector, this is far from guaranteed, nor is it exclusive when it occurs. It would, therefore, be unwise not to attempt to solve QCD to the best of our ability, the better to prepare ourselves for both the largest possible discovery reach and the highest attainable subsequent precision.

Moreover, QCD is the richest gauge theory we have, so far, encountered. Its emergent phenomena, unitarity properties, colour structure, non-perturbative dynamics, quantum versus classical limits, interplay between scale-invariant and scale-dependent properties and its wide range of phenomenological applications are still very much topics of active investigation, about which we continue to learn.

In addition, or perhaps as a consequence, the field of QCD is currently experiencing something of a revolution. On the perturbative side, new methods to compute scattering amplitudes with very high particle multiplicities are being developed, together with advanced techniques for combining such amplitudes with all-orders resummation frameworks. On the non-perturbative side, the wealth of data on soft-physics processes from the LHC is forcing us to reconsider the reliability of the standard fragmentation models, and heavy-ion collisions are providing new insights into the collective behaviour of hadronic matter. The study of cosmic rays impinging on the Earth’s atmosphere challenges our ability to extrapolate fragmentation models from collider energy scales to the region of ultra-high-energy cosmic rays. And finally, dark-matter annihilation processes in space may produce hadrons, whose spectra are sensitive to the modelling of fragmentation.

In the following, we shall focus on QCD for mainstream collider physics. This includes the basics of the gauge group  $SU(3)$ , colour factors, the running of  $\alpha_s$ , factorization, hard processes, IR safety, parton showers and matching, event generators, hadronization and the so-called underlying event. While not covering everything, hopefully these topics can also serve at least as stepping stones to more specialized issues that have been left out, such as twistor-inspired techniques, heavy flavours, polarization or forward physics, or to topics more tangential to other fields, such as axions, lattice QCD or heavy-ion physics.

## 1.1 A first hint of colour

Looking for new physics, as we do now at the LHC, it is instructive to consider the story of the discovery of colour. The first hint was arguably the  $\Delta^{++}$  baryon, discovered in 1951 [9]. The title and part of the abstract from this historical paper are reproduced in Fig. 1. In the context of the quark model—which first had to be developed, successively joining together the notions of spin, isospin, strangeness, and the

**Meson-Nucleon Scattering and Nucleon Isobars\***

KEITH A. BRUECKNER  
*Department of Physics, Indiana University, Bloomington, Indiana*  
 (Received December 17, 1951)

“[...] It is concluded that the apparently anomalous features of the scattering can be interpreted to be an indication of a resonant meson-nucleon interaction corresponding to a nucleon isobar with spin  $\frac{3}{2}$ , isotopic spin  $\frac{3}{2}$ , and with an excitation energy of 277 MeV.”

**Fig. 1:** The title and part of the abstract of the 1951 paper [9] (published in 1952) in which the existence of the  $\Delta^{++}$  baryon was deduced, based on data from Sachs and Steinberger at Columbia [10] and from Anderson *et al.* at Chicago [11]. Further studies at Chicago were quickly performed in Ref. [12, 13]. See also the memoir by Nagle [14].

eightfold way<sup>2</sup>—the flavour and spin content of the  $\Delta^{++}$  baryon is

$$|\Delta^{++}\rangle = |u_{\uparrow} u_{\uparrow} u_{\uparrow}\rangle, \quad (1)$$

clearly a highly symmetric configuration. However, since the  $\Delta^{++}$  is a fermion, it must have an overall antisymmetric wave function. In 1965, 14 years after its discovery, this was finally understood by the introduction of colour as a new quantum number associated with the group SU(3) [15, 16]. The  $\Delta^{++}$  wave function can now be made antisymmetric by arranging its three quarks antisymmetrically in this new degree of freedom,

$$|\Delta^{++}\rangle = \epsilon^{ijk} |u_{i\uparrow} u_{j\uparrow} u_{k\uparrow}\rangle, \quad (2)$$

and hence solving the mystery.

More direct experimental tests of the number of colours were provided first by measurements of the decay width of  $\pi^0 \rightarrow \gamma\gamma$  decays, which is proportional to  $N_C^2$ , and later by the famous ‘ $R$ ’ ratio in  $e^+e^-$  collisions ( $R = \sigma(e^+e^- \rightarrow q\bar{q})/\sigma(e^+e^- \rightarrow \mu^+\mu^-)$ ), which is proportional to  $N_C$ , see, e.g., Ref. [3]. Below, in Section 1.2 we shall see how to calculate such colour factors.

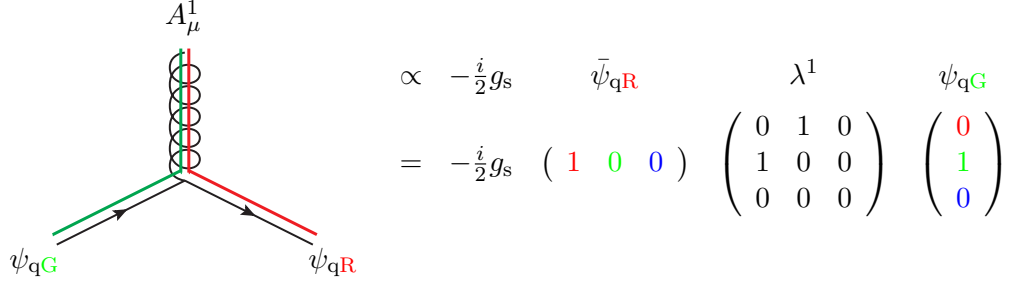
## 1.2 The Lagrangian of QCD

QCD is based on the gauge group SU(3), the Special Unitary group in three (complex) dimensions, whose elements are the set of unitary  $3 \times 3$  matrices with determinant one. Since there are nine linearly independent unitary complex matrices<sup>3</sup>, one of which has determinant  $-1$ , there are a total of eight independent directions in this matrix space, corresponding to eight different generators as compared with the single one of quantum electrodynamics (QED). In the context of QCD, we normally represent this group using the so-called *fundamental*, or *defining*, representation, in which the generators of SU(3) appear as a set of eight traceless and hermitean matrices, to which we return below. We shall refer to indices enumerating the rows and columns of these matrices (from 1 to 3) as *fundamental* indices, and we use the letters  $i, j, k, \dots$ , to denote them. We refer to indices enumerating the generators (from 1 to 8), as *adjoint* indices<sup>4</sup>, and we use the first letters of the alphabet ( $a, b, c, \dots$ ) to denote them. These matrices can operate both on each other (representing combinations of successive gauge transformations) and on a set of 3-vectors, the latter of which represent quarks in colour space; the quarks are *triplets* under SU(3). The matrices can be thought of as representing gluons in colour space (or, more precisely, the gauge

<sup>2</sup>In physics, the ‘eightfold way’ refers to the classification of the lowest-lying pseudoscalar mesons and spin-1/2 baryons within octets in SU(3)-flavour space (u, d, s). The  $\Delta^{++}$  is part of a spin-3/2 baryon decuplet, a ‘tenfold way’ in this terminology.

<sup>3</sup>A complex  $N \times N$  matrix has  $2N^2$  degrees of freedom, on which unitarity provides  $N^2$  constraints.

<sup>4</sup>The dimension of the *adjoint*, or *vector*, representation is equal to the number of generators,  $N^2 - 1 = 8$  for SU(3), while the dimension of the fundamental representation is the degree of the group,  $N = 3$  for SU(3).



**Fig. 2:** Illustration of a qg vertex in QCD, before summing/averaging over colours: a gluon in a state represented by  $\lambda^1$  interacts with quarks in the states  $\psi_{qR}$  and  $\psi_{qG}$ .

transformations carried out by gluons), and hence there are eight different gluons; the gluons are *octets* under SU(3).

The Lagrangian density of QCD is

$$\mathcal{L} = \bar{\psi}_q^i (i\gamma^\mu) (D_\mu)_{ij} \psi_q^j - m_q \bar{\psi}_q^i \psi_{qi} - \frac{1}{4} F_{\mu\nu}^a F^{a\mu\nu}, \quad (3)$$

where  $\psi_q^i$  denotes a quark field with (fundamental) colour index  $i$ ,  $\psi_q = (\psi_{qR}, \psi_{qG}, \psi_{qB})^T$ ,  $\gamma^\mu$  is a Dirac matrix that expresses the vector nature of the strong interaction, with  $\mu$  being a Lorentz vector index,  $m_q$  allows for the possibility of non-zero quark masses (induced by the standard Higgs mechanism or similar),  $F_{\mu\nu}^a$  is the gluon field strength tensor for a gluon with (adjoint) colour index  $a$  (i.e.,  $a \in [1, \dots, 8]$ ) and  $D_\mu$  is the covariant derivative in QCD,

$$(D_\mu)_{ij} = \delta_{ij} \partial_\mu - ig_s t_{ij}^a A_\mu^a, \quad (4)$$

with  $g_s$  the strong coupling (related to  $\alpha_s$  by  $g_s^2 = 4\pi\alpha_s$ ; we return to the strong coupling in more detail below)  $A_\mu^a$  the gluon field with colour index  $a$ , and  $t_{ij}^a$  proportional to the hermitean and traceless Gell–Mann matrices of SU(3),

$$\lambda^1 = \begin{pmatrix} 0 & 1 & 0 \\ 1 & 0 & 0 \\ 0 & 0 & 0 \end{pmatrix}, \lambda^2 = \begin{pmatrix} 0 & -i & 0 \\ i & 0 & 0 \\ 0 & 0 & 0 \end{pmatrix}, \lambda^3 = \begin{pmatrix} 1 & 0 & 0 \\ 0 & -1 & 0 \\ 0 & 0 & 0 \end{pmatrix}, \lambda^4 = \begin{pmatrix} 0 & 0 & 1 \\ 0 & 0 & 0 \\ 1 & 0 & 0 \end{pmatrix}$$

$$\lambda^5 = \begin{pmatrix} 0 & 0 & -i \\ 0 & 0 & 0 \\ i & 0 & 0 \end{pmatrix}, \lambda^6 = \begin{pmatrix} 0 & 0 & 0 \\ 0 & 0 & 1 \\ 0 & 1 & 0 \end{pmatrix}, \lambda^7 = \begin{pmatrix} 0 & 0 & 0 \\ 0 & 0 & -i \\ 0 & i & 0 \end{pmatrix}, \lambda^8 = \begin{pmatrix} \frac{1}{\sqrt{3}} & 0 & 0 \\ 0 & \frac{1}{\sqrt{3}} & 0 \\ 0 & 0 & \frac{-2}{\sqrt{3}} \end{pmatrix}. \quad (5)$$

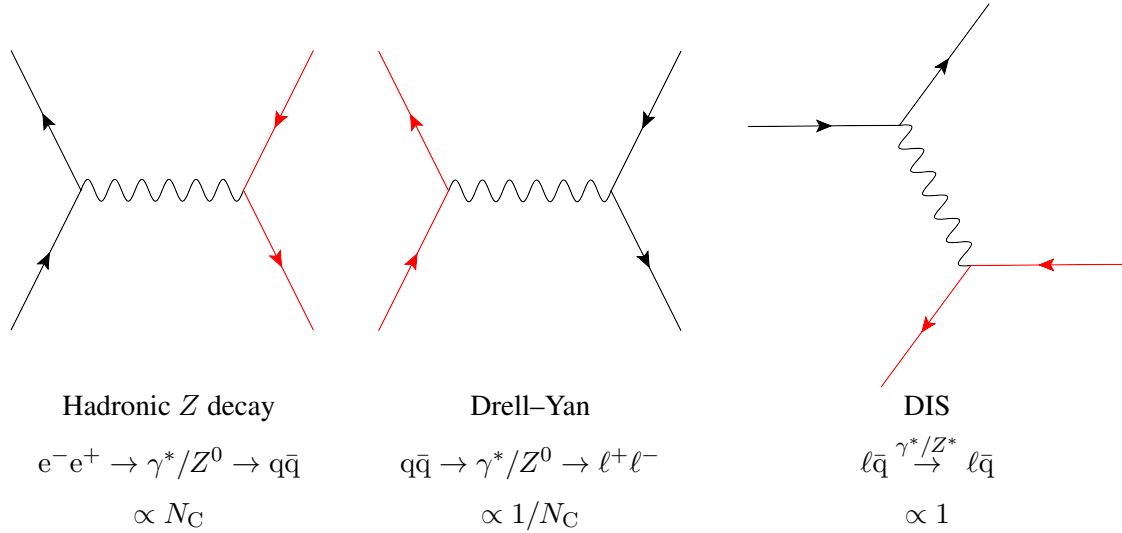
These generators are just the SU(3) analogues of the Pauli matrices in SU(2). By convention, the constant of proportionality is normally taken to be

$$t_{ij}^a = \frac{1}{2} \lambda_{ij}^a. \quad (6)$$

This choice, in turn, determines the normalization of the coupling  $g_s$ , via Eq. (4), and fixes the values of the SU(3) Casimirs and structure constants, to which we return below.

An example of the colour flow for a quark–gluon interaction in colour space is given in Fig. 2. Normally, of course, we sum over all the colour indices, so this example merely gives a pictorial representation of what one particular (non-zero) term in the colour sum looks like.

## QCD



**Fig. 3:** Illustration of the three crossings of the interaction of a lepton current (black) with a quark current (red) via an intermediate photon or  $Z$  boson, with corresponding colour factors.

### 1.3 Colour factors

Typically, we do not measure colour in the final state—instead we average over all possible incoming colours and sum over all possible outgoing ones, wherefore QCD scattering amplitudes (squared), in practice, always contain sums over quark fields contracted with Gell–Mann matrices. These contractions in turn produce traces which yield the *colour factors* that are associated with each QCD process, and which basically count the number of ‘paths through colour space’ that the process at hand can take<sup>5</sup>.

A very simple example of a colour factor is given by the decay process  $Z \rightarrow q\bar{q}$ . This vertex contains a simple  $\delta_{ij}$  in colour space; the outgoing quark and antiquark must have identical (anti-)colours. Squaring the corresponding ME and summing over final-state colours yields a colour factor of

$$e^+ e^- \rightarrow Z \rightarrow q\bar{q} \quad : \quad \sum_{\text{colours}} |M|^2 \propto \delta_{ij} \delta_{ji}^* = \text{Tr}\{\delta\} = N_C = 3, \quad (7)$$

since  $i$  and  $j$  are quark (i.e., three-dimensional fundamental) indices.

A next-to-simplest example is given by  $q\bar{q} \rightarrow \gamma^*/Z \rightarrow \ell^+ \ell^-$  (usually referred to as the Drell–Yan process [17]), which is just a crossing of the previous one. By crossing symmetry, the squared ME, including the colour factor, is exactly the same as before, but since the quarks are, here, incoming, we must *average* rather than sum over their colours, leading to


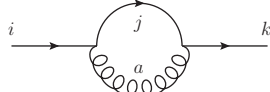
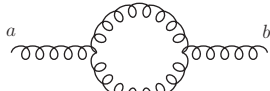
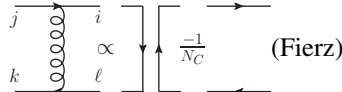
$$q\bar{q} \rightarrow Z \rightarrow e^+ e^- \quad : \quad \frac{1}{9} \sum_{\text{colours}} |M|^2 \propto \frac{1}{9} \delta_{ij} \delta_{ji}^* = \frac{1}{9} \text{Tr}\{\delta\} = \frac{1}{3}, \quad (8)$$

where the colour factor now expresses a *suppression* which can be interpreted as due to the fact that only quarks of matching colours are able to collide and produce a  $Z$  boson. The chance that a quark and an antiquark picked at random from the colliding hadrons have matching colours is  $1/N_C$ .

Similarly,  $\ell q \rightarrow \ell q$  via  $t$ -channel photon exchange (usually called deep inelastic scattering—DIS—with ‘deep’ referring to a large virtuality of the exchanged photon), constitutes yet another crossing of the same basic process, see Fig. 3. The colour factor in this case comes out as unity.

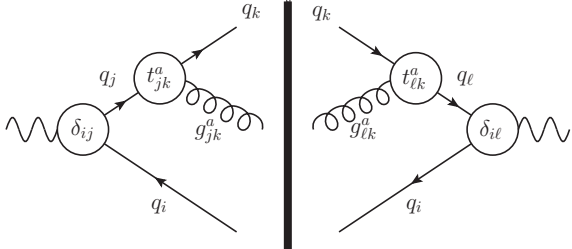
<sup>5</sup>The convention choice represented by Eq. (6) introduces a ‘spurious’ factor of two for each power of the coupling  $\alpha_s$ . Although one could, in principle, absorb that factor into a redefinition of the coupling, effectively redefining the normalization of ‘unit colour charge’, the standard definition of  $\alpha_s$  is now so entrenched that alternative choices would be counter-productive, at least in the context of a pedagogical review.

**Table 1:** Trace relations for  $t$  matrices (convention-independent). More relations can be found in Ref. [2, Section 1.2] and in Ref. [1, Appendix A.3].

Trace relation	Indices	Occurs in diagram squared
$\text{Tr}\{t^a t^b\} = T_R \delta^{ab}$	$a, b \in [1, \dots, 8]$	
$\sum_a t_{ij}^a t_{jk}^a = C_F \delta_{ik}$	$a \in [1, \dots, 8]$ $i, j, k \in [1, \dots, 3]$	
$\sum_{c,d} f^{acd} f^{bcd} = C_A \delta^{ab}$	$a, b, c, d \in [1, \dots, 8]$	
$t_{ij}^a t_{k\ell}^a = T_R \left( \delta_{jk} \delta_{i\ell} - \frac{1}{N_C} \delta_{ij} \delta_{k\ell} \right)$	$i, j, k, \ell \in [1, \dots, 3]$	

To illustrate what happens when we insert (and sum over) quark–gluon vertices, such as the one depicted in Fig. 2, we take the process  $Z \rightarrow 3$  jets. The colour factor for this process can be computed as follows, with the accompanying illustration showing a corresponding diagram (squared) with explicit colour-space indices on each vertex:

$$\begin{aligned}
 Z \rightarrow qg\bar{q} : \\
 \sum_{\text{colours}} |M|^2 &\propto \delta_{ij} t_{jk}^a (t_{\ell k}^a \delta_{i\ell}^*)^* \\
 &= \text{Tr}\{t^a t^a\} \\
 &= \frac{1}{2} \text{Tr}\{\delta\} = 4,
 \end{aligned}$$


(9)

where the last  $\text{Tr}\{\delta\} = 8$ , since the trace runs over the eight-dimensional adjoint indices.

The tedious task of taking traces over  $t$  matrices can be greatly alleviated by use of the relations given in Table 1. In the standard normalization convention for the  $\text{SU}(3)$  generators, Eq. (6), the Casimirs of  $\text{SU}(3)$  appearing in Table 1 are<sup>6</sup>

$$T_R = \frac{1}{2} \quad C_F = \frac{4}{3} \quad C_A = N_C = 3. \quad (10)$$

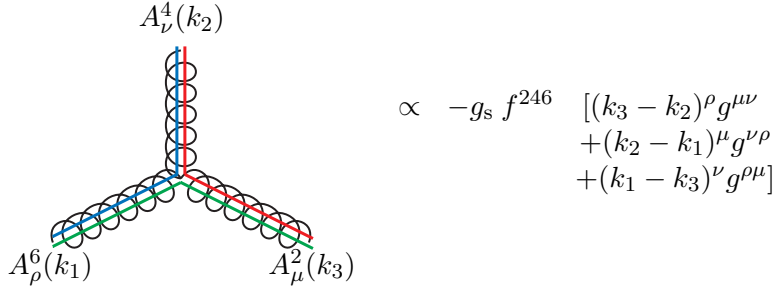
In addition, the gluon self-coupling on the third line in Table 1 involves factors of  $f^{abc}$ . These are called the *structure constants* of QCD and they enter via the non-Abelian term in the gluon-field-strength tensor appearing in Eq. (3),

$$F_{\mu\nu}^a = \partial_\mu A_\nu^a - \partial_\nu A_\mu^a + g_s f^{abc} A_\mu^b A_\nu^c. \quad (11)$$

The structure constants of  $\text{SU}(3)$  are listed in the box below. They define the *adjoint*, or *vector*, representation of  $\text{SU}(3)$  and are related to the fundamental-representation generators via the commutator relations

$$t^a t^b - t^b t^a = [t^a, t^b] = i f^{abc} t_c, \quad (12)$$

<sup>6</sup>See, e.g., Ref. [1, Appendix A.3] for how to obtain the Casimirs in other normalization conventions.



**Fig. 4:** Illustration of a ggg vertex in QCD, before summing/averaging over colours: interaction between gluons in the states  $\lambda^2$ ,  $\lambda^4$ , and  $\lambda^6$  is represented by the structure constant  $f^{246}$ .

or equivalently,

$$if^{abc} = 2\text{Tr}\{t^c[t^a, t^b]\}. \quad (13)$$

Thus, it is a matter of choice whether one prefers to express colour space on a basis of fundamental-representation  $t$  matrices, or via the structure constants  $f$ , and one can go back and forth between the two.

<b>Structure constants of SU(3)</b>	
$f_{123} = 1$	(14)
$f_{147} = f_{246} = f_{257} = f_{345} = \frac{1}{2}$	(15)
$f_{156} = f_{367} = -\frac{1}{2}$	(16)
$f_{458} = f_{678} = \frac{\sqrt{3}}{2}$	(17)
Antisymmetric in all indices	
All other $f_{abc} = 0$	

Expanding the  $F_{\mu\nu}F^{\mu\nu}$  term of the Lagrangian using Eq. (11), we see that there is a 3-gluon and a 4-gluon vertex that involve  $f^{abc}$ , the latter of which has two powers of  $f$  and two powers of the coupling.

Finally, the last line of Table 1 is not really a trace relation but instead a useful so-called Fierz transformation, which expresses products of  $t$  matrices in terms of Kronecker  $\delta$  functions. It is often used, for instance, in shower Monte Carlo applications, to assist in mapping between colour flows in  $N_C = 3$ , in which cross sections and splitting probabilities are calculated, and those in  $N_C \rightarrow \infty$  ('leading colour') are used to represent colour flow in the Monte Carlo (MC) 'event record'.

A gluon self-interaction vertex is illustrated in Fig. 4, to be compared with the quark–gluon interaction in Fig. 2. We remind the reader that gauge boson self-interactions are a hallmark of non-Abelian theories and that their presence leads to some of the main differences between QED and QCD. One should also keep in mind that the colour factor for the vertex in Fig. 4,  $C_A$ , is roughly twice as large as that for a quark,  $C_F$ .

### 1.4 The strong coupling

To first approximation, QCD is *scale invariant*. That is, if one 'zooms in' on a QCD jet, one will find a repeated self-similar pattern of jets within jets within jets, reminiscent of fractals. In the context of QCD, this property was originally called light-cone scaling, or Björken scaling. This type of scaling

is closely related to the class of angle-preserving symmetries, called *conformal* symmetries. In physics today, the terms ‘conformal’ and ‘scale invariant’ are used interchangeably<sup>7</sup>. Conformal invariance is a mathematical property of several QCD-‘like’ theories which are now being studied (such as  $N = 4$  supersymmetric relatives of QCD). It is also related to the physics of so-called ‘unparticles’, although that is a relation that goes beyond the scope of these lectures.

Regardless of the labelling, if the strong coupling did not run (we shall return to the running of the coupling below), Bjørken scaling would be absolutely true. QCD would be a theory with a fixed coupling, the same at all scales. This simplified picture already captures some of the most important properties of QCD, as we shall discuss presently.

In the limit of exact Bjørken scaling—QCD at fixed coupling—properties of high-energy interactions are determined only by *dimensionless* kinematic quantities, such as scattering angles (pseudorapidities) and ratios of energy scales<sup>8</sup>. For applications of QCD to high-energy collider physics, an important consequence of Bjørken scaling is, thus, that the rate of bremsstrahlung jets, with a given transverse momentum, scales in direct proportion to the hardness of the fundamental partonic-scattering process they are produced in association with. This agrees well with our intuition about accelerated charges; the harder you ‘kick’ them, the harder the radiation they produce.

For instance, in the limit of exact scaling, a measurement of the rate of 10 GeV jets produced in association with an ordinary Z boson could be used as a direct prediction of the rate of 100 GeV jets that would be produced in association with a 900 GeV  $Z'$  boson, and so forth. Our intuition about how many bremsstrahlung jets a given type of process is likely to have should, therefore, be governed, first and foremost, by the *ratios* of scales that appear in that particular process, as has been highlighted in a number of studies focusing on the mass and  $p_\perp$  scales appearing, for example, in beyond-the-standard-model (BSM) physics processes [18–21]. Bjørken scaling is also fundamental to the understanding of jet substructure in QCD, see, for example, Refs. [22, 23].

On top of the underlying scaling behaviour, the running coupling will introduce a dependence on the absolute scale, implying more radiation at low scales than at high ones. The running is logarithmic with energy and is governed by the so-called *beta function*,

$$Q^2 \frac{\partial \alpha_s}{\partial Q^2} = \frac{\partial \alpha_s}{\partial \ln Q^2} = \beta(\alpha_s), \quad (18)$$

where the function driving the energy dependence, the beta function, is defined as

$$\beta(\alpha_s) = -\alpha_s^2 (b_0 + b_1 \alpha_s + b_2 \alpha_s^2 + \dots), \quad (19)$$

with LO (one-loop) and NLO (two-loop) coefficients

$$b_0 = \frac{11C_A - 4T_R n_f}{12\pi}, \quad (20)$$

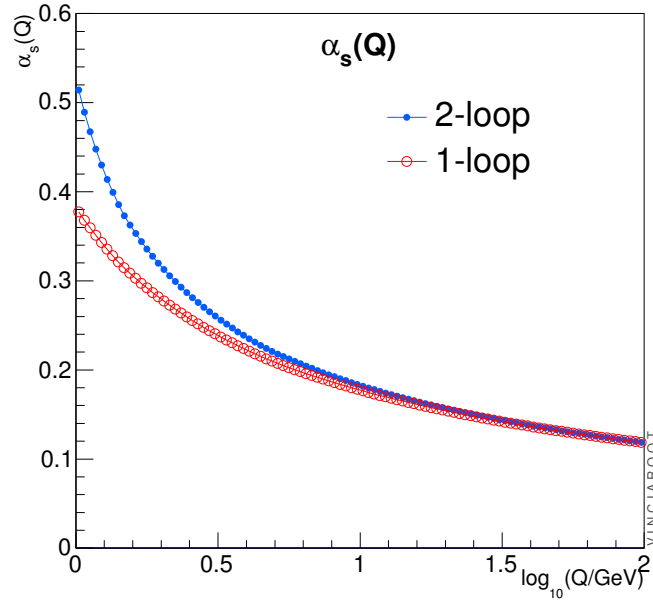
$$b_1 = \frac{17C_A^2 - 10T_R C_A n_f - 6T_R C_F n_f}{24\pi^2} = \frac{153 - 19n_f}{24\pi^2}. \quad (21)$$

In the  $b_0$  coefficient, the first term is due to gluon loops while the second is due to quark loops. Similarly, the first term of the  $b_1$  coefficient arises from double gluon loops, while the second and third represent mixed quark–gluon loops. At higher loop orders, the  $b_i$  coefficients depend explicitly on the renormalization scheme that is used. A brief discussion can be found in the Particle Data Group (PDG) review on

<sup>7</sup>Strictly speaking, conformal symmetry is more restrictive than just scale invariance, but examples of scale-invariant field theories that are not conformal are rare.

<sup>8</sup>Originally, the observed approximate agreement with this was used as a powerful argument for pointlike substructure in hadrons; since measurements at different energies are sensitive to different resolution scales, independence of the absolute energy scale is indicative of the absence of other fundamental scales in the problem and hence of pointlike constituents.





**Fig. 5:** Illustration of the running of  $\alpha_s$  at one- (open circles) and two-loop order (filled circles), starting from the same value of  $\alpha_s(M_Z) = 0.12$ .

QCD [24], with more elaborate ones contained in Refs. [2, 3]. Note that, if there are additional coloured particles beyond the standard-model ones, loops involving those particles enter at energy scales above the masses of the new particles, thus modifying the running of the coupling at high scales. This is discussed, for example, for supersymmetric models in Ref. [25].

Numerically, the value of the strong coupling is usually specified by giving its value at the specific reference scale  $Q^2 = M_Z^2$ , from which we can obtain its value at any other scale by solving Eq. (18),

$$\alpha_s(Q^2) = \alpha_s(M_Z^2) \frac{1}{1 + b_0 \alpha_s(M_Z^2) \ln \frac{Q^2}{M_Z^2} + \mathcal{O}(\alpha_s^2)}, \quad (22)$$

with relations including the  $\mathcal{O}(\alpha_s^2)$  terms available, for example, in Ref. [2]. Relations between scales not involving  $M_Z^2$  can obviously be obtained by just replacing  $M_Z^2$  by some other scale  $Q'^2$  everywhere in Eq. (22). A comparison of running at one- and two-loop order, in both cases starting from  $\alpha_s(M_Z) = 0.12$ , is given in Fig. 5. As is evident from the figure, the two-loop running is somewhat faster than the one-loop.

As an application, let us prove that the logarithmic running of the coupling implies that an intrinsically multi-scale problem can be converted to a single-scale one, up to corrections suppressed by two powers of  $\alpha_s$ , by taking the geometric mean of the scales involved. This follows from expanding an arbitrary product of individual  $\alpha_s$  factors around an arbitrary scale  $\mu$ , using Eq. (22),

$$\begin{aligned} \alpha_s(\mu_1) \alpha_s(\mu_2) \cdots \alpha_s(\mu_n) &= \prod_{i=1}^n \alpha_s(\mu) \left( 1 + b_0 \alpha_s \ln \left( \frac{\mu^2}{\mu_i^2} \right) + \mathcal{O}(\alpha_s^2) \right) \\ &= \alpha_s^n(\mu) \left( 1 + b_0 \alpha_s \ln \left( \frac{\mu^{2n}}{\mu_1^2 \mu_2^2 \cdots \mu_n^2} \right) + \mathcal{O}(\alpha_s^2) \right), \end{aligned} \quad (23)$$

whereby the specific single-scale choice  $\mu^n = \mu_1 \mu_2 \cdots \mu_n$  (the geometric mean) can be seen to push the difference between the two sides of the equation one order higher than would be the case for any other

combination of scales<sup>9</sup>.

The appearance of the number of flavours,  $n_f$ , in  $b_0$  implies that the slope of the running depends on the number of contributing flavours. Since full QCD is best approximated by  $n_f = 3$  below the charm threshold, by  $n_f = 4$  and 5 from there to the  $b$  and  $t$  thresholds, respectively, and then by  $n_f = 6$  at scales higher than  $m_t$ , it is, therefore, important to be aware that the running changes slope across quark-flavour thresholds. Likewise, it would change across the threshold for any coloured new-physics particles that might exist, with a magnitude depending on the particles' colour and spin quantum numbers.

The negative overall sign of Eq. (19), combined with the fact that  $b_0 > 0$  (for  $n_f \leq 16$ ), leads to the famous result<sup>10</sup> that the QCD coupling effectively *decreases* with energy, called asymptotic freedom, for the discovery of which the Nobel prize in physics was awarded to D. Gross, H. Politzer and F. Wilczek in 2004. An extract of the prize announcement runs as follows.

*What this year's Laureates discovered was something that, at first sight, seemed completely contradictory. The interpretation of their mathematical result was that the closer the quarks are to each other, the weaker is the 'colour charge'. When the quarks are really close to each other, the force is so weak that they behave almost as free particles<sup>a</sup>. This phenomenon is called 'asymptotic freedom'. The converse is true when the quarks move apart: the force becomes stronger when the distance increases<sup>b</sup>.*

<sup>a</sup>More correctly, it is the coupling rather than the force which becomes weak as the distance decreases. The  $1/r^2$  Coulomb singularity of the force is only dampened, not removed, by the diminishing coupling.

<sup>b</sup>More correctly, it is the potential which grows, linearly, while the force becomes constant.

Among the consequences of asymptotic freedom is that perturbation theory becomes better behaved at higher absolute energies, due to the effectively decreasing coupling. Perturbative calculations for our 900 GeV  $Z'$  boson from before should, therefore, be slightly faster converging than equivalent calculations for the 90 GeV one. Furthermore, since the running of  $\alpha_s$  explicitly breaks Björken scaling, we also expect to see small changes in jet shapes and in jet-production ratios as we vary the energy. For instance, since high- $p_\perp$  jets start out with a smaller effective coupling, their intrinsic shape (irrespective of boost effects) is somewhat narrower than for low- $p_\perp$  jets, an issue which can be important for jet calibration. Our current understanding of the running of the QCD coupling is summarized by the plot in Fig. 6, taken from a recent comprehensive review by S. Bethke [26, 27].

As a final remark on asymptotic freedom, note that the decreasing value of the strong coupling with energy must eventually cause it to become comparable to the electromagnetic and weak ones, at some energy scale. Beyond that point, which may lie at energies of order  $10^{15}$ – $10^{17}$  GeV (although it may be lower if as-yet-undiscovered particles generate large corrections to the running), we do not know what the further evolution of the combined theory will actually look like, or whether it will continue to exhibit asymptotic freedom.

Now consider what happens when we run the coupling in the other direction, towards smaller energies. Taken at face value, the numerical value of the coupling diverges rapidly at scales below 1 GeV, as illustrated by the curves disappearing off the left-hand edge of the plot in Fig. 6. To make this divergence explicit, one can rewrite Eq. (22) in the following form,

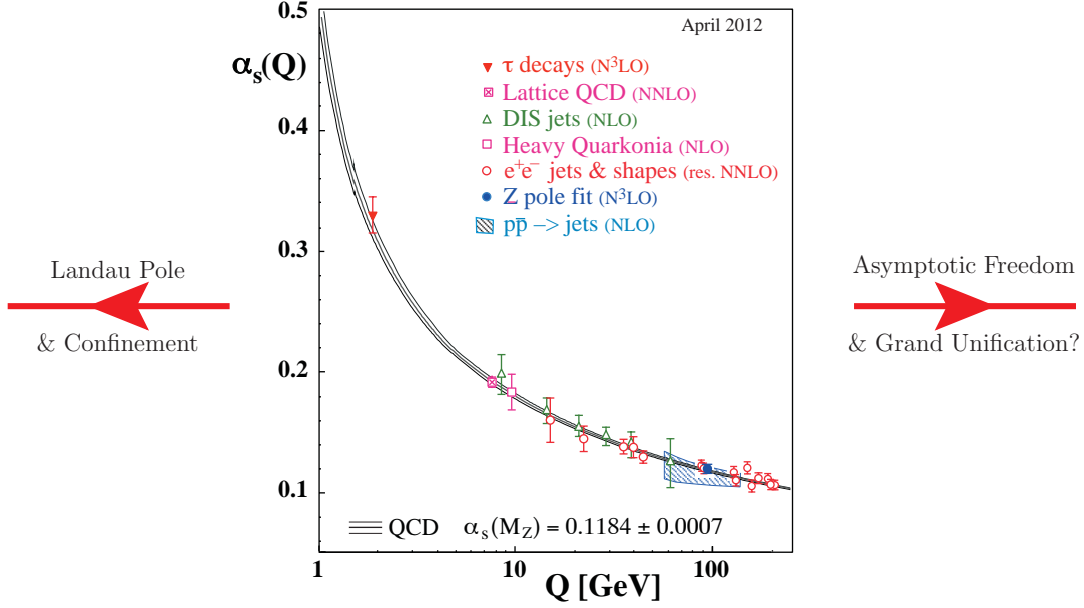
$$\alpha_s(Q^2) = \frac{1}{b_0 \ln \frac{Q^2}{\Lambda^2}}, \quad (24)$$

where

$$\Lambda \sim 200 \text{ MeV} \quad (25)$$

<sup>9</sup>In a fixed-order calculation, the individual scales  $\mu_i$ , would correspond, for example, to the  $n$  hardest scales appearing in an IR-safe sequential-clustering algorithm applied to the given momentum configuration.

<sup>10</sup>Perhaps the highest pinnacle of fame for Eq. (19) was reached when the sign of it featured in an episode of the TV series 'Big Bang Theory'.



**Fig. 6:** Illustration of the running of  $\alpha_s$  in a theoretical calculation (band) and in physical processes at different characteristic scales, from Refs. [24, 26]. The little kinks at  $Q = m_c$  and  $Q = m_b$  are caused by discontinuities in the running across the flavour thresholds.

specifies the energy scale at which the perturbative coupling would nominally become infinite, called the Landau pole. (Note, however, that this only parameterizes the purely *perturbative* result, which is not reliable at strong coupling, so Eq. (24) should not be taken to imply that the physical behaviour of full QCD should exhibit a divergence for  $Q \rightarrow \Lambda$ .)

Finally, one should be aware that there is a multitude of different ways of defining both  $\Lambda$  and  $\alpha_s(M_Z)$ . At the very least, the numerical value one obtains depends both on the renormalization scheme used (with the dimensional-regularization-based ‘modified minimal subtraction’ scheme,  $\overline{\text{MS}}$ , being the most common one) and on the perturbative order of the calculations used to extract them. As a rule of thumb, fits to experimental data typically yield smaller values for  $\alpha_s(M_Z)$  the higher the order of the calculation used to extract it (see, e.g., Refs. [24, 26–28]), with  $\alpha_s(M_Z)|_{\text{LO}} \gtrsim \alpha_s(M_Z)|_{\text{NLO}} \gtrsim \alpha_s(M_Z)|_{\text{NNLO}}$ . Further, since the number of flavours changes the slope of the running, the location of the Landau pole for fixed  $\alpha_s(M_Z)$  depends explicitly on the number of flavours used in the running. Thus, each value of  $n_f$  is associated with its own value of  $\Lambda$ , with the following matching relations across thresholds guaranteeing continuity of the coupling at one loop,

$$n_f = 5 \leftrightarrow 6 \quad : \quad \Lambda_6 = \Lambda_5 \left( \frac{\Lambda_5}{m_t} \right)^{\frac{2}{21}} \quad \Lambda_5 = \Lambda_6 \left( \frac{m_t}{\Lambda_6} \right)^{\frac{2}{23}}, \quad (26)$$

$$n_f = 4 \leftrightarrow 5 \quad : \quad \Lambda_5 = \Lambda_4 \left( \frac{\Lambda_4}{m_b} \right)^{\frac{2}{23}} \quad \Lambda_4 = \Lambda_5 \left( \frac{m_b}{\Lambda_5} \right)^{\frac{2}{25}}, \quad (27)$$

$$n_f = 3 \leftrightarrow 4 \quad : \quad \Lambda_4 = \Lambda_3 \left( \frac{\Lambda_3}{m_c} \right)^{\frac{2}{25}} \quad \Lambda_3 = \Lambda_4 \left( \frac{m_c}{\Lambda_4} \right)^{\frac{2}{27}}. \quad (28)$$

It is sometimes stated that QCD only has a single free parameter, the strong coupling. However, even in the perturbative region, the beta function depends explicitly on the number of quark flavours, as we have seen, and thereby also on the quark masses. Furthermore, in the non-perturbative region around or below  $\Lambda_{\text{QCD}}$ , the value of the perturbative coupling, as obtained, for example, from Eq. (24),

gives little or no insight into the behaviour of the full theory. Instead, universal functions (such as parton densities, form factors, fragmentation functions, etc), effective theories (such as the operator product expansion, chiral perturbation theory, or heavy quark effective theory), or phenomenological models (such as Regge theory or the string and cluster hadronization models) must be used, which in turn depend on additional non-perturbative parameters whose relation to, for example,  $\alpha_s(M_Z)$ , is not a priori known.

For some of these questions, such as hadron masses, lattice QCD can furnish important additional insight, but for multi-scale and/or time-evolution problems, the applicability of lattice methods is still severely restricted; the lattice formulation of QCD requires a Wick rotation to Euclidean space. The time-coordinate can then be treated on an equal footing with the other dimensions, but intrinsically Minkowskian problems, such as the time evolution of a system, are inaccessible. The limited size of current lattices also severely constrain the scale hierarchies that it is possible to ‘fit’ between the lattice spacing and the lattice size.

### 1.5 Colour states

A final example of the application of the underlying  $SU(3)$  group theory to QCD is given by considering which colour states we can obtain by combinations of quarks and gluons. The simplest example of this is the combination of a quark and antiquark. We can form a total of nine different colour–anticolour combinations, which fall into two irreducible representations of  $SU(3)$ :

$$3 \otimes \bar{3} = 8 \oplus 1. \quad (29)$$

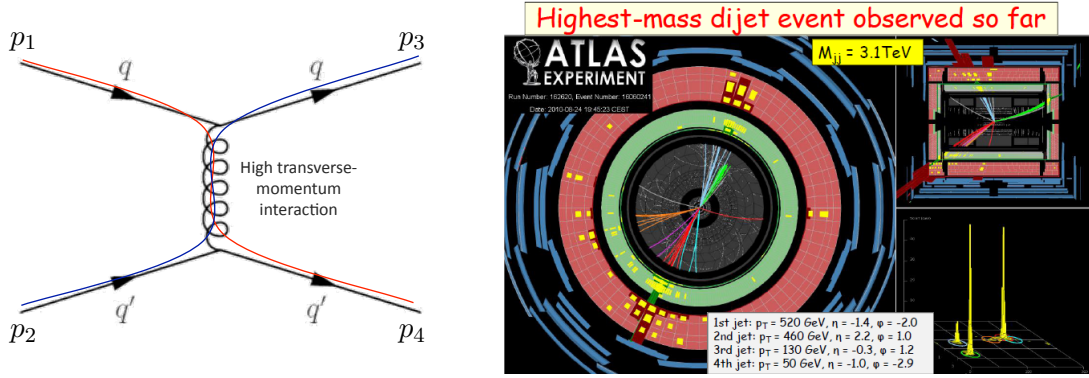
The singlet corresponds to the symmetric wave function  $\frac{1}{\sqrt{3}} (|R\bar{R}\rangle + |G\bar{G}\rangle + |B\bar{B}\rangle)$ , which is invariant under  $SU(3)$  transformations (the definition of a singlet). The other eight linearly independent combinations (which can be represented by one for each Gell–Mann matrix, with the singlet corresponding to the identity matrix) transform into each other under  $SU(3)$ . Thus, although we sometimes talk about colour-singlet states as being made up, for example, of ‘red–antired’, that is not quite precise language. The actual state  $|R\bar{R}\rangle$  is *not* a pure colour singlet. Although it does have a non-zero *projection* onto the singlet wave function above, it also has non-zero projections onto the two members of the octet that correspond to the diagonal Gell–Mann matrices. Intuitively, one can also easily realize this by noting that an  $SU(3)$  rotation of  $|R\bar{R}\rangle$  would in general turn it into a different state, say  $|B\bar{B}\rangle$ , whereas a true colour singlet would be invariant. Finally, we can also realize from Eq. (29) that a random (colour-uncorrelated) quark–antiquark pair has a  $1/N^2 = 1/9$  chance to be in an overall colour-singlet state; otherwise it is in an octet.

Similarly, there are also nine possible quark–quark (or antiquark–antiquark) combinations, six of which are symmetric under interchange of the two quarks and three of which are antisymmetric:

$$6 = \left( \begin{array}{c} |RR\rangle \\ |GG\rangle \\ |BB\rangle \\ \frac{1}{\sqrt{2}} (|RG\rangle + |GR\rangle) \\ \frac{1}{\sqrt{2}} (|GB\rangle + |BG\rangle) \\ \frac{1}{\sqrt{2}} (|BR\rangle + |RB\rangle) \end{array} \right), \quad \bar{3} = \left( \begin{array}{c} \frac{1}{\sqrt{2}} (|RG\rangle - |GR\rangle) \\ \frac{1}{\sqrt{2}} (|GB\rangle - |BG\rangle) \\ \frac{1}{\sqrt{2}} (|BR\rangle - |RB\rangle) \end{array} \right). \quad (30)$$

The members of the sextet transform into (linear combinations of) each other under  $SU(3)$  transformations, and similarly for the members of the antitriplet, and hence neither of these can be reduced further. The breakdown into irreducible  $SU(3)$  multiplets is, therefore,

$$3 \otimes 3 = 6 \oplus \bar{3}. \quad (31)$$



**Fig. 7:** *Left:* Rutherford scattering of quarks in QCD, exemplifying the type of process that dominates the short-distance interaction cross section at hadron colliders. *Right:* an example of what such a reaction looks like in a detector, in this case the ATLAS experiment.

Thus, an uncorrelated pair of quarks has a  $1/3$  chance to add to an overall anti-triplet state (corresponding to coherent superpositions like ‘red + green = antiblue’<sup>11</sup>); otherwise it is in an overall sextet state.

Note that the emphasis on the quark–(anti)quark pair being *uncorrelated* is important; production processes that correlate the produced partons, like  $Z \rightarrow q\bar{q}$  or  $g \rightarrow q\bar{q}$ , will project out specific components (here the singlet and octet, respectively). Note also that, if the quark and (anti)quark are on opposite sides of the universe (i.e., living in two different hadrons), the QCD *dynamics* will not care what overall colour state they are in, so for the formation of multi-partonic states in QCD, obviously the spatial part of the wave functions (causality at the very least) will also play a role. Here, we are considering *only* the colour part of the wave functions. Some additional examples are

$$8 \otimes 8 = 27 \oplus 10 \oplus \bar{10} \oplus 8 \oplus 8 \oplus 1, \quad (32)$$

$$3 \otimes 8 = 15 \oplus 6 \oplus 3, \quad (33)$$

$$3 \otimes 6 = 10 \oplus 8, \quad (34)$$

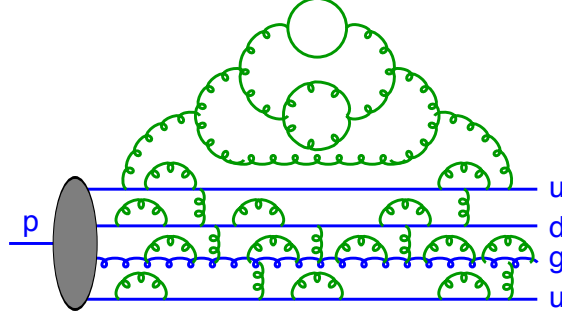
$$3 \otimes 3 \otimes 3 = (6 \oplus \bar{3}) \otimes 3 = 10 \oplus 8 \oplus 8 \oplus 1. \quad (35)$$

Physically, the ‘27’ in the first line corresponds to a completely incoherent addition of the colour charges of two gluons; the decuplets are slightly more coherent (with a lower total colour charge), the octets yet more, and the singlet corresponds to the combination of two gluons that have precisely equal and opposite colour charges, so that their total charge is zero. Further extensions and generalizations of these combination rules can be obtained, for example, using the method of the Young tableaux [29, 30].

## 2 Hard processes

Our main tool for solving QCD at high energy scales,  $Q \gg \Lambda_{\text{QCD}}$ , is perturbative quantum field theory, the starting point for which is matrix elements (MEs) which can be calculated systematically at fixed orders in the strong coupling  $\alpha_s$ . At least at the lowest order (LO), the procedure is standard textbook material [1] and it has also by now been highly automated, by the advent of tools like MADGRAPH [31], CALCHEP [32] / COMPHEP [33], and several others [34–40]. Here, we require only that the reader has a basic familiarity with the methods involved from graduate-level particle physics courses based, for example, on Refs. [1, 3]. Our main concerns are the uses to which these calculations are put, their limitations and ways to improve on the results obtained with them.

<sup>11</sup>In the context of hadronization models, this coherent superposition of two quarks in an overall antitriplet state is sometimes called a ‘diquark’ (at low  $m_{q\bar{q}}$ ) or a ‘string junction’ (at high  $m_{q\bar{q}}$ ), see Section 5.1; it corresponds to the antisymmetric ‘red + green = antiblue’ combination needed to create a baryon wavefunction.



**Fig. 8:** Illustration of partonic fluctuations inside a proton beam (from Ref. [41])

For illustration, take one of the most commonly occurring processes in hadron collisions: Rutherford scattering of two quarks via a  $t$ -channel gluon exchange—Fig. 7—which at leading order has the differential cross section

$$qq' \rightarrow qq' \quad : \quad \frac{d\sigma}{d\hat{t}} = \frac{\pi}{\hat{s}^2} \frac{4}{9} \alpha_s^2 \frac{\hat{s}^2 + \hat{u}^2}{\hat{t}^2}, \quad (36)$$

with the  $2 \rightarrow 2$  Mandelstam variables (‘hatted’ to emphasize that they refer to a partonic  $2 \rightarrow 2$  scattering rather than the full  $pp \rightarrow \text{jets}$  process)

$$\hat{s} = (p_1 + p_2)^2, \quad (37)$$

$$\hat{t} = (p_3 - p_1)^2 = -\hat{s} \frac{(1 - \cos \hat{\theta})}{2}, \quad (38)$$

$$\hat{u} = (p_4 - p_1)^2 = -\hat{s} \frac{(1 + \cos \hat{\theta})}{2}. \quad (39)$$

Reality, however, is more complicated; the picture on the right-hand pane of Fig. 7 shows a real dijet event, as recorded by the ATLAS experiment. The complications to be addressed when going from left to right in Fig. 7 are: (1) additional jets, a.k.a. real-emission corrections, which can significantly change the topology of the final state, potentially shifting jets in or out of an experimentally defined acceptance region; (2) loop factors, a.k.a. virtual corrections, change the number of available quantum paths through phase space, and hence modify the normalization of the cross section (total *and* differential); and (3) additional corrections are generated by confinement and by the so-called underlying event. These corrections must be taken into account to complete our understanding of QCD and connect the short-distance physics with macroscopic experiments. Apart from the perturbative expansion itself, the most powerful tool we have to organize this vast calculation, is factorization.

## 2.1 Factorization

In high-energy scattering problems involving hadrons in the initial state, we immediately face the complication that hadrons are composite, with a time-dependent structure illustrated in Fig. 8; there are partons within clouds of further partons, constantly being emitted and absorbed. Thus, before we can use perturbatively calculated partonic-scattering MEs, we must first address the partonic structure of the colliding hadron(s).

For the hadron to remain intact, the fluctuations inside it must involve momentum transfers smaller than the confinement scale. Indeed, high-virtuality fluctuations are suppressed by powers of

$$\frac{\alpha_s \Lambda^2}{|k|^2}, \quad (40)$$

with  $\Lambda$  the confinement scale ( $\sim 200$  MeV, see Section 1.4) and  $|k|$  the virtuality of the fluctuation. Thus, most fluctuations occur over timescales of  $\sim 1/\Lambda$ .

A hard perturbative probe, on the other hand, such as the exchanged photon in DIS (Fig. 3), interacts over a much shorter timescale  $1/Q \ll 1/\Lambda$ , during which the partonic fluctuations in the struck hadron appear almost frozen. The hard probe effectively takes an instantaneous snapshot of the hadron structure, at a characteristic resolution given by  $\sim 1/Q$ .

This is formalized by the *factorization theorem* [42] (see also the TASI lectures by George Sterman [43]), which expresses the independence of long-wavelength (soft) structure on the nature of the hard (short-distance) process. Originally formulated for DIS, factorization allows us to write the cross section for lepton–hadron scattering as a convolution of a non-perturbative but universal (i.e., process-independent) parton density function (PDF) and a perturbatively calculable partonic-scattering cross section. Denoting the fraction of the hadron momentum carried by parton  $i$  by  $x_i$ ,

$$\vec{p}_i = x_i \vec{p}_h, \quad (41)$$

we may write the lepton–hadron cross section in factorized form (see, e.g., Refs. [3, 44]),

$$\sigma_{\ell h} = \sum_i \int_0^1 dx_i \int d\Phi_f f_{i/h}(x_i, \mu_F^2) \frac{d\hat{\sigma}_{\ell i \rightarrow f}(x_i, \Phi_f, \mu_F^2)}{dx_i d\Phi_f}, \quad (42)$$

with  $i$  an index running over all possible parton types<sup>12</sup> in the incoming hadron and  $f$  enumerating all possible (partonic) final states, with Lorentz-invariant phase space,  $\Phi_f$ .

The *PDFs*,  $f_{i/h}$ , parameterize the distribution of partons inside the target hadron. They are not a priori calculable and must be constrained by fits to data. This is discussed in Section 2.2.

The *partonic cross section*,  $d\hat{\sigma}$ , knows nothing of the target hadron apart from the fact that it contained the struck parton. It is calculable within perturbation theory, as will be discussed in Section 2.3.

The dividing line between the two is drawn at an arbitrary (‘user-defined’) scale,  $\mu_F$ , called the *factorization scale*. There is some arbitrariness involved in choosing a value for  $\mu_F$ . Some heuristic arguments to guide in the choice of factorization scale are the following. On the long-distance side, the PDFs include a (re)summation of fluctuations inside fluctuations up to virtualities of order  $\mu_F$ . It would, therefore, not make much sense to take  $\mu_F$  significantly larger than the scales characterizing resolved particles on the short-distance side of the calculation (i.e., the particles appearing explicitly in  $\Phi_f$ ); otherwise the PDFs would be including sums over fluctuations that happen on timescales shorter than those probed by the physical process. Similarly,  $\mu_F$  should also not be taken much lower than the scale(s) appearing in the hard process. For MEs characterized by a single well-defined scale, such as the  $Q^2$  scale in DIS or the invariant-mass scale  $\hat{s}$  in Drell–Yan production ( $q\bar{q} \rightarrow Z/\gamma^* \rightarrow \ell^+ \ell^-$ ), such arguments essentially fix the preferred scale choice to  $\mu_F = Q$  or  $\mu_F = \sqrt{\hat{s}}$ , respectively, which may then be varied by a factor of two (or larger) around the nominal value in order to estimate uncertainties. For multi-scale problems, however, such as  $pp \rightarrow Z/W + n$  jets, there are several a priori equally good choices available, from the lowest to the highest QCD scales that can be constructed from the final-state momenta, usually with several dissenting groups of theorists arguing over which particular choice is best. Suggesting that one might simply *measure* the scale would not really be an improvement, as the factorization scale is fundamentally unphysical and therefore unobservable (similarly to gauge or convention choices). One plausible strategy is to look at higher-order (NLO or NNLO) calculations, in which correction terms appear that cancel the dependence on the scale choice, stabilizing the final result. From such comparisons, a ‘most stable’ initial scale choice can, in principle, be determined, which then furnishes a reasonable starting point, but we emphasize that the question *is* intrinsically ambiguous, and

<sup>12</sup>Typically, only quarks and gluons are included in this sum, but also photons and even leptons can, in principle, be included. Similarly, PDFs are normally used to describe hadrons, but can also be defined, for example, to describe the cloud of virtual photons (and fermion pairs) surrounding an electron.

no golden recipe is likely to magically give all the right answers. The best we can do is to vary the value of  $\mu_F$  not only by an overall factor, but also by exploring different possible forms for its functional dependence on the momenta appearing in  $\Phi_f$ . A complementary useful discussion of the pros and cons of different factorization scale choices can be found in the TASI lectures by Tilman Plehn [45].

Secondly, and more technically, at NLO and beyond one also has to settle on a *factorization scheme* in which to do the calculations. For all practical purposes, students focusing on LHC physics are only likely to encounter one such scheme, the modified minimal-subtraction ( $\overline{\text{MS}}$ ) scheme already mentioned in the discussion of the definition of the strong coupling in Section 1.4. At the level of these lectures, we shall therefore not elaborate further on this choice here.

We note that factorization can also be applied multiple times, to break up a complicated calculation into simpler pieces that can be treated as approximately independent. This will be very useful when dealing with successive emissions in a parton shower, Section 3.2, or when factoring off decays of long-lived particles from a hard production process, Section 3.4.

We round off the discussion of factorization by mentioning a few caveats the reader should be aware of. (See Ref. [43] for a more technical treatment.)

Firstly, the proof only applies to the first term in an operator product expansion in ‘twist’ = mass dimension – spin. Since operators with higher mass dimensions are suppressed by the hard scale to some power, this leading twist approximation becomes exact in the limit  $Q \rightarrow \infty$ , while at finite  $Q$  it neglects corrections of order

$$\text{Higher Twist : } \frac{[\ln(Q^2/\Lambda^2)]^{m < 2n}}{Q^{2n}} \quad (n = 2 \text{ for DIS}). \quad (43)$$

In Section 5, we shall discuss some corrections that go beyond this approximation, in the context of multiple parton–parton interactions.

Secondly, the proof only really applies to inclusive cross sections in DIS [42] and in Drell–Yan [46]. For all other hadron-initiated processes, factorization is an ansatz. For a general hadron–hadron process, we write the assumed factorizable cross section as

$$d\sigma_{h_1 h_2} = \sum_{i,j} \int_0^1 dx_i \int_0^1 dx_j \sum_f \int d\Phi_f f_{i/h_1}(x_i, \mu_F^2) f_{j/h_2}(x_j, \mu_F^2) \frac{d\hat{\sigma}_{ij \rightarrow f}}{dx_i dx_j d\Phi_f}. \quad (44)$$

Note that, if  $d\hat{\sigma}$  is divergent (as, e.g., Rutherford scattering is) then the integral over  $d\Phi_f$  must be regulated, for example, by imposing some explicit minimal transverse-momentum cut and/or other phase-space restrictions.

## 2.2 Parton densities

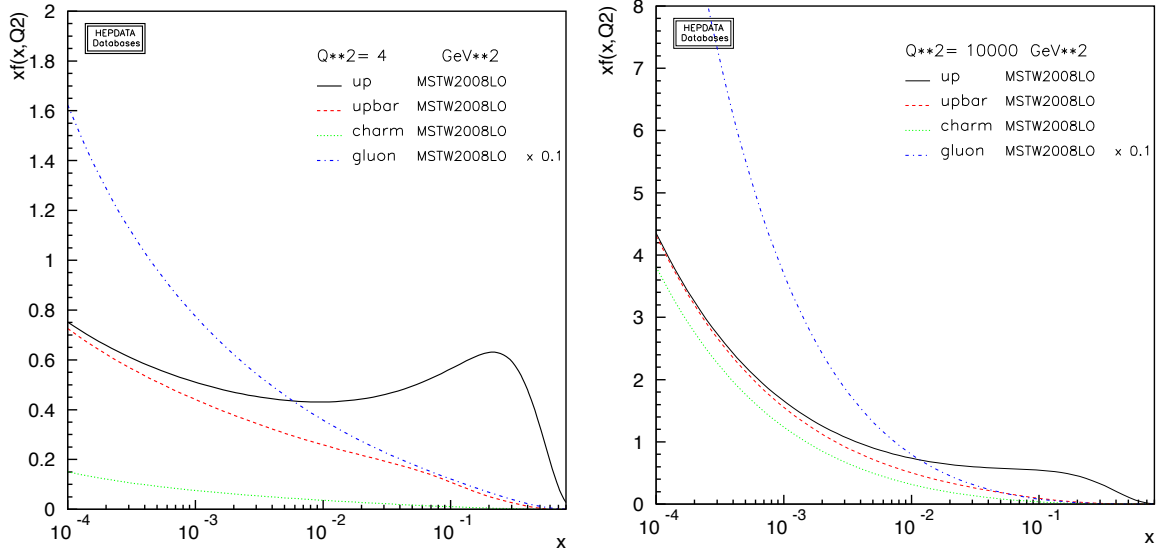
The PDF,  $f_{i/h}(x, \mu_F^2)$ , represents the effective density of partons of type/flavour  $i$ , as a function of the momentum fraction<sup>13</sup>  $x_i$ , when a hadron of type  $h$  is probed at the factorization scale  $\mu_F$ . The PDFs are non-perturbative functions which are not a priori calculable, but a perturbative differential equation governing their evolution with  $\mu_F$  can be obtained by requiring that physical-scattering cross sections, such as the one for DIS in Eq. (42), be independent of  $\mu_F$  to the calculated orders [47]. The resulting *renormalization group equation* (RGE) is called the DGLAP<sup>14</sup> equation and can be used to ‘run’ the PDFs from one perturbative resolution scale to another (its evolution kernels are the same as those used in parton showers, to which we return in Section 3.2).

This means that we only need to determine the form of the PDF as a function of  $x$  in a single (arbitrary) scale,  $\mu_0$ . We can then get its form at any other scale  $\mu_F$  by simple RGE evolution. In the

<sup>13</sup>Recall: the  $x$  fraction is defined in Eq. (41).

<sup>14</sup>DGLAP: Dokshitzer–Gribov–Lipatov–Altarelli–Parisi [47–49].





**Fig. 9:** Illustration of the change of the  $u$  (black),  $\bar{u}$  (red, dashed),  $c$  (green, dotted), and  $g$  (blue, dot-dashed) distributions, from  $Q = \mu_F = 2 \text{ GeV}$  (left) to  $Q = \mu_F = 100 \text{ GeV}$  (right). Note that a factor 0.1 has been applied to the gluon distribution. Plots made using the HEPDATA online tool [55].

context of PDF fits (constraining the form of the PDF functions by fitting cross sections to experimental data, for example, from DIS [50, 51], Drell–Yan [52, 53], and  $pp \rightarrow \text{jets}$  [54]), the reference scale  $\mu_0$  is usually taken to be relatively low, of order one or a few GeV.

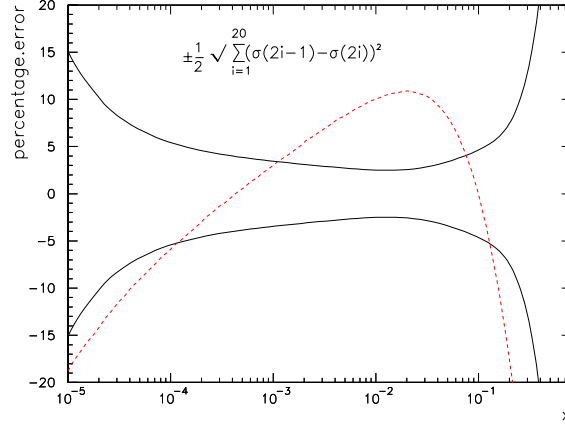
The behaviour of the PDFs as we evolve  $\mu_F$  from a low scale, 2 GeV, to a high one, 100 GeV, is illustrated in Fig. 9, for the MSTW<sup>15</sup> 2008 LO<sup>16</sup> PDF set [56]. At low  $Q = \mu_F = 2 \text{ GeV}$  (left), the proton structure is dominated by a few hard quarks (a ‘valence bump’ is clearly visible around  $x \sim 0.2$ ), while at higher scales  $Q = 100 \text{ GeV}$  (right) we predominantly resolve fluctuations within fluctuations, yielding increasingly large gluon- and sea-quark distributions with rather small  $x$  values, while the valence quarks play a progressively smaller role.

We note that different collaborations, like CTEQ, MSTW, NNPDF, etc., use different ansätze for the form of  $f(x, \mu_0^2)$ . They may also include different data in the fits, and/or treat or weight the data differently. Thus, results from different groups may not always be mutually compatible. An example is given in Fig. 10, which shows the difference between the CTEQ6L1 gluon PDF [57] (red dashed) and the MSTW 2008 LO PDF [56], normalized to MSTW (which would thus be a flat line at zero), at  $\mu_F = 10 \text{ GeV}$ . The  $y$ -axis shows the relative difference between the sets, in percent. Also shown are the 90% CL contours computed from the uncertainty variations included in the MSTW 2008 LO set (black). Using only the MSTW uncertainty band, one would arrive at an estimated  $\sim 5\%$  uncertainty over most of the  $x$  range, while including the CTEQ6L1 set would increase that to  $\sim 10\%$ . At NLO, this discrepancy is reduced, but not removed. A significant effort is currently being undertaken within the PDF community to agree on common, and more comprehensive, ways of defining PDF uncertainty bands [54, 58]. This is complicated due to the different ways of defining  $f(x, \mu_0^2)$  and due to the experimental data sets not always being fully compatible with one another. For the time being, it is recommended to try at least sets from two different groups, for a comprehensive uncertainty estimate.

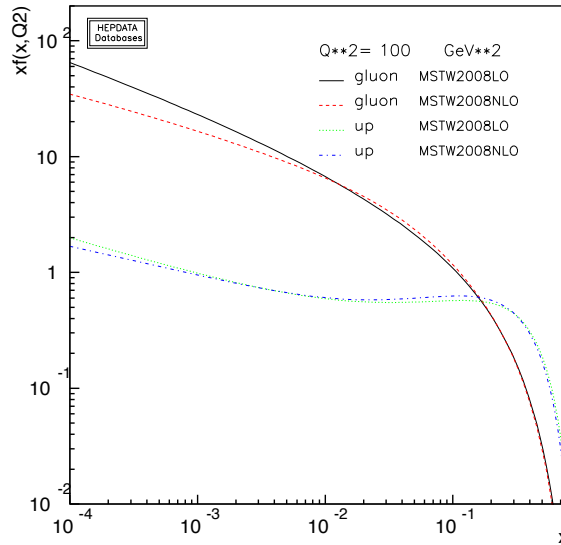
Occasionally, the words *structure functions* and *parton densities* are used interchangeably. However, there is an important distinction between the two, which we find often in (quantum) physics: the

<sup>15</sup>MSTW: Martin–Stirling–Thorne–Watt.

<sup>16</sup>The ‘LO’ means that the fit was performed using LO MEs in the cross section formulae.



**Fig. 10:** Illustration of the difference between the MSTW 2008 and CTEQ6 LO gluon PDFs at  $\mu_F = 10$  GeV. All curves are normalized to the central MSTW 2008 prediction. The black solid lines show the 90% CL MSTW variations, while the dashed red line shows the CTEQ6L1 distribution.



**Fig. 11:** Illustration of the change between PDF fits using LO and NLO MEs: the  $g$  distribution at LO (black) and NLO (red, dashed), and the  $u$  distribution at LO (green, dotted) and NLO (blue, dot-dashed), for the MSTW 2008 PDF sets [56], at  $Q = \mu_F = 10$  GeV. Plots made using the HEPDATA online tool [55].

former is a physical observable used to parameterize the DIS cross sections (see, e.g., Ref. [3]), while the latter is a ‘fundamental’ quantity extracted from it. In particular, since the parton densities are not, themselves, physically observable, they can only be defined within a specific factorization scheme, order by order in perturbation theory. The only exception is at leading order, at which they have the simple physical interpretation of parton-number densities. When going to higher orders, we tend to keep the simple intuitive picture from LO in mind, but one should be aware that the fundamental relationship between PDFs and measured quantities is now more complicated (due to the interplay between the PDFs and the real and virtual corrections to the LO cross section), and that the parton densities no longer have a clear probabilistic interpretation starting from NLO.

The reader should also be aware that there is some ambiguity whether NLO PDFs should be used for LO calculations. In principle, the higher-order PDFs are better constrained and the difference

between, for example, an NLO and an LO set should formally be beyond LO precision, so that one might be tempted to simply use the highest-order available PDFs for any calculation. However, higher-order terms can sometimes be absorbed, at least partially, into effective lower-order coefficients. In the context of PDFs, the fit parameters of lower-order PDFs will attempt to compensate for missing higher-order contributions in the matrix elements. To the extent those higher-order contributions are *universal*, this is both desirable and self-consistent. This leads to some typical qualitative differences between LO and NLO PDFs, illustrated in Fig. 11: NLO PDFs tend to be smaller at low  $x$  and slightly larger at high  $x$ , than LO ones. Thus, it is quite possible that using an NLO PDF in conjunction with LO MEs can give a worse agreement with data than LO PDFs do.

Finally, another oft-raised question concerns which PDF sets to use for the parton-shower evolution in Monte Carlo generators. Importantly, the equations driving the initial-state showers in Monte Carlo models are only sensitive to *ratios* of PDFs [59]. Since the shower evolution typically only has leading-logarithmic (LL) precision, it should be theoretically consistent to use any (LO or better) PDF set to drive the evolution. However, similarly to above, there will be subleading differences between different choices, and one is justified in worrying about the level of physical effects that could be generated. Unfortunately, there is currently no way to ensure 100% self-consistency. Since PDF fits are not done with MC codes, but instead use analytical resummation models (see, e.g., the TASI lectures by Sterman [43]), which are not identical to their MC counterparts, the PDF fits are essentially ‘tuned’ to a slightly different resummation than that incorporated in a given MC model. In practice, not much is known about the size and impact of this ambiguity [60]. Known differences include: the size of phase space (purely collinear massless PDF evolution versus the finite-transverse-momentum massive MC phase space), the treatment of momentum conservation and recoil effects, additional higher-order effects explicitly or implicitly included in the MC evolution, choice of renormalization scheme and scale, and, for those MC algorithms that do not rely on collinear (DGLAP, see Ref. [3]) splitting kernels (e.g., the various kinds of dipole evolution algorithms, see Ref. [61]), differences in the effective factorization scheme.

As a baseline, we recommend simply using whatever PDF set the given MC model was originally tuned with, since this should de facto (by fitting the available data) reabsorb as much of the inconsistency as possible. Furthermore, it should be emphasized that underlying-event and minimum-bias models based on multi-parton interactions (see Section 5.2) usually make the explicit assumption that the PDFs can be interpreted as physical number densities even down to very low  $Q$  and  $x$ , a property which is generally only true for LO PDFs. It must therefore be strongly discouraged to use (N)NLO PDF sets in this context.

### 2.3 Fixed-order QCD

Consider the production of an arbitrary final state,  $F$  (e.g., a Higgs boson, a  $t\bar{t}$  pair, etc). Schematically, we may express the (perturbative) all-orders differential cross section for an observable  $\mathcal{O}$ , in the following way:

$$\left. \frac{d\sigma_F}{d\mathcal{O}} \right|_{\text{ME}} = \underbrace{\sum_{k=0}^{\infty} \int d\Phi_{F+k}}_{\Sigma \text{ legs}} \left| \underbrace{\sum_{\ell=0}^{\infty} \mathcal{M}_{F+k}^{(\ell)}}_{\Sigma \text{ loops}} \right|^2 \delta(\mathcal{O} - \mathcal{O}(\Phi_{F+k})), \quad (45)$$

where, for compactness, we have suppressed all PDF and luminosity normalization factors.  $\mathcal{M}_{F+k}^{(\ell)}$  is the amplitude for producing  $F$  in association with  $k$  additional final-state partons, ‘legs’ and with  $\ell$  additional loops. The sums start at  $k = 0$  and  $\ell = 0$ , corresponding to the leading order for producing  $F$ , while higher terms represent real and virtual corrections, respectively.

The purpose of the  $\delta$  function is to project out hypersurfaces of constant value of  $\mathcal{O}$  in the full  $d\Phi_{F+k}$  phase space, with  $\mathcal{O}(\Phi_{F+k})$  a function that defines  $\mathcal{O}$  evaluated on each specific momentum

configuration,  $\Phi_{F+k}$ . (Without the  $\delta$  function, the formula would give the total integrated cross section, instead of the cross section differentially in  $\mathcal{O}$ .)

We recover the various fixed-order truncations of perturbative QCD (pQCD) by limiting the nested sums in Eq. (45) to include only specific values of  $k + \ell$ . Thus,

$$\begin{aligned} k = 0, \ell = 0 &\implies \text{leading order (usually tree-level) for } F \text{ production} \\ k = n, \ell = 0 &\implies \text{leading order for } F + n \text{ jets} \\ k + \ell \leq n, &\implies \text{N}^n\text{LO for } F \text{ (includes N}^{n-1}\text{LO for } F + 1 \text{ jet, N}^{n-2}\text{LO for } F + \\ &\text{2 jets, and so on up to LO for } F + n \text{ jets).} \end{aligned}$$

For  $k \geq 1$ , we are not considering inclusive  $F$  production; instead, we are considering the process  $F + k$  jets. If we simply integrate over all momenta, as implied by the integration over  $d\Phi_{F+k}$  in Eq. (45), we would be including configurations in which one or more of the  $k$  partons are collinear or soft. Such configurations are IR divergent in QCD and hence must be regulated. Since we talk about *collinear* and *soft* divergences (the origins of which will be discussed in more detail in Sections 2.4 and 3.2), cuts on *angles* and *energies* and/or cuts on combinations, like *transverse momenta*, can be used to cut away the problematic regions of phase space.

Recall, however, that pQCD is approximately scale invariant. This implies that a regularization cut on a dimensionful quantity, like energy or transverse momentum, should be formulated as a *ratio* of scales, rather than as an absolute number. For example, a jet with  $p_\perp = 50$  GeV would be considered hard and well-separated if produced in association with an ordinary  $Z$  boson (with hard scale  $M_Z = 91.2$  GeV), while the same jet would be considered soft if produced in association with a 900 GeV  $Z'$  boson (see Refs. [18, 19] for more explicit examples).

The essence of the point is that, if the regularization scale is taken too low, logarithmic enhancements of the type

$$\alpha_s^n \ln^{m \leq 2n} \left( \frac{Q_F^2}{Q_k^2} \right) \quad (46)$$

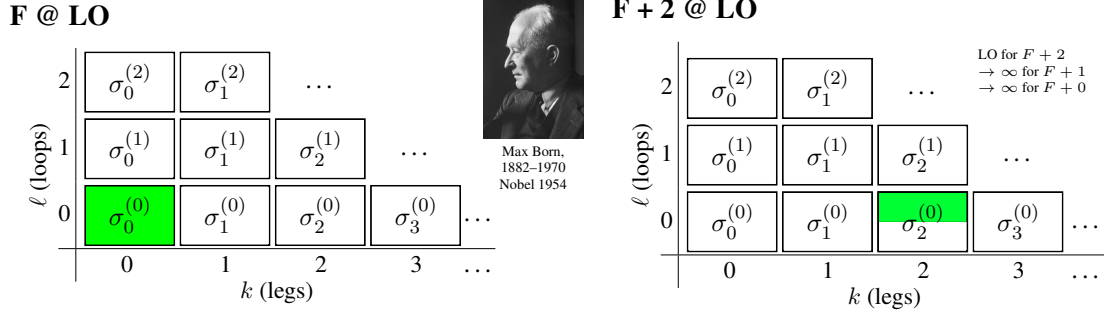
will generate progressively larger corrections, order by order, which will spoil any fixed-order truncation of the perturbative series. Here,  $Q_F$  is the hard scale associated with the process under consideration, while  $Q_k$  is the scale associated with an additional parton,  $k$ .

A good rule of thumb is that if  $\sigma_{k+1} \approx \sigma_k$  (at whatever order you are calculating), then the perturbative series is converging too slowly for a fixed-order truncation of it to be reliable. For fixed-order perturbation theory to be applicable, you must place your cuts on the hard process such that  $\sigma_{k+1} \ll \sigma_k$ . In the discussion of parton showers in Section 3.2, we shall see how the region of applicability of perturbation theory can be extended.

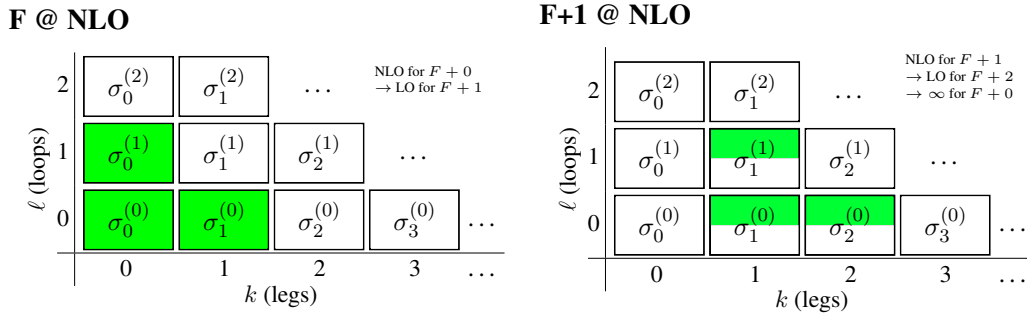
The virtual amplitudes, for  $\ell \geq 1$ , are divergent for any point in phase space. However, as encapsulated by the famous KLN theorem [62, 63], unitarity (which essentially expresses probability conservation) puts a powerful constraint on the infrared (IR) divergences<sup>17</sup>, forcing them to cancel exactly against those coming from the unresolved real emissions that we had to cut out above, order by order, making the complete answer for fixed  $k + \ell = n$  finite<sup>18</sup>. Nonetheless, since this cancellation happens between contributions that formally live in different phase spaces, a main aspect of loop-level higher-order calculations is how to arrange for this cancellation in practice, either analytically or numerically, with many different methods currently on the market. We shall discuss the idea behind subtraction approaches in Section 2.4.

<sup>17</sup>The loop integrals also exhibit ultra-violet (UV) divergences, but these are dealt with by renormalization.

<sup>18</sup>Formally, the KLN theorem states that the sum over degenerate quantum states is finite. In the context of fixed-order perturbation theory, this is exemplified by states with infinitely collinear and/or soft radiation being degenerate with the corresponding states with loop corrections; they cannot be told apart by any physical observable.



**Fig. 12:** Coefficients of the perturbative series covered by LO calculations. *Left:*  $F$  production at LO. *Right:*  $F + 2$  jets at LO, with the half-shaded box illustrating the restriction to the region of phase space with exactly 2 resolved jets. The total power of  $\alpha_s$  for each coefficient is  $n = k + \ell$ . (Photo of Max Born from nobelprize.org.)



**Fig. 13:** Coefficients of the perturbative series covered by NLO calculations. *Left:*  $F$  production at NLO. *Right:*  $F + 1$  jet at NLO, with half-shaded boxes illustrating the restriction to the region of phase space with exactly one resolved jet. The total power of  $\alpha_s$  for each coefficient is  $n = k + \ell$ .

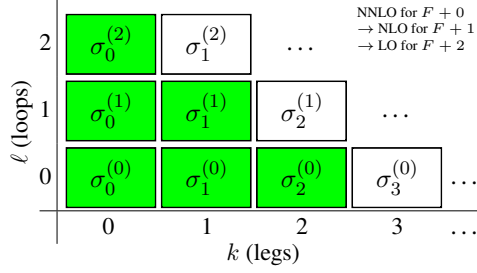
A convenient way of illustrating the terms of the perturbative series that a given ME-based calculation includes is given in Fig. 12. In the left-hand pane, the shaded box corresponds to the lowest-order ‘Born-level’ ME squared. This coefficient is non-singular and hence can be integrated over all of phase space, which we illustrate by letting the shaded area fill all of the relevant box. A different kind of leading-order calculation is illustrated in the right-hand pane of Fig. 12, where the shaded box corresponds to the LO ME squared for  $F + 2$  jets. This coefficient diverges in the part of phase space where one or both of the jets are unresolved (i.e., soft or collinear), and hence integrations can only cover the hard part of phase space, which we reflect by only shading the upper half of the relevant box.

Figure 13 illustrates the inclusion of NLO virtual corrections. To prevent confusion, first a point on notation: by  $\sigma_0^{(1)}$ , we intend

$$\sigma_0^{(1)} = \int d\Phi_0 \, 2\text{Re}[\mathcal{M}_0^{(1)} \mathcal{M}_0^{(0)*}], \quad (47)$$

which is of order  $\alpha_s$  relative to the Born level. Compare, for example, with the expansion of Eq. (45) to order  $k + \ell = 1$ . In particular,  $\sigma_0^{(1)}$  should *not* be confused with the integral over the one-loop ME squared (which would be of relative order  $\alpha_s^2$  and hence forms part of the NNLO coefficient  $\sigma_0^{(2)}$ ). Returning to Fig. 13, the unitary cancellations between real and virtual singularities imply that we can now extend the integration of the real correction in the left-hand pane over all of phase space, while retaining a finite

## F @ NNLO



**Fig. 14:** Coefficients of the perturbative series covered by an NNLO calculation. The total power of  $\alpha_s$  for each coefficient is  $n = k + \ell$ . Green shading represents the full perturbative coefficient at the respective  $k$  and  $\ell$ .

total cross section,

$$\begin{aligned}\sigma_0^{\text{NLO}} &= \int d\Phi_0 |\mathcal{M}_0^{(0)}|^2 + \int d\Phi_1 |\mathcal{M}_1^{(0)}|^2 + \int d\Phi_0 2\text{Re}[\mathcal{M}_0^{(1)} \mathcal{M}_0^{(0)*}] \\ &= \sigma_0^{(0)} + \sigma_1^{(0)} + \sigma_0^{(1)},\end{aligned}\quad (48)$$

with  $\sigma_0^{(0)}$  the finite Born-level cross section, and the positive divergence caused by integrating the second term over all of phase space is cancelled by a negative divergence coming from the integration over loop momenta in the third term. One method for arranging the cancellation of singularities—subtraction—is discussed in Section 2.4.

However, if our starting point for the NLO calculation is a process which already has a non-zero number of hard jets, we must continue to impose that at least that number of jets must still be resolved in the final-state integrations,

$$\begin{aligned}\sigma_1^{\text{NLO}}(p_{\perp\text{min}}) &= \int_{p_{\perp} > p_{\perp\text{min}}} d\Phi_1 |\mathcal{M}_1^{(0)}|^2 + \int_{p_{\perp 1} > p_{\perp\text{min}}} d\Phi_2 |\mathcal{M}_2^{(0)}|^2 + \int_{p_{\perp} > p_{\perp\text{min}}} d\Phi_1 2\text{Re}[\mathcal{M}_1^{(1)} \mathcal{M}_1^{(0)*}] \\ &= \sigma_1^{(0)}(p_{\perp} > p_{\perp\text{min}}) + \sigma_2^{(0)}(p_{\perp 1} > p_{\perp\text{min}}) + \sigma_1^{(1)}(p_{\perp} > p_{\perp\text{min}}),\end{aligned}\quad (49)$$

where the restriction to at least one jet having  $p_{\perp} > p_{\perp\text{min}}$  has been illustrated in the right-hand pane of Fig. 13 by shading only the upper part of the relevant boxes. In the second term in Eq. (49), the notation  $p_{\perp 1}$  is used to denote that the integral runs over the phase space in which at least one ‘jet’ (which may consist of one or two partons) must be resolved with respect to  $p_{\perp\text{min}}$ . Here, therefore, an explicit dependence on the algorithm used to define ‘a jet’ enters for the first time. This is discussed in more detail in the 2009 ESHEP lectures by Salam [4].

To extend the integration to cover also the case of two unresolved jets, we must combine the left- and right-hand parts of Fig. 13 and add the new coefficient

$$\sigma_0^{(2)} = |\mathcal{M}_0^{(1)}|^2 + 2\text{Re}[\mathcal{M}_0^{(2)} \mathcal{M}_0^{(0)*}],\quad (50)$$

as illustrated by the diagram in Fig. 14.

## 2.4 The subtraction idea

According to the KLN theorem, the IR singularities coming from integrating over collinear and soft real-emission configurations should cancel, order by order, by those coming from the IR divergent-loop integrals. This implies that we should be able to rewrite, for example, the NLO cross section, Eq. (48), as

$$\sigma^{\text{NLO}} = \sigma^{\text{Born}} + \text{Finite} \left\{ \int d\Phi_{F+1} |\mathcal{M}_{F+1}^{(0)}|^2 \right\} + \text{Finite} \left\{ \int d\Phi_F 2\text{Re}[\mathcal{M}_F^{(1)} \mathcal{M}_F^{(0)*}] \right\},\quad (51)$$

with the second and third terms having had their common (but opposite-sign) singularities cancelled out and some explicitly finite quantities remaining.

The first step towards this goal is to classify all IR singularities that could appear in the amplitudes. We know that the IR limits are universal, so they can be classified using a set of process-independent functions that only has to be worked out once and for all. A widely used such set of functions are the *Catani–Seymour* (CS) dipole functions [64, 65], a method which by now has even been partially automated [66, 67]. Here, we shall instead use a formalism based on *antennae* [68–70]. The distinction between the two is basically that one antenna is made up of two dipole ‘ends’, and hence the antenna formalism tends to generate somewhat fewer terms. At NLO, however, there is no fundamental incompatibility—the antennae we use here can always be partitioned into two dipole ends, if so desired. (Note: only the antenna method has been successfully generalized to NNLO [71, 72]. Other NNLO techniques, not covered here, are *sector decomposition*, see Refs. [73, 74], and the generic formalism for hadroproduction of colourless states presented in Ref. [75].)

At NLO, the idea with subtraction is thus to rewrite the NLO cross section by adding and subtracting a simple function,  $d\sigma_S$ , that encapsulates all the IR limits,

$$\begin{aligned} \sigma^{\text{NLO}} &= \sigma^{\text{Born}} + \underbrace{\int d\Phi_{F+1} \left( |\mathcal{M}_{F+1}^{(0)}|^2 - d\sigma_S^{\text{NLO}} \right)}_{\text{finite by universality}} \\ &\quad + \underbrace{\int d\Phi_F 2\text{Re}[\mathcal{M}_F^{(1)} \mathcal{M}_F^{(0)*}] + \int d\Phi_{F+1} d\sigma_S^{\text{NLO}}}_{\text{finite by KLN}}. \end{aligned} \quad (52)$$

The task now is to construct a suitable form for  $d\sigma_S$ . A main requirement is that it should be sufficiently simple that the integral in the last term can be done analytically, in dimensional regularization, so that the IR poles it generates can be cancelled against those from the loop term.

To build a set of universal terms that parameterize the IR singularities of any amplitude, we start from the observation that gauge theory amplitudes factorize in the *soft limit*, as follows:

$$|\mathcal{M}_{F+1}(\dots, i, j, k, \dots)|^2 \xrightarrow{j_g \rightarrow 0} g_s^2 N_C \left( \frac{2s_{ik}}{s_{ij}s_{jk}} - \frac{2m_i^2}{s_{ij}^2} - \frac{2m_k^2}{s_{jk}^2} \right) |\mathcal{M}_F(\dots, i, k, \dots)|^2, \quad (53)$$

where parton  $j$  is a soft gluon, partons  $i$ ,  $j$ , and  $k$  form a chain of colour-space index contractions (we say they are *colour-connected*),  $g_s$  is the strong coupling, and the terms in parentheses are called the *soft-eikonal factor*. We here show it including mass corrections, which appear if  $i$  and  $k$  have non-zero rest masses, with the invariants  $s_{ab}$  then defined as

$$s_{ab} \equiv 2p_a \cdot p_b = (p_a + p_b)^2 - m_a^2 - m_b^2. \quad (54)$$

The colour factor,  $N_C$ , is valid for the leading-colour contribution, regardless of whether the  $i$  and  $k$  partons are quarks or gluons. At subleading colour, an additional soft-eikonal factor identical to the one above but with a colour factor proportional to  $-1/N_C$  arises for each  $q\bar{q}$  pair combination. This, for example, modifies the effective colour factor for  $q\bar{q} \rightarrow qg\bar{q}$  from  $N_C$  to  $N_C(1 - 1/N_C) = 2C_F$ , in agreement with the colour factor for quarks being  $C_F$  rather than  $C_A$ .

Similarly, amplitudes also factorize in the *collinear limit* (partons  $i$  and  $j$  are parallel, so  $s_{ij} \rightarrow 0$ ), in which the eikonal factor above is replaced by the famous DGLAP splitting kernels [47–49], which were already mentioned in Section 2.2, in the context of PDF evolution. They are also the basis of conventional parton-shower models, to which we return in Section 3.2.

Essentially, what antenna functions, CS dipoles, and the like, all do, is to combine the soft (eikonal) and collinear (Altarelli–Parisi) limits into one universal set of functions that achieve the correct limiting

behaviour for *both* soft and collinear radiation. To give an explicit example, the *antenna function* for gluon emission from a colour-connected  $q\bar{q}$  pair can be derived from the MEs squared for the process  $Z^0 \rightarrow q\bar{q} \rightarrow qg\bar{q}$  [76],

$$\frac{|\mathcal{M}(Z^0 \rightarrow q_i g_j \bar{q}_k)|^2}{|\mathcal{M}(Z^0 \rightarrow q_I \bar{q}_K)|^2} = g_s^2 2C_F \left[ \underbrace{\frac{2s_{ik}}{s_{ij}s_{jk}}}_{\text{eikonal}} + \frac{1}{s_{IK}} \underbrace{\left( \frac{s_{jk}}{s_{ij}} + \frac{s_{ij}}{s_{jk}} \right)}_{\text{collinear}} \right], \quad (55)$$

where we have neglected mass corrections (see Refs. [77, 78] for massive expressions) and we recognize the universal eikonal soft factor from Eq. (53) in the first term. The two additional terms are less singular, and are required to obtain the correct collinear (Altarelli–Parisi) limits as  $s_{ij} \rightarrow 0$  or  $s_{jk} \rightarrow 0$ .

However, since the singularity structure is universal, we could equally well have used the process  $H^0 \rightarrow q\bar{q} \rightarrow qg\bar{q}$  to derive the antenna function. Our antenna function would then have come out as [78],

$$\frac{|\mathcal{M}(H^0 \rightarrow q_i g_j \bar{q}_k)|^2}{|\mathcal{M}(H^0 \rightarrow q_I \bar{q}_K)|^2} = g_s^2 2C_F \left[ \underbrace{\frac{2s_{ik}}{s_{ij}s_{jk}}}_{\text{eikonal}} + \frac{1}{s_{IK}} \underbrace{\left( \frac{s_{jk}}{s_{ij}} + \frac{s_{ij}}{s_{jk}} \right)}_{\text{collinear}} + \underbrace{\frac{2}{s_{IK}}}_{\text{finite}} \right], \quad (56)$$

where the additional term,  $2/s_{IK}$ , is non-singular (‘finite’) over all of phase space. Thus, we here see an explicit example that the singularities are process independent while the non-singular terms are process dependent. Since we add and subtract the same term in Eq. (52), the final answer does not depend on the choice of finite terms. We say that they correspond to different *subtraction schemes*. One standard antenna subtraction scheme, which uses the antenna function defined in Eq. (55) rather than the one in Eq. (56), is the Gehrmann–Gehrmann–de Ridder–Glover (GGG) one, given in Ref. [70].

If there is more than one colour antenna in the Born-level process, the form of  $d\sigma_S$  is obtained as a sum over terms, each of which captures one specific soft limit and either all or ‘half’ of a collinear one, depending on the specific scheme and the type of parton,

$$d\sigma_S = \sum_j A_{IK \rightarrow ijk} |\mathcal{M}_F(\dots, I, K, \dots)|^2, \quad (57)$$

with the sum running over all singular  $3 \rightarrow 2$  ‘clusterings’ of the  $(F + 1)$ -parton state to  $F$  partons. An analysis of the different ways of partitioning the collinear singularity of gluons among neighbouring antenna is beyond the scope of this introduction, but useful discussions can be found in Ref. [79–81].

## 2.5 Infrared safety

A further requirement for being able to perform calculations within pQCD is that the observable be *IR safe*. Note that by ‘IR’, we here mean any limit that involves a low scale (i.e., any non-UV limit), without regard to whether it is collinear or soft.

The property of IR safety defines a special class of observables which have *minimal sensitivity* to long-distance physics, and which can be consistently computed in pQCD. An observable is IR safe if:

1. (*safety against soft radiation*): adding any number of infinitely soft particles should not change the value of the observable;
2. (*safety against collinear radiation*): splitting an existing particle up into two co-moving particles, with arbitrary fractions  $z$  and  $1 - z$ , respectively, of the original momentum, should not change the value of the observable.



If both of these conditions are satisfied, any long-distance non-perturbative corrections will be suppressed by the ratio of the long-distance scale to the short-distance one to some (observable-dependent) power, typically

$$\text{IR-safe observables: IR corrections} \propto \frac{Q_{\text{IR}}^2}{Q_{\text{UV}}^2} \quad (58)$$

where  $Q_{\text{UV}}$  denotes a generic hard scale in the problem, and  $Q_{\text{IR}} \sim \Lambda_{\text{QCD}} \sim \mathcal{O}(1 \text{ GeV})$ .

Due to this *power suppression*, IR-safe observables are not so sensitive to our lack of ability to solve the strongly coupled IR physics, unless of course we go to processes for which the relevant hard scale,  $Q_{\text{UV}}$ , is small (such as minimum-bias, soft jets, or small-scale jet substructure). Even when a high scale is present, however, as in resonance decays, jet fragmentation or underlying-event-type studies, IR safety only guarantees us that IR corrections are small, not that they are zero. Thus, ultimately, we run into a precision barrier even for IR-safe observables, which only a reliable understanding of the long-distance physics itself can address.

To constrain models of long-distance physics, one needs IR *sensitive* observables. Hence it is not always the case that IR-safe observables are preferable—the purpose decides the tool. Instead of the suppressed corrections above, the perturbative prediction for such observables contains logarithms of the type already encountered in Eq. (46),

$$\text{IR sensitive observables: IR corrections} \propto \alpha_s^n \log^{m \leq 2n} \left( \frac{Q_{\text{UV}}^2}{Q_{\text{IR}}^2} \right), \quad (59)$$

which grow increasingly large as  $Q_{\text{IR}}/Q_{\text{UV}} \rightarrow 0$ . As an example, consider such a fundamental quantity as particle multiplicities (= number of particles); in the absence of non-trivial IR effects, the number of partons tends logarithmically to infinity as the IR cutoff is lowered. Similarly, the distinction between a charged and a neutral pion only occurs in the very last phase of hadronization, and hence observables that only include charged tracks, for instance, are always IR sensitive<sup>19</sup>.

Two important categories of IR-safe observables that are widely used are *event shapes* and *jet algorithms*. Jet algorithms are perhaps nowhere as pedagogically described as in the 2009 ESHEP lectures by Salam [4, Chapter 5]. Event shapes in the context of hadron colliders have not yet been as widely explored, but the basic phenomenology is introduced also by Salam and collaborators in Ref. [82], with first measurements reported by CMS and ATLAS [83, 84] and a proposal to use them also for the characterization of soft-QCD (‘minimum-bias’) events put forth in Ref. [85].

Let us here merely emphasize that the real reason to prefer IR-safe jet algorithms over unsafe ones is not that they necessarily give very different or ‘better’ answers in the experiment—experiments are IR-safe by definition, and the difference between IR-safe and unsafe algorithms may not even be visible when running the algorithm on experimental data—but that it is only possible to compute pQCD predictions for the IR-safe ones. Any measurement performed with an IR-unsafe algorithm can only be compared to calculations that include a detailed hadronization model. This both limits the number of calculations that can be compared to and also adds an a priori unknown sensitivity to the details of the hadronization description, details which one would rather investigate and constrain separately, in the framework of more dedicated fragmentation studies.

For LHC phenomenology, the preferred IR-safe algorithm for jet reconstruction is currently the *anti- $k_T$*  one [86], with size parameter  $R$  varying between 0.4 and 0.7, although larger sizes can be motivated in certain contexts, for example, to look for highly energetic jets and/or the boosted decay products of high-mass objects [23, 87]. This algorithm generates circular-looking jets, so subtracting the energy believed to be associated with the *underlying event* (UE, see Section 5.2) is particularly simple.

<sup>19</sup>This remains true in principle even if the tracks are clustered into jets, although the energy clustered in this way does provide a lower bound on  $Q_{\text{UV}}$  in the given event, since ‘charged + neutral > charged-only’.

For jet substructure, typically either the ‘kT’ or ‘Cambridge/Aachen’ algorithms are used, see, for example, Ref. [23, 87]. The clustering measures used in these algorithms more closely mimic the singularity structure of QCD bremsstrahlung and they are therefore particularly well suited to ‘unravel’ a tree of QCD branchings [4], such as those a parton shower generates. The Cambridge/Aachen algorithm may also be used to characterize the underlying event, see Ref. [88].

### 3 Monte Carlo event generators

In this section, we discuss the physics of Monte Carlo event generators and their mathematical foundations, at an introductory level. We shall attempt to convey the main ideas as clearly as possible without burying them in an avalanche of technical details. References to more detailed discussions are included where applicable. We assume the reader is already familiar with the contents of the preceding section on hard processes.

The task of a Monte Carlo event generator is to calculate everything that happens in a high-energy collision, from the hard short-distance physics to the long wavelengths of hadronization and hadron decays. Obviously, this requires some compromises to be made. General-purpose generators like HERWIG [39, 89], PYTHIA [90, 91], and SHERPA [92], start from low-order (LO or NLO) descriptions of the perturbative hard physics and then attempt to include the ‘most significant’ corrections, such as higher-order ME corrections and parton showers, resonance decays and finite-width effects, underlying event, beam remnants, hadronization and hadron decays. Each of them had slightly different origins, which carries through to the emphasis placed on various physics aspects today.

- PYTHIA. Successor to JETSET (begun in 1978). Originated in hadronization studies. Main feature: the Lund string fragmentation model.
- HERWIG. Successor to EARWIG (begun in 1984). Originated in perturbative coherence studies. Main feature: angular-ordered parton showers.
- SHERPA. Begun in 2000. Originated in studies of the matching of hard-emission MEs with parton showers. Main feature: CKKW matching.

There is also a large number of more specialized generators, mainly for hard processes within and beyond the Standard Model (SM), a few that offer alternative shower models, and ones specializing in soft-inclusive and/or heavy-ion physics.

An important aspect of contemporary generators is the ability to combine specialized ones with general-purpose ones, via interfaces. The most common interface between partonic hard-process and parton-shower generators is the Les Houches event file standard, defined in Ref. [93, 94] and ‘spoken’ by most modern generator tools. For interfaces to experimental analysis packages (like RIVET [95]) and detector simulations (like GEANT [96]), typically the HepMC standard is used [97].

Hard processes were the topic of Section 2. In this section, we shall focus mainly on parton showers, with some brief comments on resonance decays at the end. Section 4 then concerns the matching of MEs and parton showers. Finally, models of hadronization and the UE are the topic of Section 5.

Several of the discussions below rely on material from the section on Monte Carlo event generators in the PDG review of particle physics [24] and on the more comprehensive review by the *MCnet* collaboration in Ref. [5]. The latter also contains brief descriptions of the physics implementations of each of the main general-purpose event generators on the market, together with a guide on how to use (and not use) them in various connections, and a collection of comparisons to important experimental distributions. We highly recommend readers to obtain a copy of that review, as it is the most comprehensive and up-to-date review of event generators currently available. Another useful and pedagogical review on event generators is contained in the 2006 ESHEP lectures by Torbjörn Sjöstrand [41], with a more recent update in Ref. [98].

**Table 2:** Relative uncertainty after  $n$  evaluations, in one and  $d$  dimensions, for two traditional numerical integration methods and stochastic Monte Carlo. The last column shows the number of function evaluations that are required per point, in  $d$  dimensions.

Relative uncertainty with $n$ points	1-Dim	$d$ -Dim	$n_{\text{eval}}/\text{point}$
Trapezoidal rule	$1/n^2$	$1/n^{2/d}$	$2^d$
Simpson's rule	$1/n^4$	$1/n^{4/d}$	$3^d$
Monte Carlo	$1/\sqrt{n}$	$1/\sqrt{n}$	1

### 3.1 The Monte Carlo method

A ubiquitous problem in fundamental physics is the following: given a source located some distance from a detector, predict the number of counts that should be observed within the solid angle spanned by the detector (or within a bin of its phase-space acceptance), as a function of the properties of the source, the intervening medium and the efficiency of the detector. Essentially, the task is to compute integrals of the form

$$N_{\text{Count}}(\Delta\Omega) = \int_{\Delta\Omega} d\Omega \frac{d\sigma}{d\Omega}, \quad (60)$$

with  $d\sigma$  a differential cross section for the process of interest.

In particle physics, phase space has three dimensions per final-state particle (minus four for overall four-momentum-conservation). Thus, for problems with more than a few outgoing particles, the dimensionality of phase space increases rapidly. At LEP, for instance, the total multiplicity of neutral + charged hadrons (before weak decays) was typically  $\sim 30$  particles, for about 86 dimensions.

The standard one-dimensional numerical-integration methods give very slow convergence rates for higher-dimensional problems. For illustration, a table of convergence rates in one and  $d$  dimensions is given in Table 2, comparing the trapezoidal (2-point) rule and Simpson's (3-point) rule to random-number-based Monte Carlo. In one dimension, the  $1/n^2$  convergence rate of the trapezoidal rule is much faster than the stochastic  $1/\sqrt{n}$  of random-number Monte Carlo, and Simpson's rule converges even faster. However, as we go to  $d$  dimensions, the convergence rate of the  $n$ -point rules all degrade with  $d$  (while the number of function evaluations required for each 'point' simultaneously increases). The MC convergence rate, on the other hand, remains the simple stochastic  $1/\sqrt{n}$ , independent of  $d$ , and each point still only requires one function evaluation. These are some of the main reasons that MC is the preferred numerical integration technique for high-dimensional problems. In addition, the random phase-space vectors it generates can be re-used in many ways, for instance as an input to iterative solutions, to compute many different observables simultaneously and/or to hand 'events' to propagation and detector-simulation codes.

Therefore, virtually all numerical cross-section calculations are based on Monte Carlo techniques in one form or another, the simplest being the RAMBO algorithm [99] which can be expressed in about half a page of code and generates a flat scan over  $n$ -body phase space<sup>20</sup>.

However, due to the IR singularities in pQCD, and due to the presence of short-lived resonances, the functions to be integrated,  $|\mathcal{M}_{F+k}|^2$ , can be highly non-uniform, especially for large  $k$ . This implies that we will have to be clever in the way we sample phase space if we want the integration to converge in any reasonable amount of time—simple algorithms like RAMBO quickly become inefficient for  $k$  greater than a few. To address this bottleneck, the simplest step up from RAMBO is to introduce generic (i.e., automated) importance-sampling methods, such as those offered by the VEGAS algorithm [100, 101]. This is still the dominant basic technique, although most modern codes do employ several additional refinements, such as several different copies of VEGAS running in parallel (multi-channel integration),

<sup>20</sup>Strictly speaking, RAMBO is only truly uniform for massless particles. Its massive variant makes up for phase-space biases by returning weighted momentum configurations.



*“This risk, that convergence is only given with a certain probability, is inherent in Monte Carlo calculations and is the reason why this technique was named after the world’s most famous gambling casino. Indeed, the name is doubly appropriate because the style of gambling in the Monte Carlo casino, not to be confused with the noisy and tasteless gambling houses of Las Vegas and Reno, is serious and sophisticated.”*

*F. James, “Monte Carlo theory and practice”,  
Rept. Prog. Phys. 43 (1980) 1145*

**Fig. 15:** *Left:* The casino in Monaco. *Right:* extract from Ref. [7] concerning the nature of Monte Carlo techniques.

to further optimize the sampling. Alternatively, a few algorithms incorporate the singularity structure of QCD explicitly in their phase-space sampling, either by directly generating momenta distributed according to the leading-order QCD singularities, in a sort of ‘QCD-preweighted’ analogue of RAMBO, called SARGE [102], or by using all-orders Markovian parton showers to generate them (VINCIA [80, 81]).

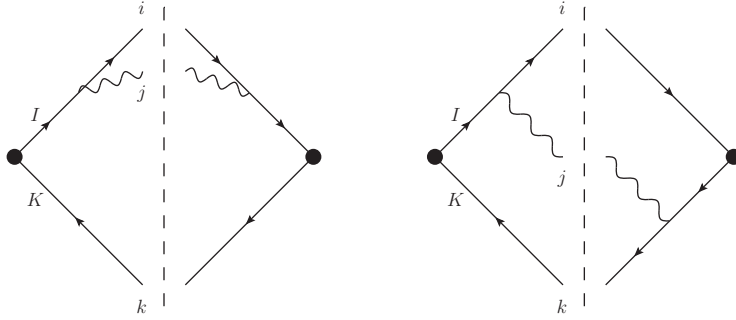
The price of using random numbers is that we must generalize our notion of convergence. In calculus, we say that a sequence  $\{A\}$  converges to  $B$  if an  $n$  exists for which the difference  $|A_{i>n} - B| < \epsilon$  for any  $\epsilon > 0$ . In random-number-based techniques, we cannot completely rule out the possibility of very pathological sequences of ‘dice rolls’ leading to large deviations from the true goal, and hence we are restricted to say that  $\{A\}$  converges to  $B$  if an  $n$  exists for which *the probability* for  $|A_{i>n} - B| < \epsilon$ , for any  $\epsilon > 0$ , is greater than  $P$ , for any  $P \in [0, 1]$  [7]. This risk, that convergence is only given with a certain probability, is the reason why Monte Carlo techniques were named after the famous casino in Monaco, illustrated in Fig. 15.

### 3.2 Theoretical basis of parton showers

In Section 2, we noted two conditions that had to be valid for fixed-order truncations of the perturbative series to be valid. Firstly, the strong coupling  $\alpha_s$  must be small for perturbation theory to be valid at all. This restricts us to the region in which all scales  $Q_i \gg \Lambda_{\text{QCD}}$ . We shall maintain this restriction in this section, that, we are still considering *pQCD*. Secondly, however, in order to be allowed to *truncate* the perturbative series, we had to require  $\sigma_{k+1} \ll \sigma_k$ , that is, the corrections at successive orders must become successively smaller, which—due to the enhancements from soft/collinear singular (conformal) dynamics—effectively restricted us to consider only the phase-space region in which all jets are ‘hard and well-separated’, equivalent to requiring all  $Q_i/Q_j \approx 1$ . In this section, we shall see how to lift this restriction, extending the applicability of perturbation theory into regions that include scale hierarchies,  $Q_i \gg Q_j \gg \Lambda_{\text{QCD}}$ , such as those which occur for soft jets, jet substructure, etc.

In fact, the simultaneous restriction to all resolved scales being larger than  $\Lambda_{\text{QCD}}$  and no large hierarchies is extremely severe, if taken at face value. Since we collide and observe hadrons ( $\rightarrow$  low scales) while simultaneously wishing to study short-distance physics processes ( $\rightarrow$  high scales), it would appear trivial to conclude that fixed-order pQCD is not applicable to collider physics at all. So why do we still use it?

The answer lies in the fact that we actually never truly perform a fixed-order calculation in QCD. Let us repeat the factorized formula for the cross section, Eq. (44), now inserting also a function,  $D$ , to



**Fig. 16:** Diagrams (squared) giving rise to collinear (*left*) and soft (*right*) singularities

represent the fragmentation of the final-state partons into observable hadrons,

$$\frac{d\sigma}{d\mathcal{O}} = \sum_{i,j} \int_0^1 dx_i dx_j \sum_f \int d\Phi_f f_{i/h_1}(x_i, \mu_F^2) f_{j/h_2}(x_j, \mu_F^2) \frac{d\hat{\sigma}_{ij \rightarrow f}}{d\hat{\mathcal{O}}} D_f(\hat{\mathcal{O}} \rightarrow \mathcal{O}, \mu_F^2), \quad (61)$$

with  $\hat{\mathcal{O}}$  denoting the observable evaluated on the partonic final state, and  $\mathcal{O}$  the observable evaluated on the hadronic final state, after fragmentation. Although the partonic cross section,  $d\hat{\sigma}_{ij \rightarrow f}$ , does represent a fixed-order calculation, the parton densities,  $f_{i/h_1}$  and  $f_{j/h_2}$ , include so-called resummations of perturbative corrections *to all orders* from the initial scale of the order of the mass of the proton, up to the factorization scale,  $\mu_F$  (see Section 2.2 and/or the TASI lectures by Sterman [43]). Note that the oft-stated mantra that the PDFs are purely non-perturbative functions is therefore misleading. True, they are defined as essentially non-perturbative functions at some very low scale,  $\mu_0 \sim$  a few GeV, but, if  $\mu_F$  is taken large, they necessarily incorporate a significant amount of perturbative physics as well. On the ‘fixed-order side’, all we have left to ensure in  $d\sigma_{ij \rightarrow f}$  is then that there are no large hierarchies remaining between  $\mu_F$  and the QCD scales appearing in  $\Phi_f$ . Likewise, in the final state, the fragmentation functions,  $D_f$ , include infinite-order resummations of perturbative corrections all the way *from*  $\mu_F$  down to some low scale, with similar caveats concerning mantras about their non-perturbative nature as for the PDFs.

### 3.2.1 Step one: Infinite legs

The infinite-order resummations that are included in objects such as the PDFs and fragmentation functions in Eq. (61) (and in their parton-shower equivalents) rely on some very simple and powerful properties of gauge-field theories that were already touched on in Section 2. In particular, we saw in Section 2.4 that we can represent all the IR limits of any NLO amplitude with a set of simple universal functions, based solely on knowing which partons are colour-connected (i.e., have colour-space index contractions) with one another.

The diagrams in Fig. 16 show the basic origin of the universal IR singularities of gauge-theory amplitudes. On the left is shown a diagram (squared) in which an emission with small  $s_{ij}$  interferes with itself. In the collinear limit,  $s_{ij} \rightarrow 0$ , the propagator of the parent parton,  $I$ , goes on shell; the singularity of the associated propagator factor is the origin of the  $1/s_{ij}$  collinear singularities. On the right is shown the interference between a diagram with emission from parton  $I$  and a diagram with emission from parton  $K$ . The resulting term has propagator singularities when both partons  $I$  and  $K$  go on shell, which can happen simultaneously if parton  $j$  is soft. This generates the  $2s_{ik}/(s_{ij}s_{jk})$  soft singularity, also called the soft-eikonal factor or the dipole factor.

We now understand the fundamental origin of the IR singularities, why they are universal, and why amplitudes factorize in the soft and collinear limits—the singularities are simply generated by inter-

**Fig. 17:** Illustration of the branching phase space for  $q\bar{q} \rightarrow qg\bar{q}$ , with the original dipole-antenna oriented horizontally, the two parents sharing the transverse component of recoil, and the azimuthal angle  $\phi$  (representing rotations of the emitted parton around the dipole axis) chosen such that the gluon is radiated upwards. From Ref. [80].

mediate parton propagators going on shell, which is independent of the nature of the hard process, and hence can be factorized from it.

Thus, for each pair of (massless) colour-connected partons  $I$  and  $K$  in  $F$ , the squared amplitude for  $F + 1$  gluon,  $|\mathcal{M}_{F+1}|^2$ , will include a factor

$$|\mathcal{M}_{F+1}|^2 = \underbrace{g_s^2 N_C \left( \frac{2s_{ik}}{s_{ij}s_{jk}} + \text{collinear terms} \right)}_{\text{antenna function}} |\mathcal{M}_F|^2, \quad (62)$$

where  $g_s^2 = 4\pi\alpha_s$  is the strong coupling,  $i$  and  $k$  represent partons  $I$  and  $K$  after the branching (i.e., they include possible recoil effects) and  $s_{ij}$  is the invariant between parton  $i$  and the emitted parton,  $j$ .

The branching phase space of a colour dipole (i.e., a pair of partons connected by a colour-index contraction) is illustrated in Fig. 17. Expressed in the branching invariants,  $s_{ij}$  and  $s_{jk}$ , the phase space has a characteristic triangular shape, imposed by the relation  $s = s_{ij} + s_{jk} + s_{ik}$  (assuming massless partons). Sketchings of the post-branching parton momenta have been inserted in various places in the figure, for illustration. The soft singularity is located at the origin of the plot and the collinear regions lie along the axes.

The collinear terms for a  $q\bar{q} \rightarrow qg\bar{q}$  ‘antenna’ are unambiguous and are given in Section 2.4. Since gluons are in the adjoint representation, they carry both a colour and an anticolour index (one corresponding to the rows and the other to the columns of the Gell–Mann matrices), and there is therefore some ambiguity concerning how to partition collinear radiation among the two antennae they participate in. This is discussed in more detail in Ref. [80]. Differences are subleading, however, and for our purposes here we shall consider gluon antenna ends as radiating just like quark ones. The difference between quark and gluon radiation then arise mainly because gluons participate in two antennae, while quarks only participate in one. This is related to the difference between the colour factors,  $C_A \sim 2C_F$ .

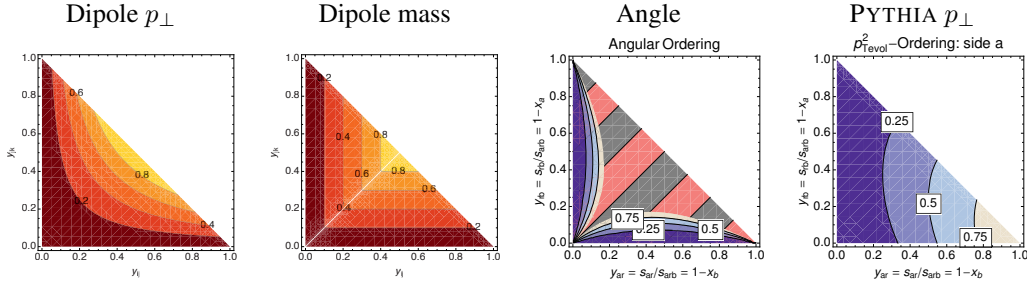
The problem that plagued the fixed-order truncations in Section 2 is clearly visible in Eq. (62): if we integrate over the entire phase space including the region  $s_{ij} \rightarrow 0$ ,  $s_{jk} \rightarrow 0$ , we end up with a double pole. If we instead regulate the divergence by cutting off the integration at some minimal *perturbative cutoff scale*  $\mu_{\text{IR}}^2$ , we end up with a logarithm squared of that scale. This is a typical example of ‘large logarithms’ being generated by the presence of scale hierarchies. Also note that the precise definition of  $\mu_{\text{IR}}$  is not unique. Any scale choice that properly isolates the singularities from the rest of phase space will do, with some typical choices being, for example, invariant-mass and/or transverse-momentum scales.

Before we continue, it is worth noting that Eq. (62) is often rewritten in other forms to emphasize specific aspects of it. One such rewriting is thus to reformulate the invariants  $s_{ij}$  appearing in it in terms of energies and angles,

$$s_{ij} = 2E_i E_j (1 - \cos \theta_{ij}). \quad (63)$$

Rewritten in this way, the differentials can become partial fractions,

$$\frac{ds_{ij}}{s_{ij}} \frac{ds_{jk}}{s_{jk}} \propto \frac{dE_j}{E_j} \frac{d\theta_{ij}}{\theta_{ij}} + \frac{dE_j}{E_j} \frac{d\theta_{jk}}{\theta_{jk}}. \quad (64)$$



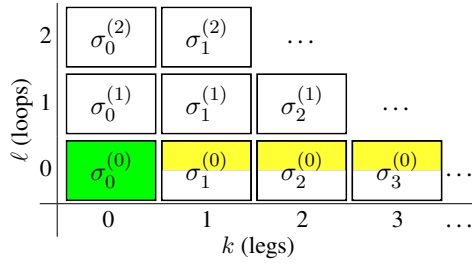
**Fig. 18:** A selection of parton-shower evolution variables, represented as contours over the dipole phase space. Note: the right-most variable corresponds to evolution of only one of the parents, the one with no collinear singularity along the bottom of the plot.

This kind of rewriting enables an intuitively appealing categorization of the singularities as related to vanishing energies and angles, explaining why they are called *soft* and *collinear*, respectively. Arguments based on this rewriting have led to important insights in QCD. For instance, within the framework of conventional parton showers, it was shown in a sequence of publications (see Refs. [103, 104] and references therein) that the destructive interference effects between two or more colour-connected partons (*coherence*) can be described by using the angle of the emissions as the shower-ordering variable. One should still keep in mind, however, that Lorentz-non-invariant formulations come with similar caveats and warnings as do gauge-non-invariant formulations of quantum field theory: while they can be practical to work with at intermediate stages of a calculation, one should be careful with any physical conclusions that rely explicitly on them.

We shall therefore here restrict ourselves to a Lorentz-invariant formalism based directly on Eq. (62), pioneered by the dipole formulation of QCD cascades [76]. The collinear limit is then replaced by a more general *single-pole* limit in which a single parton-parton invariant vanishes (as, for instance, when a pair of partons become collinear), while the soft limit is replaced by one in which two (or more) invariants involving the same parton vanish simultaneously (as, for instance by that parton becoming soft in a frame defined by two or more hard partons). This avoids frame-dependent ambiguities from entering into the language, at the price of a slight reinterpretation of what is meant by collinear and soft.

In the generator landscape, *angular ordering* is used by the HERWIG [104] and HERWIG++ [105] programs, and an *angular veto* is imposed on the virtuality-ordered evolution in PYTHIA 6 [106]. Variants of the dipole approach is used by the ARIADNE [107], SHERPA [108, 109], and VINCIA [110] programs, while the  $p_{\perp}$ -ordered showers in PYTHIA 6 and 8 represent a hybrid, combining collinear splitting kernels with dipole kinematics [111]. Phase-space contours of equal value of some of these choices are illustrated in Fig. 18. During the shower evolution, each model effectively ‘sweeps’ over phase space in the order implied by these contours. For example, a  $p_{\perp}$ -ordered dipole shower (left-most plot in Fig. 18) will treat a hard-collinear branching as occurring ‘earlier’ than a soft one, while a mass-ordered dipole shower (second plot) will tend to do the opposite. This affects the tower of virtual corrections generated by each shower model via the so-called Sudakov factor, discussed below. Experimental tests of the subleading aspects of shower models can therefore be quite important, see Ref. [112] for a recent example.

Independently of rewritings and philosophy, the real power of Eq. (62) lies in the fact that it is *universal*. Thus, for *any* process  $F$ , we can apply Eq. (62) in order to get an approximation for  $d\sigma_{F+1}$ . We may then, for instance, take our newly obtained expression for  $F+1$  as our arbitrary process and crank Eq. (62) again, to obtain an approximation for  $d\sigma_{F+2}$ , and so forth. What we have here is therefore a very simple recursion relation that can be used to generate approximations to leading-order cross sections with arbitrary numbers of additional legs. The quality of this approximation is governed by how many terms besides the leading one shown in Eq. (53) are included in the game. Including all possible terms,

**F @ LO×LL(non-unitary)**

**Fig. 19:** Coefficients of the perturbative series covered by LO + LL approximations to higher-multiplicity tree-level ME. Green (darker) shading represents the full perturbative coefficient at the respective  $k$  and  $\ell$ . Yellow (lighter) shading represents an LL approximation to it. Half-shaded boxes indicate phase spaces in which we are prohibited from integrating over the IR singular region, as discussed in Sections 2.3 and 4.

the most general form for the cross section at  $F + n$  jets, restricted to the phase-space region above some IR-cutoff scale  $\mu_{\text{IR}}$ , has the following algebraic structure,

$$\sigma_{F+n}^{(0)} = \alpha_s^n (\ln^{2n} + \ln^{2n-1} + \ln^{2n-2} + \dots + \ln + \mathcal{F}) \quad (65)$$

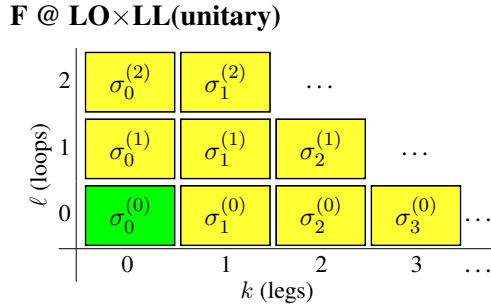
where we use the notation  $\ln^\lambda$  without an argument to denote generic functions of *transcendentality*  $\lambda$  (the logarithmic function to the power  $\lambda$  being a ‘typical’ example of a function with transcendentality  $\lambda$  appearing in cross section expressions, but also dilogarithms and higher logarithmic functions<sup>21</sup> of transcendentality  $> 1$  should be implicitly understood to belong to our notation  $\ln^\lambda$ ). The last term,  $\mathcal{F}$ , represents a rational function of transcendentality, 0. We shall also use the nomenclature *singular* and *finite* for the  $\ln^\lambda$  and  $\mathcal{F}$  terms, respectively, a terminology which reflects their respective behaviour in the limit  $\mu_{\text{IR}} \rightarrow 0$ .

The simplest approximation one can build on Eq. (65), dropping all but the leading  $\ln^{2n}$  term in the parenthesis, is thus the *leading-transcendentality* approximation. This approximation is better known as the double logarithmic approximation, since it generates the correct coefficient for terms which have two powers of logarithms for each power of  $\alpha_s$ , while terms of lower transcendentality are not guaranteed to have the correct coefficients. In so-called LL parton-shower algorithms, one generally expects to reproduce the correct coefficients for the  $\ln^{2n}$  and  $\ln^{2n-1}$  terms. In addition, several formally subleading improvements are normally also introduced in such algorithms (such as explicit momentum conservation, gluon polarization and other spin-correlation effects [113–115], higher-order coherence effects [103], renormalization scale choices [116], finite-width effects [117], etc), as a means to improve the agreement with some of the more subleading coefficients as well, if not in every phase-space point then at least on average. Although LL showers do not magically acquire NLL (next-to-leading-log) precision from such procedures, one, therefore, still expects a significantly better average performance from them than from corresponding ‘strict’ LL analytical resummations. A side effect of this is that it is often possible to ‘tune’ shower algorithms to give better-than-nominal agreement with experimental distributions, by adjusting the parameters controlling the treatment of subleading effects. One should remember, however, that there is a limit to how much can be accomplished in this way—at some point, agreement with one process will only come at the price of disagreement with another, and at this point further tuning would be meaningless.

Applying such an iterative process on a Born-level cross section, one obtains the description of the full perturbative series illustrated in Fig. 19. The yellow (lighter) shades, used here for  $k \geq 1$ , indicate that the coefficient obtained is not the exact one, but rather an approximation to it that only

<sup>21</sup>Note: due to the theorems that allow us, for instance, to rewrite dilogarithms in different ways with logarithmic and lower ‘spillover’ terms, the coefficients at each  $\lambda$  are only well-defined up to reparameterization ambiguities involving the terms with transcendentality greater than  $\lambda$ .





**Fig. 20:** Coefficients of the perturbative series covered by LO + LL calculations, imposing unitarity order by order for each  $n = k + \ell$ . Green (darker) shading represents the full perturbative coefficient at the respective  $k$  and  $\ell$ . Yellow (lighter) shading represents an LL approximation to it.

gets its leading singularities right. However, since this is still only an approximation to infinite-order *tree-level* cross sections (we have not yet included any virtual corrections), we cannot yet integrate this approximation over all of phase space, as illustrated by the yellow boxes being only half filled in Fig. 19; otherwise, the summed-total cross section would still be infinite. This particular approximation would therefore still appear to be very useless indeed—on one hand, it is only guaranteed to get the singular terms right, but on the other, it does not actually allow us to integrate over the singular region. In order to obtain a truly *all-orders* calculation, the constraint of unitarity must also be explicitly imposed, which furnishes an approximation to all-orders loop corrections as well. Let us therefore emphasize that Fig. 19 is included for pedagogical purposes only; all resummation calculations, whether analytical or parton-shower based, include virtual corrections as well and consequently yield finite total cross sections, as will now be described.

### 3.2.2 Step two: Infinite loops

Order-by-order unitarity, such as used in the KLN theorem, implies that the singularities caused by integration over unresolved radiation in the tree-level MEs must be cancelled, order by order, by equal but opposite-sign singularities in the virtual corrections at the same order. That is, from Eq. (62), we immediately know that the one-loop correction to  $d\sigma_F$  *must* contain a term,

$$2\text{Re}[\mathcal{M}_F^{(0)} \mathcal{M}_F^{(1)*}] \supset -g_s^2 N_C \left| \mathcal{M}_F^{(0)} \right|^2 \int \frac{ds_{ij} ds_{jk}}{16\pi^2 s_{ijk}} \left( \frac{2s_{ik}}{s_{ij} s_{jk}} + \text{less singular terms} \right), \quad (66)$$

that cancels the divergence coming from Eq. (62) itself. Further, since this is universally true, we may apply Eq. (66) again to get an approximation to the corrections generated by Eq. (62) at the next order and so on. By adding such terms explicitly, order by order, we may now bootstrap our way around the entire perturbative series, using Eq. (62) to move horizontally and Eq. (66) to move along diagonals of constant  $n = k + \ell$ . Since real-virtual cancellations are now explicitly restored, we may finally extend the integrations over all of phase space, resulting in the picture shown in Fig. 20.

The picture shown in Fig. 20, not the one in Fig. 19, corresponds to what is actually done in *resummation* calculations, both of the analytic and parton-shower types<sup>22</sup>. Physically, there is a significant and intuitive meaning to the imposition of unitarity, as follows.

Take a jet algorithm, with some measure of jet resolution,  $Q$ , and apply it to an arbitrary sample of events, say dijets. At a very crude resolution scale, corresponding to a high value for  $Q$ , you find that

<sup>22</sup>In the way these calculations are formulated in practice, they in fact rely on one additional property, called exponentiation, that allows us to move along straight vertical lines in the loops-and-legs diagrams. However, since the two different directions furnished by Eqs. (62) and (66) are already sufficient to move freely in the full two-dimensional coefficient space, we shall use exponentiation without extensively justifying it here.

everything is clustered back to a dijet configuration, and the two-jet cross section is equal to the total inclusive cross section,

$$\sigma_{\text{tot}} = \sigma_{F;\text{incl}}. \quad (67)$$

At finer resolutions, decreasing  $Q$ , you see that some events that were previously classified as two-jet events contain additional, lower-scale jets, that you can now resolve, and hence those events now migrate to the three-jet bin, while the total inclusive cross section of course remains unchanged,

$$\sigma_{\text{tot}} = \sigma_{F;\text{incl}} = \sigma_{F;\text{excl}}(Q) + \sigma_{F+1;\text{incl}}(Q), \quad (68)$$

where ‘incl’ and ‘excl’ stands for inclusive and exclusive cross sections<sup>23</sup>, respectively, and the  $Q$ -dependence in the two terms on the right-hand side must cancel so that the total inclusive cross section is independent of  $Q$ . Later, some three-jet events now migrate further, to four and higher jets, while still more two-jet events migrate *into* the three-jet bin, etc. For arbitrary  $n$  and  $Q$ , we have

$$\sigma_{F+n;\text{incl}}(Q) = \sigma_{F;\text{incl}} - \sum_{m=0}^{n-1} \sigma_{F+m;\text{excl}}(Q). \quad (69)$$

This equation expresses the trivial fact that the cross section for  $n$  or more jets can be computed as the total inclusive cross section for  $F$  minus a sum over the cross sections for  $F$  + exactly  $m$  jets including all  $m < n$ . On the theoretical side, it is these negative terms which must be included in the calculation, for each order  $n = k + \ell$ , to restore unitarity. Physically, they express that, at a given scale  $Q$ , each event will be classified as having *either* zero, one, two, or whatever jets. Or, equivalently, for each event we gain in the three-jet bin as  $Q$  is lowered, we must lose one event in the two-jet one; the negative contribution to the two-jet bin is exactly minus the integral of the positive contribution to the three-jet one, and so on. We may perceive this *detailed balance* as an *evolution* of the event structure with  $Q$ , for each event, which is effectively what is done in parton-shower algorithms, to which we shall return in Section 3.3.

### 3.3 Perturbation theory with Markov chains

Consider again the Born-level cross section for an arbitrary hard process,  $F$ , differentially in an arbitrary IR-safe observable  $\mathcal{O}$ , as obtained from Eq. (45):

$$\left. \frac{d\sigma_F^{(0)}}{d\mathcal{O}} \right|_{\text{Born}} = \int d\Phi_F |\mathcal{M}_F^{(0)}|^2 \delta(\mathcal{O} - \mathcal{O}(\Phi_F)), \quad (70)$$

where the integration runs over the full final-state on-shell phase space of  $F$  (this expression and those below would also apply to hadron collisions were we to include integrations over the PDFs in the initial state), and the  $\delta$  function projects out a one-dimensional slice defined by  $\mathcal{O}$  evaluated on the set of final-state momenta which we denote  $\Phi_F$ .

To make the connection to parton showers, we insert an operator,  $\mathcal{S}$ , that acts on the Born-level final state *before* the observable is evaluated, that is,

$$\left. \frac{d\sigma_F}{d\mathcal{O}} \right|_{\mathcal{S}} = \int d\Phi_F |\mathcal{M}_F^{(0)}|^2 \mathcal{S}(\Phi_F, \mathcal{O}). \quad (71)$$

Formally, this operator—the evolution operator—will be responsible for generating all (real and virtual) higher-order corrections to the Born-level expression. The measurement  $\delta$  function appearing explicitly in Eq. (70) is now implicit in  $\mathcal{S}$ .

<sup>23</sup>  $F$  inclusive =  $F$  plus anything.  $F$  exclusive =  $F$  and only  $F$ . Thus,  $\sigma_{F;\text{incl}} = \sum_{k=0}^{\infty} \sigma_{F+k;\text{excl}}$

Algorithmically, parton showers cast  $\mathcal{S}$  as an iterative Markov (i.e., history-independent) chain, with an evolution parameter,  $Q_E$ , that formally represents the factorization scale of the event, below which all structure is summed over inclusively. Depending on the particular choice of shower algorithm,  $Q_E$  may be defined as a parton virtuality (virtuality-order showers), as a transverse-momentum scale ( $p_\perp$ -ordered showers) or as a combination of energies times angles (angular ordering). Regardless of the specific form of  $Q_E$ , the evolution parameter will go towards zero as the Markov chain develops, and the event structure will become more and more exclusively resolved. A transition from a perturbative evolution to a non-perturbative one can also be inserted, when the evolution reaches an appropriate scale, typically around 1 GeV. This scale, called the *hadronization scale*, thus represents the lowest perturbative scale that can appear in the calculations, with all perturbative corrections below it summed over inclusively.

Working out the precise form that  $\mathcal{S}$  must have in order to give the correct expansions discussed in Section 3.2 takes a bit of algebra and is beyond the scope we aim to cover in these lectures. Heuristically, the procedure is as follows. We noted that the singularity structure of QCD is universal and that at least its first few terms are known to us. We also saw that we could iterate that singularity structure, using universality and unitarity, thereby bootstrapping our way around the entire perturbative series. This was illustrated by Fig. 20 in Section 3.2.

Skipping intermediate steps, the form of the all-orders pure-shower Markov chain, for the evolution of an event between two scales  $Q_1 > Q_E > Q_2$ , is,

$$\begin{aligned} \mathcal{S}(\Phi_F, Q_1, Q_2, \mathcal{O}) &= \underbrace{\Delta(\Phi_F, Q_1, Q_2) \delta(\mathcal{O} - \mathcal{O}(\Phi_F))}_{F + 0 \text{ exclusive above } Q_2} \\ &+ \underbrace{\sum_r \int_{Q_{E2}}^{Q_{E1}} \frac{d\Phi_{F+1}^r}{d\Phi_F} S_r(\Phi_{F+1}) \Delta(\Phi_F, Q_1, Q_{F+1}) \mathcal{S}(\Phi_{F+1}, Q_{F+1}, Q_2, \mathcal{O})}_{F + 1 \text{ inclusive above } Q_2}, \end{aligned} \quad (72)$$

with the so-called *Sudakov factor*,

$$\Delta(\Phi_F, Q_1, Q_2) = \exp \left[ - \sum_r \int_{Q_2}^{Q_1} \frac{d\Phi_{F+1}^r}{d\Phi_F} S_r(\Phi_{F+1}) \right], \quad (73)$$

defining the probability that there is *no evolution* (i.e., no emissions) between the scales  $Q_1$  and  $Q_2$ , according to the *radiation functions*  $S_r$  to which we shall return below. The term on the first line of Eq. (72) thus represents all events that *did not* evolve as the resolution scale was lowered from  $Q_1$  to  $Q_2$ , while the second line contains a sum and phase-space integral over those events that *did* evolve—including the insertion of  $\mathcal{S}(\Phi_{F+1})$  representing the possible further evolution of the event and completing the iterative definition of the Markov chain.

The factor  $d\Phi_{F+1}^r/d\Phi_F$  defines the chosen phase space factorization. Our favourite is the so-called dipole-antenna factorization, whose principal virtue is that it is the simplest Lorentz-invariant factorization which is simultaneously exact over all of phase space while only involving on-shell momenta. For completeness, its form is

$$\frac{d\Phi_{F+1}^r}{d\Phi_F} = \frac{d\Phi_3^r}{d\Phi_2} = ds_{a1} ds_{1b} \frac{d\phi}{2\pi} \frac{1}{16\pi^2 s_r}, \quad (74)$$

which involves just one colour–anticolour pair for each  $r$ , with invariant mass squared  $s_r = (p_a + p_1 + p_b)^2$ . Other choices, such as purely collinear ones (only exact in the collinear limit *or* involving explicitly off-shell momenta), more global ones involving all partons in the event (more complicated, in our opinion), or less global ones with a single parton playing the dominant role as emitter, are also possible, again depending on the specific algorithm considered.

The radiation functions  $S_r$  obviously play a crucial role in these equations, driving the emission probabilities. For example, if  $S_r \rightarrow 0$ , then  $\Delta \rightarrow \exp(0) = 1$  and all events stay in the top line of Eq. (72). Thus, in regions of phase space where  $S_r$  is small, there is little or no evolution. Conversely, for  $S_r \rightarrow \infty$ , we have  $\Delta \rightarrow 0$ , implying that *all* events evolve. One possible choice for the radiation functions  $S_r$  was implicit in Eq. (62), in which we took them to include only the leading (double) singularities, with  $r$  representing colour–anticolour pairs. In general, the shower may exponentiate the entire set of universal singular terms, or only a subset of them (for example, the terms leading in the number of colours  $N_C$ ), which is why we here let the explicit form of  $S_r$  be unspecified. Suffice it to say that in traditional parton showers,  $S_r$  would simply be the DGLAP splitting kernels (see, e.g., Ref. [3]), while they would be so-called dipole or antenna radiation functions in the various dipole-based approaches to QCD (see, e.g., Ref. [64, 70, 76, 80, 81, 109]).

The procedure for how to technically ‘construct’ a shower algorithm of this kind, using random numbers to generate scales distributed according to Eq. (72), is described more fully in Ref. [80], using a notation that closely parallels the one used here. The procedure is also described at a more technical level in the review [5], although using a slightly different notation. Finally, a pedagogical introduction to Monte Carlo methods in general can be found in Ref. [7].

### 3.4 Decays of unstable particles

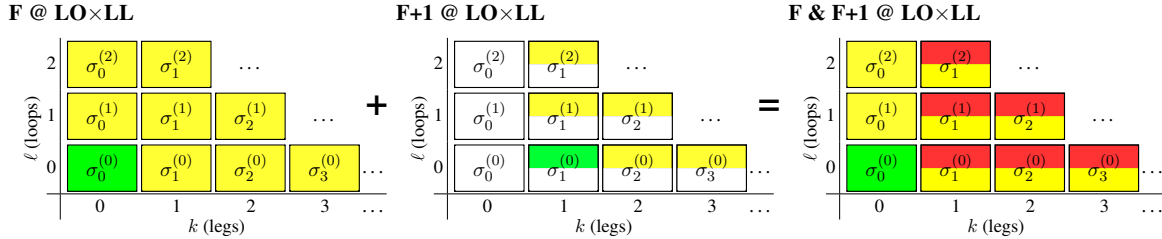
In most BSM processes and some SM ones, an important aspect of the event simulation is how decays of short-lived particles, such as top quarks, Electro-Weak and Higgs bosons and new BSM resonances, are handled. We here briefly summarize the spectrum of possibilities, but emphasize that there is no universal standard. Users are advised to check whether the treatment of a given code is adequate for the physics study at hand.

The appearance of an unstable resonance as a physical particle at some intermediate stage of the event generation implies that its production and decay processes are treated as being factorized. This is called the *narrow width approximation* and is valid up to corrections of order  $\Gamma/m_0$ , with  $\Gamma$  the width and  $m_0$  the pole mass of the particle. States whose widths are a substantial fraction of their mass should not be treated in this way, but rather as intrinsically virtual internal propagator lines.

For states treated as physical particles, two aspects are relevant: the mass distribution of the decaying particle itself and the distributions of its decay products. For the mass distribution, the simplest is to use a  $\delta$  function at  $m_0$ . The next level up, typically used in general-purpose Monte Carlo, is to use a Breit–Wigner distribution (relativistic or non-relativistic), which formally resums higher-order virtual corrections to the mass distribution. Note, however, that this still only generates an improved picture for *moderate* fluctuations away from  $m_0$ . Similarly to above, particles that are significantly off-shell (in units of  $\Gamma$ ) should not be treated as resonant, but rather as internal off-shell propagator lines. In most Monte Carlo codes, some further refinements are also included, for instance by letting  $\Gamma$  be a function of  $m$  (‘running widths’) and by limiting the magnitude of the allowed fluctuations away from  $m_0$ . See also Ref. [118] for an elaborate discussion of the Higgs boson lineshape.

For the distributions of the decay products, the simplest treatment is again to assign them their respective  $m_0$  values, with a uniform (i.e., isotropic, or ‘flat’) phase-space distribution. A more sophisticated treatment distributes the decay products according to the differential decay MEs, capturing at least the internal dynamics and helicity structure of the decay process, including Einstein-Podolsky-Rosen(EPR)-like correlations. Further refinements include polarizations of the external states [113–115] (see also Refs. [119–121] for phenomenological studies) and assigning the decay products their own Breit–Wigner distributions, the latter of which opens the possibility to include also intrinsically off-shell decay channels, like  $H \rightarrow WW^*$ . Please refer to the physics manual of the code you are using and/or make simple cross checks such as plotting the distribution of the phase-space invariants it produces.

During subsequent showering of the decay products, most parton-shower models will preserve the



**Fig. 21:** The double-counting problem caused by naively adding cross sections involving MEs with different numbers of legs.

total invariant mass of each resonance-decay system separately, so as not to skew the original resonance shape.

#### 4 Matching at LO and NLO

The essential problem that leads to ME/parton-shower matching can be illustrated in a very simple way. Assume we have computed the LO cross section for some process,  $F$ , and that we have added an LL shower to it, as in the left-hand pane of Fig. 21. We know that this only gives us an LL description of  $F + 1$ . We now wish to improve this from LL to LO by adding the actual LO ME for  $F + 1$ . Since we also want to be able to hadronize these events, etc., we again add an LL shower off them. However, since the ME for  $F + 1$  is divergent, we must restrict it to cover only the phase-space region with at least one hard resolved jet, illustrated by the half-shaded boxes in the middle pane of Fig. 21.

Adding these two samples, however, we end up counting the LL terms of the inclusive cross section for  $F + 1$  twice, since we are now getting them once from the shower off  $F$  and once from the ME for  $F + 1$ , illustrated by the dark shaded (red) areas of the right-hand pane of Fig. 21. This *double-counting* problem would grow worse if we attempted to add more MEs, with more legs. The cause is very simple. Each such calculation corresponds to an *inclusive* cross section, and hence naive addition would give

$$\sigma_{\text{tot}} = \sigma_{0;\text{incl}} + \sigma_{1;\text{incl}} = \sigma_{0;\text{excl}} + 2\sigma_{1;\text{incl}}. \quad (75)$$

Recall the definition of inclusive and exclusive cross sections, Eq. (68):  $F$  *inclusive* =  $F$  plus anything.  $F$  *exclusive* =  $F$  and only  $F$ . Thus,  $\sigma_{F;\text{incl}} = \sum_{k=0}^{\infty} \sigma_{F+k;\text{excl}}$ .

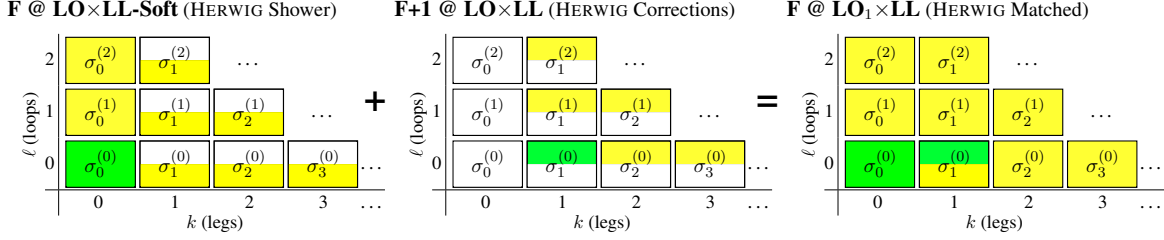
Instead, we must *match* the coefficients calculated by the two parts of the full calculation—showers and matrix elements—more systematically, for each order in perturbation theory, so that the nesting of inclusive and exclusive cross sections is respected without overcounting.

Given a parton shower and a ME generator, there are fundamentally three different ways in which we can consider matching the two [80]: slicing, subtraction and unitarity. The following subsections will briefly introduce each of these.

##### 4.1 Slicing

The most commonly encountered matching type is currently based on separating (slicing) phase space into two regions, one of which is supposed to be mainly described by hard MEs and the other of which is supposed to be described by the shower. This type of approach was first used in HERWIG [89], to include ME corrections for one emission beyond the basic hard process [122, 123]. This is illustrated in Fig. 22. The method has since been generalized by several independent groups to include arbitrary numbers of additional legs, the most well-known of these being the CKKW [124], CKKW-L [125, 126], and MLM [127, 128] approaches.

Effectively, the shower approximation is set to zero above some scale, either due to the presence of explicit dead zones in the shower, as in HERWIG, or by vetoing any emissions above a certain *matching*



**Fig. 22:** HERWIG’s original matching scheme [122, 123], in which the dead zone of the HERWIG shower was used as an effective ‘matching scale’ for one emission beyond a basic hard process.

*scale*, as in the CKKW(-L) and MLM approaches. The empty part of phase space can then be filled by separate events generated according to higher-multiplicity tree-level MEs. In the CKKW(-L) and MLM schemes, this process can be iterated to include arbitrary numbers of additional hard legs (the practical limit being around three or four, due to computational complexity).

In order to match smoothly with the shower calculation, the higher-multiplicity MEs must be associated with Sudakov form factors (representing the virtual corrections that would have been generated if a shower had produced the same phase-space configuration), and their  $\alpha_s$  factors must be chosen so that, at least at the matching scale, they become identical to the choices made on the shower side [129]. The CKKW and MLM approaches do this by constructing ‘fake parton-shower histories’ for the higher-multiplicity MEs. By applying a sequential jet clustering algorithm, a tree-like branching structure can be created that at least has the same dominant structure as that of a parton shower. Given the fake shower tree,  $\alpha_s$  factors can be chosen for each vertex with argument  $\alpha_s(p_\perp)$  and Sudakov factors can be computed for each internal line in the tree. In the CKKW method, these Sudakov factors are estimated analytically, while the MLM and CKKW-L methods compute them numerically, from the actual shower evolution.

Thus, the matched result is identical to the ME in the region above the matching scale, modulo higher-order (Sudakov and  $\alpha_s$ ) corrections. We may sketch this as

$$\text{Matched (above matching scale)} = \overbrace{\text{Exact}}^{\text{ME}} \times \overbrace{(1 + \mathcal{O}(\alpha_s))}^{\text{corrections}}, \quad (76)$$

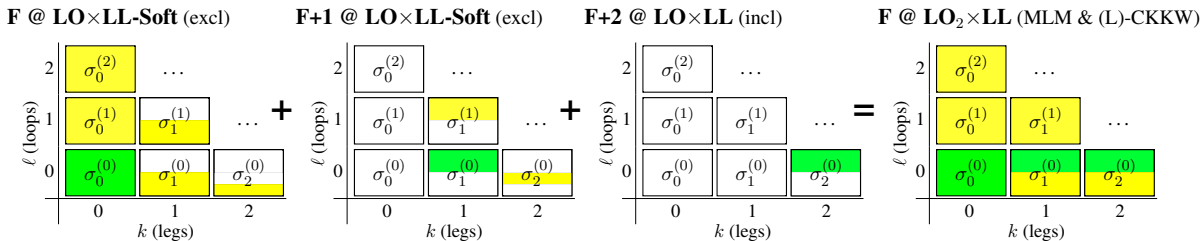
where the ‘shower corrections’ include the approximate Sudakov factors and  $\alpha_s$  reweighting factors applied to the MEs in order to obtain a smooth transition to the shower-dominated region.

Below the matching scale, the small difference between the MEs and the shower approximation can be dropped (since their leading singularities are identical and this region by definition includes no hard jets), yielding the pure shower answer in that region,

$$\begin{aligned} \text{Matched (below matching scale)} &= \overbrace{\text{Approximate}}^{\text{shower}} + \overbrace{(\text{Exact} - \text{Approximate})}^{\text{correction}} \\ &= \text{Approximate} + \text{non-singular} \\ &\rightarrow \text{Approximate}. \end{aligned} \quad (77)$$

This type of strategy is illustrated in Fig. 23.

As emphasized above, since this strategy is discontinuous across phase space, a main point here is to ensure that the behaviour across the matching scale be as smooth as possible. CKKW showed [124] that it is possible to remove any dependence on the matching scale through NLL precision by careful choices of all ingredients in the matching; technical details of the implementation (affecting the  $\mathcal{O}(\alpha_s)$  terms in Eq. (76)) are important, and the dependence on the unphysical matching scale may be larger than NLL unless the implementation matches the theoretical algorithm precisely [125, 126, 130]. Furthermore,



**Fig. 23:** Slicing, with up to two additional emissions beyond the basic process. The showers off  $F$  and  $F + 1$  are set to zero above a specific ‘matching scale’. (The number of coefficients shown was reduced a bit in these plots to make them fit in one row.)

since the Sudakov factors are generally computed using showers (MLM, CKKW-L) or a shower-like formalism (CKKW), while the real corrections are computed using MEs, care must be taken not to (re-)introduce differences that could break the detailed real-virtual balance that ensures unitarity among the singular parts, see e.g., Ref. [129].

It is advisable not to choose the matching scale too low. This is again essentially due to the approximate scale invariance of QCD imploring us to write the matching scale as a ratio, rather than as an absolute number. If one uses a very low matching scale, the higher-multiplicity MEs will already be quite singular, leading to very large LO cross sections before matching. After matching, these large cross sections are tamed by the Sudakov factors produced by the matching scheme, and hence the final cross sections may still look reasonable. But the higher-multiplicity MEs in general contain subleading singularity structures, beyond those accounted for by the shower, and hence the delicate line of detailed balance that ensures unitarity has most assuredly been overstepped. We, therefore, recommend not to take the matching scale lower than about an order of magnitude below the characteristic scale of the hard process.

One should also be aware that all strategies of this type are quite computing intensive. This is basically due to the fact that a separate phase-space generator is required for each of the  $n$ -parton correction terms, with each such sample a priori consisting of weighted events such that a separate unweighting step (often with quite low efficiency) is needed before an unweighted sample can be produced.

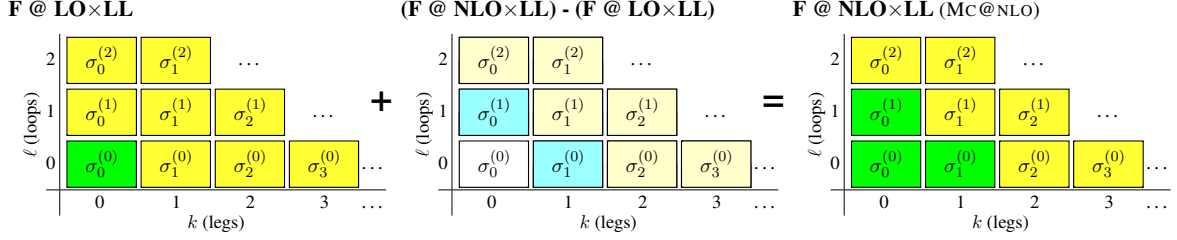
## 4.2 Subtraction

Another way of matching two calculations is by subtracting one from the other and correcting by the difference, schematically

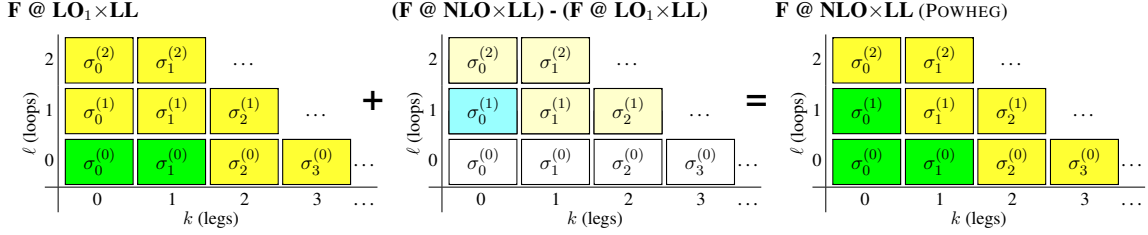
$$\text{Matched} = \overbrace{\text{Approximate}}^{\text{shower}} + \overbrace{(\text{Exact} - \text{Approximate})}^{\text{correction}}. \quad (78)$$

This looks very much like the structure of a subtraction-based NLO fixed-order calculation, Section 2.4, in which the shower approximation here plays the role of subtraction terms, and indeed this is what is used in strategies like MC@NLO [131–133], illustrated in Fig. 24. In this type of approach, however, negative-weight events will generally occur, for instance in phase-space points where the approximation is larger than the exact answer.

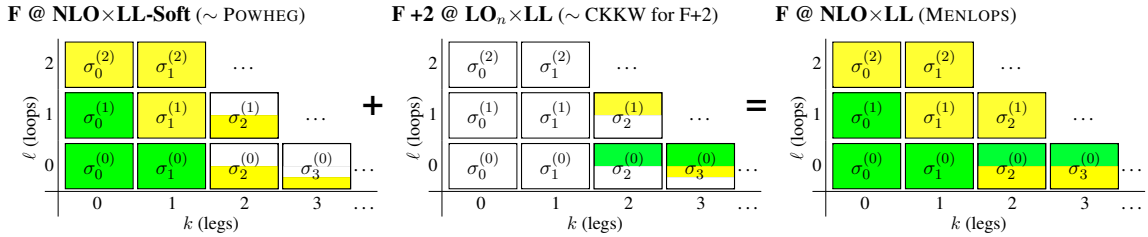
Negative weights are not in principle an insurmountable problem. Histograms can be filled with each event counted according to its weight, as usual. However, negative weights do affect efficiency. Imagine a worst-case scenario in which 1000 positive-weight events have been generated, along with 999 negative-weight ones (assuming each event weight has the same absolute value, the closest one can get to an unweighted sample in the presence of negative weights). The statistical precision of the MC answer would be equivalent to one event, for 2000 generated, i.e., a big loss in convergence rate.



**Fig. 24:** MC@NLO. In the middle pane, cyan boxes denote non-singular correction terms, while the egg-coloured ones denote showers off such corrections, which cannot lead to double-counting at the LL level.



**Fig. 25:** POWHEG. In the middle pane, cyan boxes denote non-singular correction terms, while the egg-coloured ones denote showers off such corrections, which cannot lead to double-counting at the LL level.

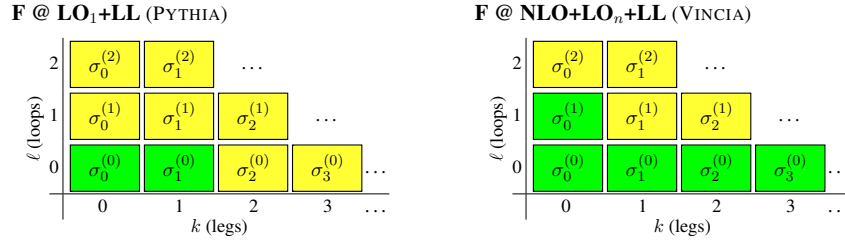


**Fig. 26:** MENLOPS. Note that each of the POWHEG and CKKW samples are composed of separate sub-samples, as illustrated in Figs. 23 and 25.

In practice, generators like MC@NLO ‘only’ produce around 10% or less events with negative weights, so the convergence rate should not be severely affected for ordinary applications. Nevertheless, the problem of negative weights motivated the development of the so-called POWHEG approach [134], illustrated in Fig. 25, which is constructed specifically to prevent negative-weight events from occurring and simultaneously to be more independent of which parton-shower algorithm it is used with. In the POWHEG method, one effectively modifies the real-emission probability for the first emission to agree with the  $F + 1$  ME (this is covered under unitarity, below). One is then left with a purely virtual correction, which will typically be positive, at least for processes for which the NLO cross section is larger than the LO one.

The advantage of these methods is obviously that NLO corrections to the Born level can be systematically incorporated. However, a systematic way of extending this strategy beyond the first additional emission is not available, save for combining them with a slicing-based strategy for the additional legs, as in MENLOPS [135], illustrated in Fig. 26. These issues are, however, no more severe than in ordinary fixed-order NLO approaches, and hence they are not viewed as disadvantages if the point of reference is an NLO computation.





**Fig. 27:** PYTHIA (left) and VINCIA (right). Unitarity-based. Only one event sample is produced by each of these methods, and hence no sub-components are shown.

### 4.3 Unitarity

The oldest, and in my view most attractive, approach [106, 136] consists of working out the shower approximation to a given fixed order, and correcting the shower splitting functions at that order by a multiplicative factor given by the ratio of the ME to the shower approximation, phase-space point by phase-space point. We may sketch this as

$$\text{Matched} = \overbrace{\text{Approximate}}^{\text{shower}} \times \frac{\overbrace{\text{Exact}}^{\text{correction}}}{\text{Approximate}}. \quad (79)$$

When these correction factors are inserted back into the shower evolution, they guarantee that the shower evolution off  $n - 1$  partons correctly reproduces the  $n$ -parton MEs, without the need to generate a separate  $n$ -parton sample. That is, the shower approximation is essentially used as a pre-weighted (stratified) all-orders phase-space generator, on which a more exact answer can subsequently be imprinted order by order in perturbation theory. Since the shower is already optimized for exactly the kind of singular structures that occur in QCD, very fast computational speeds can therefore be obtained with this method [81].

In the original approach [106, 136], used by PYTHIA [90, 91], this was only worked out for one additional emission beyond the basic hard process. In POWHEG [134, 137], it was extended to also include virtual corrections to the Born-level ME. Finally, in VINCIA, it has been extended to include arbitrary numbers of emissions at tree level [80, 81] and one emission at loop level [138], although that method has so far only been applied to final-state showers.

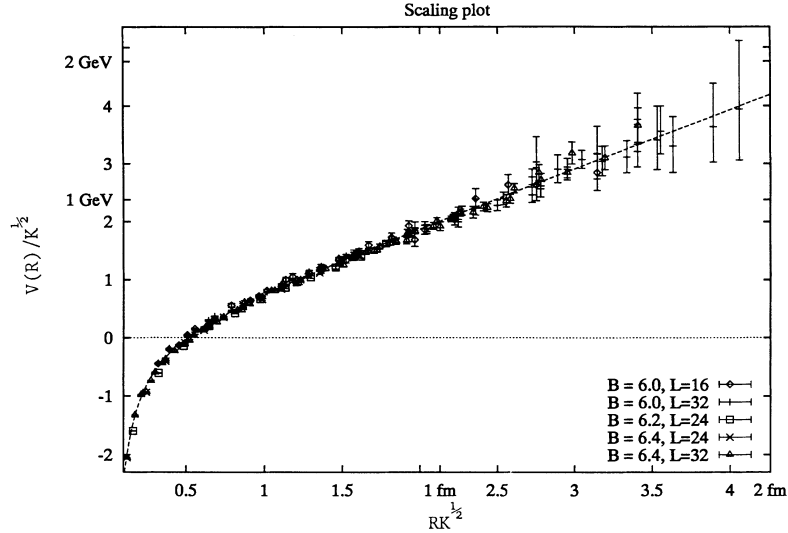
An illustration of the perturbative coefficients that can be included in each of these approaches is given in Fig. 27, as usual with green (darker shaded) boxes representing exact coefficients and yellow (light shaded) boxes representing logarithmic approximations.

Finally, two more properties unique to this method deserve a mention. Firstly, since the corrections modify the actual shower evolution kernels, the corrections are automatically *resummed* in the Sudakov exponential, which should improve the logarithmic precision once  $k \geq 2$  is included, and secondly, since the shower is *unitary*, an initially unweighted sample of  $(n - 1)$ -parton configurations remains unweighted, with no need for a separate event-unweighting or event-rejection step.

## 5 Hadronization and soft hadron–hadron physics

We here give a very brief overview of the main aspects of soft QCD that are relevant for hadron–hadron collisions, such as hadronization, minimum-bias and soft-inclusive physics, and the so-called underlying event. This will be kept at a pedestrian level and is largely based on the reviews in Refs. [5, 24, 139].

In the context of event generators, *hadronization* denotes the process by which a set of coloured partons (*after* showering) is transformed into a set of colour-singlet *primary* hadrons, which may then subsequently decay further. This non-perturbative transition takes place at the *hadronization scale*  $Q_{\text{had}}$ , which by construction is identical to the IR cutoff of the parton shower. In the absence of a first-principles



**Fig. 28:** Static quark–antiquark potential, as a function of separation distance, in quenched lattice QCD, from Ref. [140]. Note that the axes are scaled by units of the string tension  $\sqrt{\kappa} \sim 420$  MeV. Additional labels corresponding to 1 GeV and 2 GeV are also provided, on the  $y$ -axis, and to 1 fm and 2 fm, on the  $x$ -axis. A constant term,  $V_0$ , has been subtracted from all the results. The dashed line corresponds to  $V(R) = R - \pi/(12R)$ .

solution to the relevant dynamics, event generators use QCD-inspired phenomenological models to describe this transition.

The problem can be stated as follows: given a set of partons resolved at a scale of  $Q_{\text{had}} \sim 1$  GeV, we need a ‘mapping’ from this set onto a set of on-shell colour-singlet (i.e., confined) hadronic states. MC models do this in three steps:

1. Map the partonic system onto a continuum of high-mass hadronic states (called ‘strings’ or ‘clusters’).
2. Iteratively map strings/clusters onto discrete set of primary hadrons (via string breaks / cluster splittings / cluster decays).
3. Sequential decays into secondaries ( $\rho \rightarrow \pi\pi$ ,  $\Lambda \rightarrow n\pi$ ,  $\pi^0 \rightarrow \gamma\gamma$ , ...).

The physics governing this mapping is non-perturbative. However, we do have some knowledge of the properties that such a solution must have. For instance, Poincaré invariance, unitarity, and causality are all concepts that apply beyond perturbation theory. In addition, lattice QCD provides us a means of making explicit quantitative studies in a genuinely non-perturbative setting (albeit only of certain questions).

An important result in ‘quenched’ lattice QCD<sup>24</sup> is that the potential of the colour-dipole field between a charge and an anticharge appears to grow linearly with the separation of the charges, at distances greater than about 0.5 fm; this behaviour is illustrated by the plot shown in Fig. 28, from Ref. [140]. (Note that the axes are scaled by units of the string tension  $\sqrt{\kappa} \sim 420$  MeV. Additional labels corresponding to 1 GeV and 2 GeV are also provided, on the  $y$ -axis, and to 1 fm and 2 fm, on the  $x$ -axis.) This is known as ‘linear confinement’, and it forms the starting point for the *string model of hadronization*, discussed below in Section 5.1. Alternatively, a property of pQCD called ‘preconfinement’ [141] is the basis of the *cluster model of hadronization*, described in Refs. [5, 24].

In the generator landscape, PYTHIA uses string fragmentation, while HERWIG and SHERPA use cluster fragmentation. It should be emphasized that the so-called *parton level* that can be obtained by

<sup>24</sup>Quenched QCD implies no ‘dynamical’ quarks, i.e., no  $g \rightarrow q\bar{q}$  splittings allowed.

switching off hadronization in an MC generator, is not a universal concept, since each model defines the hadronization scale differently. For example, the hadronization scale can be defined by a cutoff in invariant mass, transverse momentum, or some other quantity, with different tunes using different values for the cutoff. Note that the so-called *parton level* that can be obtained by switching off hadronization in an MC generator, is not a universal concept, since each model defines the hadronization scale differently, with different tunes using different values for it. Comparisons to distributions at this level (i.e., with hadronization switched off) may therefore be used to provide an idea of the overall impact of hadronization corrections within a given model, but should be avoided in the context of physical observables. Note also that the corresponding MC *fragmentation functions* are intrinsically defined at the hadronization scale. They can therefore not be compared directly to those that are used in fixed-order/analytical-resummation contexts, which are typically defined at a factorization scale of the order of the scale of the hard process.

We use the term ‘soft hadron–hadron physics’ to comprise all scattering processes for which a hard, perturbative scale is not required to be present<sup>25</sup>. This includes elastic, diffractive, minimum-bias and pile-up processes, as well as the physics contributing to the so-called underlying event. We give a brief introduction to such processes in Section 5.2.

We round off with a discussion of the data constraints that enter in the tuning of Monte Carlo models in Section 5.4 and give an outline of a procedure that could be followed in a realistic set-up.

## 5.1 String model

Starting from early concepts developed by Artru and Mennessier [143], several hadronization models based on strings were proposed in the late 1970s and early 1980s. Of these, the most widely used today is the so-called Lund model, implemented in the PYTHIA code. We shall, therefore, concentrate on that particular model here, although many of the overall concepts would be shared by any string-inspired method. (A more extended discussion can be found in the very complete and pedagogical review of the Lund model by Andersson [6].)

Consider the production of a  $q\bar{q}$  pair from vacuum, for instance in the process  $e^+e^- \rightarrow \gamma^*/Z \rightarrow q\bar{q} \rightarrow \text{hadrons}$ . As the quarks move apart, linear confinement implies that a potential

$$V(R) = \kappa R \tag{80}$$

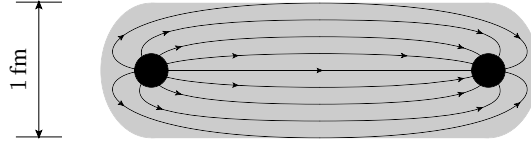
is asymptotically reached for large distances,  $R$ . At short distances, there is a Coulomb term proportional to  $1/R$  as well, cf. Fig. 28, but this is neglected in the Lund model. Such a potential describes a string with tension (energy per unit length)  $\kappa$ , with the value [140]

$$\kappa \sim (420 \text{ MeV})^2 \sim 0.18 \text{ GeV}^2 \sim 0.9 \text{ GeV/fm}, \tag{81}$$

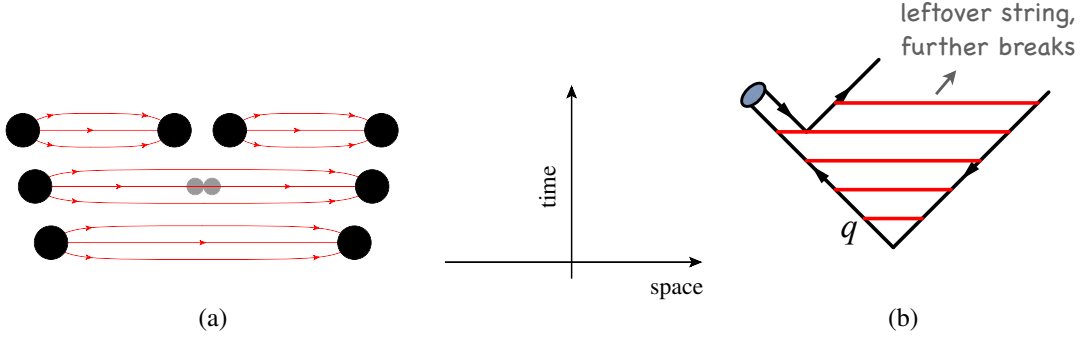
which, for comparison with the world of macroscopic objects, would be sufficient to lift a 16-ton truck [144].

The string can be thought of as parameterizing the position of the axis of a cylindrically symmetric flux tube, illustrated in Fig. 29. Such simple  $q - \bar{q}$  strings form the starting point for the string model. More complicated multi-parton topologies are treated by representing gluons as transverse ‘kinks’, e.g.,  $q - g - \bar{q}$ . The space–time evolution is then slightly more involved [6], and modifications to the fragmentation model to handle stepping across gluon corners have to be included, but the main point is that there are no separate free parameters for gluon jets. Differences with respect to quark fragmentation arise simply because quarks are only connected to a single string piece, while gluons have one on either side,

<sup>25</sup>Note, however, that while a hard scale is not *required* to be present, it is not explicitly required to be absent either. Thus, both diffractive, minimum-bias, pile-up and underlying-event processes will have tails towards high- $p_\perp$  physics as well. For example, even  $t\bar{t}$  pair production can be viewed as a tail of minimum-bias interactions, and there is a tail of diffractive processes in which hard dijets can be produced diffractively (see, e.g., Ref. [142]).



**Fig. 29:** Illustration of the transition between a Coulomb potential at short distances to the string-like one of Eq. (80) at large  $q\bar{q}$  separations.



**Fig. 30:** (a) Illustration of string breaking by quark pair creation in the string field. (b) Illustration of the algorithmic choice to process the fragmentation from the outside-in, splitting off a single on-shell hadron in each step.

increasing the energy loss per unit (invariant) time from a gluon to the string by a factor of two relative to quarks, which can be compared to the ratio of colour Casimirs  $C_A/C_F = 2.25$ . Another appealing feature of the model is that low-energy gluons are absorbed smoothly into the string, without leading to modifications. This improves the stability of the model with respect to variations of the IR behaviour of the parton shower.

As the partonic string endpoints move apart, their kinetic energy is gradually converted to potential energy, stored in the growing string spanned between them. In the ‘quenched’ approximation, in which  $g \rightarrow q\bar{q}$  splittings are not allowed, this process would continue until the endpoint quarks have lost *all* their momentum, at which point they would reverse direction and be accelerated by the now shrinking string.

In the real world, quark–antiquark fluctuations inside the string field can make the transition to become real particles by absorbing energy from the string, thereby screening the original endpoint charges from each other and breaking the string into two separate colour-singlet pieces,  $(q\bar{q}) \rightarrow (q\bar{q}') + (q'\bar{q})$ , illustrated in Fig. 30 (a). This process then continues until only ordinary hadrons remain. (We will give more details on the individual string breaks below.)

Since the string breaks are causally disconnected (as can easily be realized from space–time diagrams like the one in Fig. 30, see also Ref. [6]), they do not have to be considered in any specific time-ordered sequence. In the Lund model, the string breaks are instead generated starting with the leading (‘outermost’) hadrons, containing the endpoint quarks, and iterating inwards towards the centre of the string, alternating randomly between fragmentation off the left- and right-hand sides, respectively, Fig. 30 (b). One can thereby split off a single well-defined hadron in each step, with a mass that, for unstable hadrons, is selected according to a Breit–Wigner distribution.

The details of the individual string breaks are not known from first principles. The Lund model invokes the idea of quantum mechanical tunneling, which leads to a Gaussian suppression of the transverse momenta and masses imparted to the produced quarks,

$$\text{Prob}(m_q^2, p_{\perp q}^2) \propto \exp\left(\frac{-\pi m_q^2}{\kappa}\right) \exp\left(\frac{-\pi p_{\perp q}^2}{\kappa}\right), \quad (82)$$

where  $m_q$  is the mass of the produced quark and  $p_\perp$  is the transverse momentum imparted to it by the breakup process (with the  $\bar{q}$  having the opposite  $p_\perp$ ).

Due to the factorization of the  $p_\perp$  and  $m$  dependence implied by Eq. (82), the  $p_\perp$  spectrum of produced quarks in this model is independent of the quark flavour, with a universal average value of

$$\langle p_{\perp q}^2 \rangle = \sigma^2 = \kappa/\pi \sim (240 \text{ MeV})^2. \quad (83)$$

Bear in mind that ‘transverse’ is here defined with respect to the string axis. Thus, the  $p_\perp$  in a frame where the string is moving is modified by a Lorentz boost factor. Also bear in mind that  $\sigma^2$  is here a purely non-perturbative parameter. In a Monte Carlo model with a fixed shower cutoff  $Q_{\text{had}}$ , the effective amount of ‘non-perturbative’  $p_\perp$  may be larger than this, due to effects of additional unresolved soft-gluon radiation below  $Q_{\text{had}}$ . In principle, the magnitude of this additional component should scale with the cutoff, but in practice it is up to the user to enforce this by retuning (see Section 5.4) the effective  $\sigma$  parameter when changing the hadronization scale. Since hadrons receive  $p_\perp$  contributions from two breakups, one on either side, their average transverse momentum squared will be twice as large,

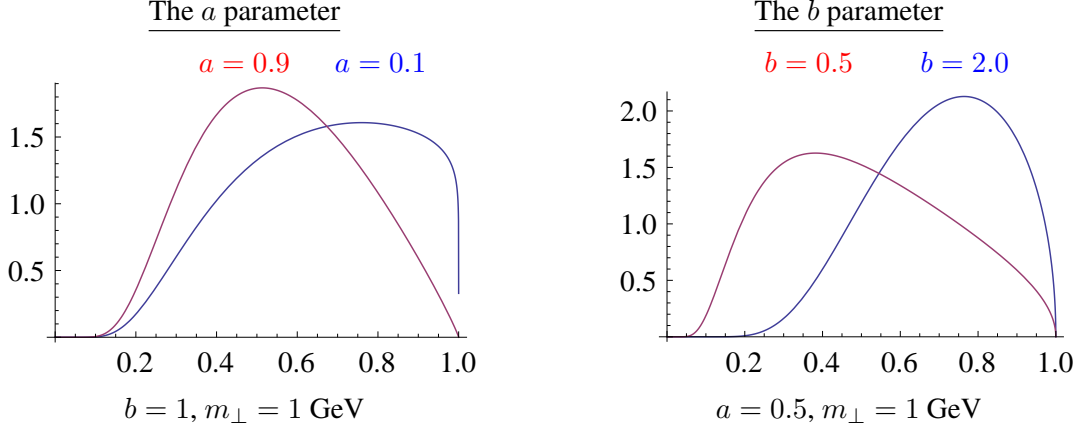
$$\langle p_{\perp h}^2 \rangle = 2\sigma^2. \quad (84)$$

The mass suppression implied by Eq. (82) is less straightforward to interpret. Since quark masses are notoriously difficult to define for light quarks, the value of the strangeness suppression must effectively be extracted from experimental measurements, for example, of the  $K/\pi$  ratio, with a resulting suppression of roughly  $s/u \sim s/d \sim 0.2\text{--}0.3$ . Inserting even comparatively low values for the charm quark mass in Eq. (82), however, one obtains a relative suppression of charm of the order of  $10^{-11}$ . Heavy quarks can therefore safely be considered to be produced only in the perturbative stages and not by the soft fragmentation.

Baryon production can be incorporated in the same basic picture [145], by allowing string breaks to occur also by the production of pairs of so-called *diquarks*, loosely bound states of two quarks in an overall  $\bar{3}$  representation (e.g., ‘red + blue  $\sim$  antigreen’, cf. the rules for colour combinations in Section 1.2). Again, the relative rate of diquark-to-quark production is not known a priori and must be extracted from experimental measurements, for example, of the  $p/\pi$  ratio. More advanced scenarios for baryon production have also been proposed, in particular the so-called popcorn model [146, 147], which is normally used in addition to the diquark picture and then acts to decrease the correlations among neighbouring baryon–antibaryon pairs by allowing mesons to be formed inbetween them. Within the PYTHIA framework, a fragmentation model including explicit *string junctions* [148] has so far only been applied to baryon-number-violating new-physics processes and to the description of beam remnants (and then acts to increase baryon stopping [149]).

This brings us to the next step of the algorithm: assignment of the produced quarks within hadron multiplets. Using a nonrelativistic classification of spin states, the fragmenting  $q$  ( $\bar{q}$ ) may combine with the  $\bar{q}'$  ( $q'$ ) from a newly created breakup to produce either a vector or a pseudoscalar meson, or, if diquarks are involved, either a spin-1/2 or spin-3/2 baryon. Unfortunately, the string model is entirely unproductive in this respect, and this is therefore the sector that contains the largest amount of free parameters. From spin counting alone, one would expect the ratio  $V/S$  of vectors to pseudoscalars to be three, but this is modified by the  $V$ – $S$  mass splittings, which implies a phase-space suppression of vector production, with corresponding suppression parameters to be extracted from data.

Especially for the light flavours, the substantial difference in phase space caused by the  $V$ – $S$  mass splittings implies a rather large suppression of vector production. Thus, for  $D^*/D$ , the effective ratio is already reduced to about  $\sim 1.0\text{--}2.0$ , while for  $K^*/K$  and  $\rho/\pi$ , extracted values range from 0.3–1.0. (Recall, as always, that these are production ratios of *primary hadrons*, hence feed-down from secondary decays of heavier hadrons complicates the extraction of these parameters from experimental data, in particular for the lighter hadron species.)



**Fig. 31:** Normalized Lund symmetric fragmentation function, for fixed  $m_{\perp} = 1$  GeV. *Left:* variation of the  $a$  parameter, from 0.1 (blue) to 0.9 (red), with fixed  $b = 1$  GeV $^{-2}$ . *Right:* variation of the  $b$  parameter, from 0.5 (red) to 2 (blue) GeV $^{-2}$ , with fixed  $a = 0.5$ .

The production of higher meson resonances is assumed to be low in a string framework<sup>26</sup>. For diquarks, separate parameters control the relative rates of spin-1 diquarks versus spin-0 ones and, likewise, have to be extracted from data, with resulting values of order  $(qq)_1/(qq)_0 \sim 0.075\text{--}0.15$ .

With  $p_{\perp}^2$  and  $m^2$  now fixed, the final step is to select the fraction,  $z$ , of the fragmenting endpoint quark's longitudinal momentum that is carried by the created hadron. In this respect, the string picture is substantially more predictive than for the flavour selection. Firstly, the requirement that the fragmentation be independent of the sequence in which breakups are considered (causality) imposes a 'left-right symmetry' on the possible form of the fragmentation function,  $f(z)$ , with the solution [150]

$$f(z) \propto \frac{1}{z}(1-z)^a \exp\left(-\frac{b(m_h^2 + p_{\perp h}^2)}{z}\right), \quad (85)$$

which is known as the *Lund symmetric fragmentation function* (normalized to unit integral). The  $a$  and  $b$  parameters, illustrated in Fig. 31, are the only free parameters of the fragmentation function, although  $a$  may in principle be flavour-dependent. Note that the explicit mass dependence in  $f(z)$  implies a harder fragmentation function for heavier hadrons (in the rest frame of the string).

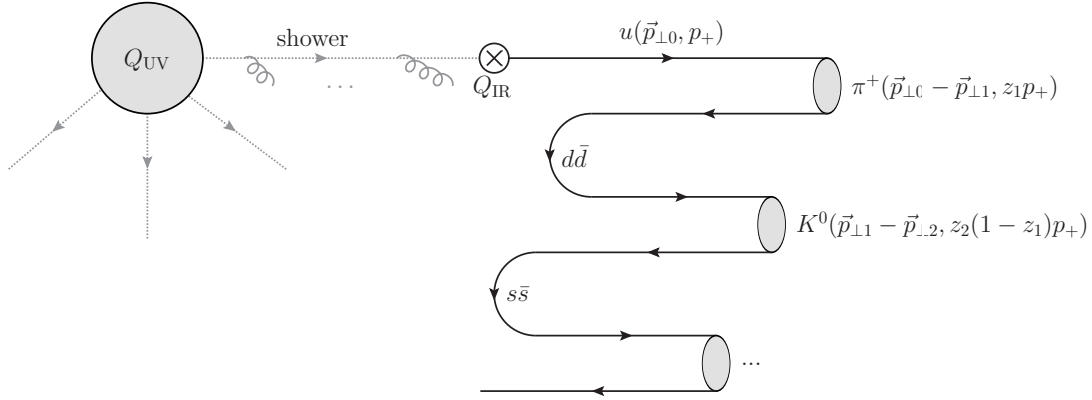
For massive endpoints (e.g.,  $c$  and  $b$  quarks), which do not move along straight lightcone sections, the exponential suppression with string area leads to modifications of the form [151],  $f(z) \rightarrow f(z)/z^{b m_Q^2}$ , with  $m_Q$  the heavy-quark mass. Strictly speaking, this is the only fragmentation function that is consistent with causality in the string model, although a few alternative forms are typically provided as well.

As a by-product, the probability distribution in invariant time  $\tau$  of  $q'\bar{q}'$  breakup vertices, or equivalently  $\Gamma = (\kappa\tau)^2$ , is also obtained, with  $dP/d\Gamma \propto \Gamma^a \exp(-b\Gamma)$  implying an area law for the colour flux [152], and the average breakup time lying along a hyperbola of constant invariant time  $\tau_0 \sim 10^{-23}$  s [6].

We may also ask, for example, how many units of rapidity does the particle production from a string span? Measuring  $p_z$  along the string direction and defining rapidity by

$$y = \frac{1}{2} \ln \left( \frac{E + p_z}{E - p_z} \right), \quad (86)$$

<sup>26</sup>The four  $L = 1$  multiplets are implemented in PYTHIA, but are disabled by default, largely because several states are poorly known and thus may result in a worse overall description when included.



**Fig. 32:** Iterative selection of flavours and momenta in the Lund string-fragmentation model

the absolute highest rapidity that can be reached, by a pion traveling exactly along the string direction and taking all of the endpoint quark’s energy, is  $y_{\max} = \ln(2E_q/m_\pi)$ . That is, the rapidity region covered by a fragmenting string scales logarithmically with the energy, and since the density of hadrons produced per unit rapidity is roughly constant (modulo endpoint effects), the average number of hadrons produced by string fragmentation likewise scales logarithmically with energy.

The iterative selection of flavours,  $p_\perp$ , and  $z$  values is illustrated in Fig. 32. A parton produced in a hard process at some high scale  $Q_{UV}$  emerges from the parton shower, at the hadronization scale  $Q_{IR}$ , with 3-momentum  $\vec{p} = (\vec{p}_{\perp 0}, p_+)$ , where the ‘+’ on the third component denotes ‘light-cone’ momentum,  $p_\pm = E \pm p_z$ . Next, an adjacent  $d\bar{d}$  pair from the vacuum is created, with relative transverse momenta  $\pm p_{\perp 1}$ . The fragmenting quark combines with the  $\bar{d}$  from the breakup to form a  $\pi^+$ , which carries off a fraction  $z_1$  of the total lightcone momentum  $p_+$ . The next hadron carries off a fraction  $z_2$  of the remaining momentum, etc.

## 5.2 Soft hadron–hadron processes

The total hadron–hadron (hh) cross section is around 100 mb at LHC energies [153], growing slowly with the CM energy,  $\sigma_{\text{tot}}(s) \propto s^{0.096}$  [154]. There are essentially four types of physics processes, which together make up  $\sigma_{\text{tot}}$ :

1. elastic scattering:  $hh \rightarrow hh$ ;
2. single diffractive dissociation:  $hh \rightarrow h + \text{gap} + X$ , with ‘gap’ denoting an empty rapidity region, and X anything that is not the original beam particle;
3. double diffractive dissociation:  $hh \rightarrow X + \text{gap} + X$  (both hadrons ‘blow up’);
4. Inelastic non-diffractive scattering: everything else.

In principle, higher ‘multi-gap’ diffractive components may be defined as well, the most important one being central diffraction (CD):  $hh \rightarrow h + \text{gap} + X + \text{gap} + h$ , see the discussion of diffraction in Section 5.2.1 below.

Some important differences exist between theoretical and experimental terminology [155]. In the experimental setting, diffraction is defined by an observable rapidity gap, with  $|\Delta y|_{\text{gap}} \gtrsim 3$  typically giving clean diffractive samples. In the MC context, however, each diffractive process type produces a whole spectrum of gaps, with small ones suppressed but not excluded. Likewise, events of non-diffractive origin may produce accidental rapidity gaps, now with large ones suppressed (exponentially) but not excluded, and in the transition region there could even be quantum mechanical interference between the two. Due to this unphysical model dependence of theoretical definitions of diffraction, we strongly

advise to phrase measurements first and foremost in terms of physical observables, and only seek to connect with theory models as a second, separate, step.

The distinction between elastic and inelastic events *is*, however, unambiguous (modulo  $pp \rightarrow pp\gamma$  events); the final state either contains just two protons, or not. The total hadron–hadron cross section can therefore be written as a sum of these two physically distinguishable components,

$$\sigma_{\text{tot}}(s) = \sigma_{\text{el}}(s) + \sigma_{\text{inel}}(s), \quad (87)$$

where  $s = (p_A + p_B)^2$  is the beam–beam centre-of-mass energy squared.

Another potentially confusing term is ‘minimum bias’ (MB). This originates from the experimental requirement of a minimal energy or number of hits in a given (experiment-dependent) instrumented region near the beam, used to determine whether there was any non-trivial activity in the event, or not. This represents the smallest possible ‘trigger bias’ that the corresponding experiment is capable of. There is thus no universal definition of ‘min-bias’; each experiment has its own. We give a brief discussion of MB in Section 5.2.2 below.

Finally, in events containing a hard parton–parton interaction, the UE can be roughly conceived of as the *difference* between QCD with and without including the remnants of the original beam hadrons. Without such ‘beam remnants’, only the hard interaction itself, and its associated parton showers and hadronization, would contribute to the observed particle production. In reality, after the partons that participate in the hard interaction have been taken out, the remnants still contain whatever is left of the incoming beam hadrons, including also a partonic substructure, which leads to the possibility of *multiple parton interactions* (MPI). We discuss MPI-based models of the UE in Section 5.3 below. Other useful reviews of MPI-based MC models can be found in Refs. [5, 139]. Analytical models are mostly formulated only for double parton scattering, see, for example, Refs. [156–159].

### 5.2.1 *Diffraction scattering*

As mentioned above, if the beam particles  $A$  and/or  $B$  are not elementary, the inelastic final states may be divided into ‘diffractive’ and ‘non-diffractive’ topologies. This is a qualitative classification, usually based on whether the final state looks like the decay of an excitation of the beam particles (diffractive<sup>27</sup>), or not (non-diffractive), or upon the presence of a large rapidity gap somewhere in the final state which would separate such excitations.

Given that an event has been labeled as diffractive, either within the context of a theoretical model, or by a final-state observable, we may distinguish between three different classes of diffractive topologies, which it is possible to distinguish between physically, at least in principle. In double-diffractive (DD) events, both of the beam particles are diffractively excited and hence none of them survive the collision intact. In single-diffractive (SD) events, only one of the beam particles gets excited and the other survives intact. The last diffractive topology is CD, in which both of the beam particles survive intact, leaving an excited system in the central region between them. (This latter topology includes ‘central exclusive production’ where a single particle is produced in the central region.) That is,

$$\sigma_{\text{inel}}(s) = \sigma_{\text{SD}}(s) + \sigma_{\text{DD}}(s) + \sigma_{\text{CD}}(s) + \sigma_{\text{ND}}(s), \quad (88)$$

where ‘ND’ (non-diffractive, here understood not to include elastic scattering) contains no gaps in the event consistent with the chosen definition of diffraction. Further, each of the diffractively excited systems in the events labeled SD, DD and CD, respectively, may in principle consist of several subsystems with gaps between them. Eq. (88) may thus be defined to be exact, within a specific definition of diffraction, even in the presence of multi-gap events. Note, however, that different theoretical models almost

<sup>27</sup>An example of a process that would be labeled as diffractive would be if one of the protons is excited to a  $\Delta^+$  which then decays back to  $p^+ + \pi^0$ , without anything else happening in the event. In general, a whole tower of possible diffractive excitations are available, which in the continuum limit can be described by a mass spectrum falling roughly as  $dM^2/M^2$ .



always use different (model-dependent) definitions of diffraction, and therefore the individual components in one model are in general not directly comparable to those of another. It is therefore important that data be presented at the level of physical observables if unambiguous conclusions are to be drawn from them.

### 5.2.2 *Minimum bias*

In principle, *everything* that produces a hit in a given experiment’s minimum-bias trigger, is a subset of MB. In particular, since there is no explicit veto on hard activity, it is useful to keep in mind that MB includes a diverse mixture of both soft and hard processes, although the fraction that is made up of hard high- $p_{\perp}$  processes is only a small tail compared to the total minimum-bias cross section<sup>28</sup>.

In theoretical contexts, the term ‘minimum-bias’ is often used with a slightly different meaning; to denote specific (classes of) inclusive soft-QCD subprocesses in a given model. Since these two usages are not exactly identical, in these lectures we have chosen to reserve the term ‘MB’ to pertain strictly to definitions of experimental measurements, and instead use the term ‘soft inclusive’ physics as a generic descriptor for the class of processes which generally dominate the various experimental ‘MB’ measurements in theoretical models. This parallels the terminology used in the review Ref. [5], from which most of the discussion here has been adapted. See Eq. (88) above for a compact overview of the types of physical processes that contribute to minimum-bias data samples. For a more detailed description of Monte Carlo models of this physics, see Ref. [5].

## 5.3 Underlying event and multiple parton interactions

In this subsection, we focus on the physics of MPI as a theoretical basis for understanding both inelastic, non-diffractive processes (MB), as well as the so-called underlying event (a.k.a. the jet pedestal effect). Keep in mind, however, that especially at low multiplicities, and when gaps are present, the contributions from diffractive processes should not be ignored.

Due to the simple fact that hadrons are composite, multi-parton interactions (several distinct parton–parton interactions in one and the same hadron–hadron collision) will always be there—but how many, and how much additional energy and tracks do they deposit in a given measurement region? The first detailed Monte Carlo model for perturbative MPI was proposed by Sjöstrand in Ref. [160], and with some variation this still forms the basis for most modern implementations [5].

The first crucial observation is that the  $t$ -channel propagators appearing in pQCD  $2 \rightarrow 2$  scattering almost go on shell at low  $p_{\perp}$ , causing the differential cross sections to become very large, behaving roughly as

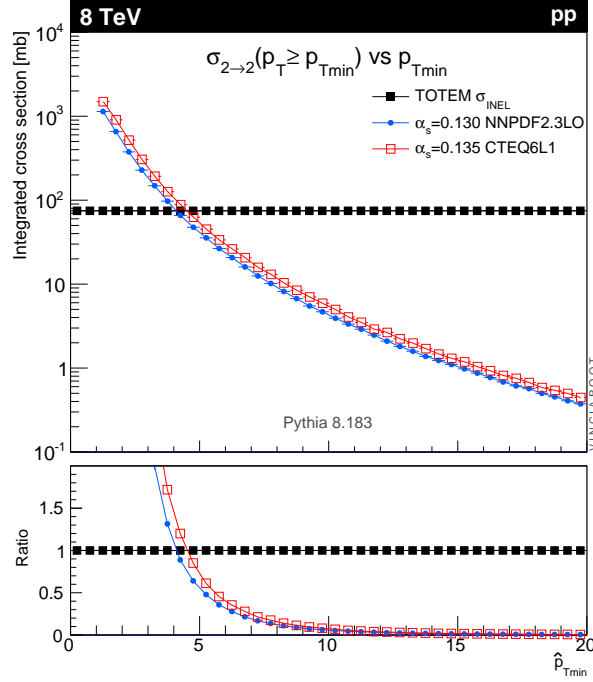
$$d\sigma_{2 \rightarrow 2} \propto \frac{dt}{t^2} \sim \frac{dp_{\perp}^2}{p_{\perp}^4}. \quad (89)$$

At LHC energies, this *parton–parton* cross section becomes larger than the total *hadron–hadron* cross section at  $p_{\perp}$  scales of order 4–5 GeV. This is illustrated in Fig. 33, in which we compare the integrated QCD parton–parton cross section (with two different  $\alpha_s$  and PDF choices) to the total inelastic cross section measured by TOTEM [153], for pp collisions at  $\sqrt{s} = 8$  TeV. In the context of MPI models, this is interpreted straightforwardly to mean that *each* hadron–hadron collision contains *several* few GeV parton–parton collisions.

In the limit that all the partonic interactions are independent and equivalent, one would simply have a Poisson distribution in the number of MPI, with average

$$\langle n \rangle(p_{\perp \min}) = \frac{\sigma_{2 \rightarrow 2}(p_{\perp \min})}{\sigma_{\text{tot}}}, \quad (90)$$

<sup>28</sup> Furthermore, since only a tiny fraction of the total minimum-bias rate can normally be stored, the minimum-bias sample would give quite poor statistics if used for hard physics studies. Instead, separate dedicated hard-process triggers are typically included in addition to the minimum-bias one, in order to ensure maximal statistics also for hard physics processes.



**Fig. 33:** Proton-proton collisions at 8 TeV. LO QCD parton-parton cross section (integrated above  $p_{T\min}$ , for two different  $\alpha_s$  and PDF choices) compared to the total inelastic hadron-hadron cross section. Towards the right of the plot, we see, as expected, that hard dijet events is only a tiny fraction of the total cross section. The fact that the curves cross at a scale of order 5 GeV is interpreted to mean that this is a characteristic scale relevant for MPI. [161].

with  $p_{\perp\min}$  a lower cutoff scale which we shall return to below, and  $\sigma_{\text{tot}}$  a measure of the inelastic hadron-hadron cross section. This simple reinterpretation in fact expresses unitarity; instead of the total interaction cross section diverging as  $p_{\perp\min} \rightarrow 0$  (which would violate unitarity), we have restated the problem so that it is now the *number of MPI per collision* that diverges, with the total cross section remaining finite.

Two important ingredients remain to fully regulate the remaining divergence. Firstly, the interactions cannot use up more momentum than is available in the parent hadron. This suppresses the large- $n$  tail of the estimate above. In PYTHIA-based models, the MPI are ordered in  $p_{\perp}$  [111, 160], and the parton densities for each successive interaction are explicitly constructed so that the sum of  $x$  fractions can never be greater than unity. In the HERWIG models [162, 163], instead the uncorrelated estimate of  $\langle n \rangle$  above is used as an initial guess, but the generation of actual MPI is stopped once the energy-momentum conservation limit is reached.

The second ingredient invoked to suppress the number of interactions, at low  $p_{\perp}$  and  $x$ , is colour screening; if the wavelength  $\sim 1/p_{\perp}$  of an exchanged coloured parton becomes larger than a typical colour-anticolour separation distance, it will only see an *average* colour charge that vanishes in the limit  $p_{\perp} \rightarrow 0$ , hence leading to suppressed interactions. This provides an IR cutoff for MPI similar to that provided by the hadronization scale for parton showers. A first estimate of the colour-screening cutoff would be the proton size,  $p_{\perp\min} \approx \hbar/r_p \approx 0.3 \text{ GeV} \approx \Lambda_{\text{QCD}}$ , but empirically this appears to be far too low. In current models, one replaces the proton radius  $r_p$  in the above formula by a ‘typical colour screening distance’, that is, an average size of a region within which the net compensation of a given colour charge occurs. This number is not known from first principles, although it may be related to saturation [164]. In current MPI models, it is perceived of simply as an effective cutoff parameter, to be determined from data.

Note that the partonic cross sections depend upon the PDF set used, and therefore the optimal value to use for the cutoff will also depend on this choice [165]. Note also that the cutoff does not have to be energy-independent. Higher energies imply that parton densities can be probed at smaller  $x$  values, where the number of partons rapidly increases. Partons then become closer packed and the colour-screening distance  $d$  decreases. The uncertainty on the scaling of the cutoff is a major concern when extrapolating between different collider energies [165–167].

We now turn to the origin of the observational fact that hard jets appear to sit on top of a higher ‘pedestal’ of underlying activity than events with no hard jets. That is, the so-called UE is much more active, with larger fluctuations, than the average min-bias event. This is interpreted as a consequence of impact-parameter-dependence: in peripheral collisions, only a small fraction of events contain any high- $p_{\perp}$  activity, whereas central collisions are more likely to contain at least one hard scattering; a high- $p_{\perp}$  triggered sample will therefore be biased towards small impact parameters,  $b$ , with a large number of MPI (and associated increased activity). The ability of a model to describe the shape of the pedestal (e.g., to describe both MB and UE distributions simultaneously) therefore depends upon its modelling of the  $b$ -dependence, and correspondingly the impact-parameter shape constitutes another main tuning parameter. A detailed discussion of impact-parameter dependent models goes beyond the scope of these lectures; see Refs. [149, 160, 168].

For hard processes at the LHC at 13 TeV, the transverse energy,  $E_T$ , in the UE is expected to be about 3.3 GeV per unit  $\Delta R = \sqrt{\Delta\phi^2 + \Delta\eta^2}$  area [167] (for a reference case of 100 GeV dijets, including both charged and neutral particles, with no cut on  $p_{\perp}$ ), although with large event-to-event fluctuations of order  $\pm 2$  GeV [169]. Thus, for example, the total  $E_T$  originating from the UE, in a cone with radius 0.4 can be estimated to be  $E_{TUE}(R = 0.4) \sim 1.6 \pm 1$  GeV, while the  $E_T$  in a cone with radius 1.0 would be  $E_{TUE}(R = 1.0) \sim 10 \pm 6$  GeV. Note that the magnetic field in realistic detectors will deflect some fraction of the soft charged component of the underlying event into helix trajectories that will hence not contribute to the energy deposition in the calorimeters.

## 5.4 Tuning

A main virtue of general-purpose Monte Carlo event generators is their ability to provide a complete and fully differential picture of collider final states, down to the level of individual particles. As has been emphasized in these lectures, the achievable accuracy depends both on the inclusiveness of the chosen observable and on the sophistication of the simulation itself. An important driver for the latter is obviously the development of improved theoretical models, for example, by including matching to higher-order MEs, more accurate resummations or better non-perturbative models, as discussed in the previous sections, but it also depends crucially on the available constraints on the remaining free parameters of the model. Using existing data (or more precise calculations) to constrain these is referred to as generator tuning.

Keep in mind that generators attempt to deliver a *global* description of the data; a tune is no good if it fits one distribution perfectly, but not any others. It is therefore crucial to study the simultaneous degree of agreement or disagreement over many, mutually complementary, distributions. A useful online resource for making such comparisons can be found at the MCPLOTS web site [170] (which relies on computing power donated by volunteers, via the LHC@home project [171]). The analyses come from the comprehensive RIVET analysis toolkit [95], which can also be run stand-alone to make your own MC tests and comparisons.

Although MC models may appear to have a bewildering number of independently adjustable parameters, it is worth noting that most of these only control relatively small (exclusive) details of the event generation. The majority of the (inclusive) physics is determined by only a few, very important ones, such as the value of the strong coupling, in the perturbative domain, and the form of the fragmentation function for massless partons, in the non-perturbative one.

Armed with a good understanding of the underlying model, an expert would therefore normally take a highly factorized approach to constraining the parameters, first constraining the perturbative ones (using IR-safe observables and/or more precise theory calculations) and thereafter the non-perturbative ones, each ordered in a measure of their relative significance to the overall modelling. This allows one to concentrate on just a few parameters and a few carefully chosen distributions at a time, reducing the full parameter space to manageable-sized chunks. Still, each step will often involve more than one single parameter, and non-factorizable correlations may still necessitate additional iterations from the beginning before a fully satisfactory set of parameters is obtained.

Recent years have seen the emergence of automated tools that attempt to reduce the amount of both computer and manpower required for this task, for instance by making full generator runs only for a limited set of parameter points, and then interpolating between these to obtain approximations to what the true generator result would have been for any intermediate parameter point, as, for example, in PROFESSOR [172]. Automating the human expert input is more difficult. Currently, this is addressed by a combination of input solicited from the generator authors (e.g., which parameters and ranges to consider, which observables constitute a complete set, etc) and the elaborate construction of non-trivial weighting functions that determine how much weight is assigned to each individual bin in each distribution. The field is still burgeoning, and future sophistications are to be expected. Nevertheless, at this point the overall quality of the tunes obtained with automated methods appear to at least be competitive with the manual ones.

However, although we have very good LHC tunes for essentially all the general-purpose generators by now, there are two important aspects which have so far been neglected, and which it is becoming increasingly urgent to address. The first is that a central tune is not really worth much, unless you know what the uncertainty on it is. A few individual proposals for systematic tuning variations have been made [166, 173], but so far there is no general approach for establishing MC uncertainties by tune variations. The second issue is that virtually all generator tuning is done at the ‘pure’ LL-shower level, and not much is known about what happens to the tuning when matrix-element matching is subsequently included.

Finally, rather than performing one global tune to all the data, as is usually done, a more systematic check on the validity of the underlying physics model could be obtained by instead performing several independent optimizations of the model parameters for a range of different phase-space windows and/or collider environments. In regions in which consistent parameter sets are obtained (with reasonable  $\Delta\chi^2$  values), the underlying model can be considered as interpolating well, that is, it is universal. If not, a breakdown in the ability of the model to span different physical regimes has been identified, and can be addressed, with the nature of the deviations giving clues as to the nature of the breakdown. With the advent of automated tools, such systematic studies are now becoming feasible, with a first example given in Ref. [165].

We round off by giving a sketch of a reasonably complete tuning procedure, without going into details about the parameters that control each of these sectors in individual Monte Carlo models (a recent detailed discussion in the context of PYTHIA 8 can be found in Ref. [161]).

1) **Keep in mind** that inabilities of models to describe data is a vital part of the feedback cycle between theory and experiment. Also keep in mind that perturbation theory at (N)LO+LL is doing *very well* if it gets within 10% of a given IR-safe measurement. An agreement of 5% should be considered the absolute sanity limit, beyond which it does not make any sense to tune further. For some quantities, for example, ones for which the underlying modelling is *known* to be poor, an order-of-magnitude agreement or worse may have to be accepted.

2) **Final-state radiation and hadronization:** mainly using LEP and other  $e^+e^-$  collider data. On the IR safe side, there are event shapes and jet observables. On the IR sensitive side, multiplicities and particle spectra. Pay attention to the high- $z$  tail of the fragmentation, where a single hadron carries a large fraction of an entire jet’s momentum (most likely to give ‘fakes’). Depending on the focus of the tuning,

attention should also be paid to identified-particle rates and ratios (perhaps with a nod to hadron-collider measurements), and to fragmentation in events containing heavy quarks and/or gluon jets. Usually, more weight is given to those particles that are most copiously produced. The scaling properties of IR-safe versus IR-sensitive contributions can be tested by comparing data at several different  $e^+e^-$  collider energies.

3) **Initial-state radiation, and ‘primordial’<sup>29</sup>  $k_T$** : the main constraining distribution is the dilepton  $p_\perp$  distribution in Drell–Yan events in hadron–hadron collisions. Ideally, one would like to use several different  $Q^2$  values, and/or complementary processes, like  $p_\perp$  (dijet) or  $p_\perp$  ( $t\bar{t}$ ). For any observables containing explicit jets, be aware that the UE can produce small horizontal shifts in jet  $p_\perp$  distributions, which may in turn result in larger-than-expected vertical changes if the distributions are falling sharply. Also note that the ISR evolution is sensitive to the choice of PDFs.

4) **Initial–final connections**: radiation from colour lines connecting the initial and final states. DIS and jet broadening in hadron collisions. This is one of the most poorly controlled parts of most MC models, highly sensitive to the treatment of coherence (see, e.g., Ref. [174] for illustrations). Keep in mind that it is *not* directly constrained by pure final-state observables, such as LEP fragmentation, nor by pure initial-state observables, such as the Drell–Yan  $p_\perp$  spectrum, which is why we list it as a separate item here. The modelling of this aspect can have important effects on specific observables, a recent example being the  $t\bar{t}$  forward-backward asymmetry at the Tevatron [175].

5) **Underlying event**: good constraints on the overall level of the underlying event can be obtained by counting the summed transverse energy (more IR safe) and/or particle multiplicities and average transverse momenta (more IR sensitive) in regions *transverse* to a hard trigger jet (more IR safe) or particle (more IR sensitive), see, for example, Ref. [176]. Constraints on the *fluctuations* of the underlying event are also important, and can be obtained, for example, by comparing to measurements of the RMS of such distributions [169]. Again, note that the UE is sensitive to the choice of PDFs [165].

6) **Colour (re-)connections and other final-state interactions**: by final-state interactions, we intend a broad spectrum of possible collective effects that may be included to a greater or lesser extent in various models. These effects include: Bose–Einstein correlations (see, e.g., Ref. [177]), rescattering (see, e.g., Ref. [178]), colour reconnections / string interactions (see, e.g., Ref. [179–181]), hydrodynamics (see, e.g., Ref. [182]), etc. As a rule, these effects are soft and/or non-perturbative and hence should not modify hard IR-safe observables appreciably. They can, however, have *drastic* effects on IR-sensitive ones, such as particle multiplicities, momentum distributions, and correlations, wherefore useful constraints are typically furnished by measurements of spectra and correlations as functions of quantities believed to serve as indicators of the strength of these phenomena (such as event multiplicity), and/or by collective-flow-type measurements. Finally, if the model includes a universal description of underlying event and soft-inclusive QCD, as many MPI-based models do, then minimum-bias data can also be used as a control sample, although one must then be careful either to address diffractive contributions properly or to include only gap-suppressed data samples. A complete MB and UE model should also be able to describe the rise of the pedestal from MB to UE, for example, in the transverse UE observables (see above).

7) **Beam remnants**: constraints on beam remnant fragmentation (see, e.g., Ref. [149]) are most easily obtained in the forward region, but, for example, the amount of baryon transport from the remnant to a given rapidity region can also be used to probe how much the colour structure of the remnant was effectively disturbed, with more baryon transport indicating a larger amount of ‘beam baryon blowup’.

<sup>29</sup>Primordial  $k_T$ : an additional soft  $p_\perp$  component that is injected on top of the  $p_\perp$  generated by the initial-state shower itself, see Ref. [5, Section 7.1].

## Acknowledgments

Thanks go to C. Brust, M. Cacciari, Y. Dokshitzer, L. Hartgring, A. Kronfeld, A. Larkoski, J. Lopez-Villarejo, C. Murphy, P. Nason, P. Pigard, S. Prestel, G. Salam, and T. Sjöstrand whose valuable comments and sharing of insight contributed to these lectures. In addition, I have used material from my 2010 ESHEP lectures [139] and 2014 AEPSHEP lectures, and from the ESHEP lectures by Mangano [183], by Salam [4, 184], by Sjöstrand [41], and by Stirling [185], as well as the recent review on Monte Carlo event generators by the MCnet collaboration [5].

## References

- [1] M.E. Peskin and D.V. Schroeder, *An Introduction to Quantum Field Theory* (Addison-Wesley, 1995).
- [2] R.K. Ellis, W.J. Stirling and B.R. Webber, *Camb. Monogr. Part. Phys. Nucl. Phys. Cosmol.* **8** (1996) 1.
- [3] G. Dissertori, I.G. Knowles and M. Schmelling, *Quantum Chromodynamics — High Energy Experiments and Theory* (Oxford Science Publications, Oxford, 2003).
- [4] Gavin P. Salam, Elements of QCD for hadron colliders, Proc. 17th European School on High-Energy Physics (ESHEP), Bautzen, Germany, 2009, arXiv:1012.4643.
- [5] A. Buckley *et al.*, *Phys. Rept.* **504**(5) (2011) 145.  
<http://dx.doi.org/10.1016/j.physrep.2011.03.005>
- [6] B. Andersson, *Camb. Monogr. Part. Phys. Nucl. Phys. Cosmol.* **7** (1997) 1.
- [7] F. James, *Rept. Prog. Phys.* **43**(9) (1980) 1145. <http://dx.doi.org/10.1088/0034-4885/43/9/002>
- [8] Stefan Weinzierl, Introduction to Monte Carlo methods (2000),  
<https://arxiv.org/abs/hep-ph/0006269>
- [9] K.A. Brueckner, *Phys. Rev.* **86**(1) (1952) 106. <http://dx.doi.org/10.1103/PhysRev.86.106>
- [10] C. Chedester *et al.*, *Phys. Rev.* **82**(6) (1951) 958. <http://dx.doi.org/10.1103/PhysRev.82.958>
- [11] E. Fermi *et al.*, *Phys. Rev.* **85**(5) (1952) 935. <http://dx.doi.org/10.1103/PhysRev.85.935>
- [12] H.L. Anderson *et al.*, *Phys. Rev.* **85**(5) (1952) 936. <http://dx.doi.org/10.1103/PhysRev.85.936>
- [13] H.L. Anderson *et al.*, *Phys. Rev.* **86**(3) (1952) 413. <http://dx.doi.org/10.1103/PhysRev.86.413>
- [14] D.E Nagle, The delta: The first pion nucleon resonance: Its discovery and applications, LALP-84-27, DE84 017107, based on a lecture given at the University of Chicago Symposium in honor of H.L. Anderson, May 11, 1982 (1984).
- [15] O.W. Greenberg, *Phys. Rev. Lett.* **13**(20) (1964) 598.  
<http://dx.doi.org/10.1103/PhysRevLett.13.598>
- [16] M.Y. Han and Y. Nambu, *Phys. Rev.* **139**(4B) (1965) B1006.  
<http://dx.doi.org/10.1103/PhysRev.139.B1006>
- [17] S.D. Drell and T.-M. Yan, *Phys. Rev. Lett.* **25**(5) (1970) 316.  
<http://dx.doi.org/10.1103/PhysRevLett.25.316>
- [18] T. Plehn, D. Rainwater and P.Z. Skands, *Phys. Lett. B* **645**(2-3) (2007) 217.  
<http://dx.doi.org/10.1016/j.physletb.2006.12.009>
- [19] J. Alwall, S. de Visscher and F. Maltoni, *J. High Energy Phys.* **0902** (2009) 017.  
<http://dx.doi.org/10.1088/1126-6708/2009/02/017>
- [20] A. Papaefstathiou and B. Webber, *J. High Energy Phys.* **06** (2009) 069.  
<http://dx.doi.org/10.1088/1126-6708/2009/06/069>
- [21] D. Krohn, L. Randall and L.-T. Wang, On the feasibility and utility of ISR tagging (2011),  
<https://arxiv.org/abs/1101.0810>

- [22] C.K. Vermilion, PhD Thesis, Jet substructure at the Large Hadron Collider: Harder, better, faster, stronger (2011), <https://arxiv.org/abs/1101.1335>
- [23] A. Altheimer *et al.*, *J. Phys. G: Nucl. Part. Phys. G* **39**(6) (2012) 063001.  
<http://dx.doi.org/10.1088/0954-3899/39/6/063001>
- [24] J. Beringer *et al.*, *Phys. Rev. D* **86**(1) (2012) 010001.  
<http://dx.doi.org/10.1103/PhysRevD.86.010001>
- [25] S.P. Martin, A Supersymmetry primer (1997), [http://dx.doi.org/10.1142/9789812839657\\_0001](http://dx.doi.org/10.1142/9789812839657_0001)
- [26] S. Bethke, *Nucl. Phys. Proc. Suppl.* **234** (2013) 229.  
<http://dx.doi.org/10.1016/j.nuclphysbps.2012.12.020>
- [27] S. Bethke, *Eur. Phys. J. C* **64**(4) (2009) 689. <http://dx.doi.org/10.1140/epjc/s10052-009-1173-1>
- [28] G. Dissertori, A. Gehrmann-De Ridder *et al.*, *J. High Energy Phys.* **0908** (2009) 036.  
<http://dx.doi.org/10.1088/1126-6708/2009/08/036>
- [29] A. Young, *Proc. London Math. Soc.* **33** (1901) 97.
- [30] B.E. Sagan, in *Invariant Theory and Tableaux*, Ed. D. Stanton (Springer, 1990), p. 262.  
<http://www.mth.msu.edu/users/sagan/Papers/Old/uyt.pdf>.
- [31] J. Alwall *et al.*, *J. High Energy Phys.* **1106** (2011) 128.  
[http://dx.doi.org/10.1007/JHEP06\(2011\)128](http://dx.doi.org/10.1007/JHEP06(2011)128)
- [32] A. Pukhov, Calcchep 2.3: MSSM, structure functions, event generation, 1, and generation of matrix elements for other packages (2004), <https://arxiv.org/abs/hep-ph/0412191>
- [33] E. Boos *et al.*, *Nucl. Instrum. Meth. A* **534**(1-2) (2004) 50.  
<http://dx.doi.org/10.1016/j.nima.2004.07.096>
- [34] A. Kanaki and C.G. Papadopoulos, *Comput. Phys. Commun.* **132**(3) (2000) 306.  
[http://dx.doi.org/10.1016/S0010-4655\(00\)00151-X](http://dx.doi.org/10.1016/S0010-4655(00)00151-X)
- [35] F. Krauss, R. Kuhn and G. Soff, *J. High Energy Phys.* **0202** (2002) 044.  
<http://dx.doi.org/10.1088/1126-6708/2002/02/044>
- [36] M. Moretti, T. Ohl and Jurgen Reuter, O'Mega: An optimizing matrix element generator (2001), <https://arxiv.org/abs/hep-ph/0102195>
- [37] W. Kilian, T. Ohl and J. Reuter, *Eur. Phys. J. C* **71** (2011) 1742.  
<http://dx.doi.org/10.1140/epjc/s10052-011-1742-y>
- [38] A. Cafarella, C.G. Papadopoulos and M. Worek, *Comput. Phys. Commun.* **180**(10) (2009) 1941.  
<http://dx.doi.org/10.1016/j.cpc.2009.04.023>
- [39] M. Bähr *et al.*, *Eur. Phys. J. C* **58**(4) (2008) 639.  
<http://dx.doi.org/10.1140/epjc/s10052-008-0798-9>
- [40] T. Gleisberg and S. Hoeche, *J. High Energy Phys.* **0812** (2008) 039.  
<http://dx.doi.org/10.1088/1126-6708/2008/12/039>
- [41] T. Sjöstrand. Monte Carlo Generators (2006), <https://arxiv.org/abs/hep-ph/0611247>
- [42] J.C. Collins and D.E. Soper, *Nucl. Phys. B* **194**(3) (1982) 445.  
[http://dx.doi.org/10.1016/0550-3213\(82\)90021-9](http://dx.doi.org/10.1016/0550-3213(82)90021-9)
- [43] G.F. Sterman. Partons, factorization and resummation, TASI 95 (1995), <https://arxiv.org/abs/hep-ph/9606312>
- [44] R. Brock *et al.*, *Rev. Mod. Phys.* **67**(1) (1995) 157.  
<http://dx.doi.org/10.1103/RevModPhys.67.157>
- [45] T. Plehn, LHC Phenomenology for Physics Hunters (2008), pp. 125–180,  
[http://dx.doi.org/10.1142/9789812838360\\_0003](http://dx.doi.org/10.1142/9789812838360_0003)
- [46] J.C. Collins *et al.*, *Nucl. Phys. B* **250**(1-4) (1985) 199.  
[http://dx.doi.org/10.1016/0550-3213\(85\)90479-1](http://dx.doi.org/10.1016/0550-3213(85)90479-1)

- [47] G. Altarelli and G. Parisi, *Nucl. Phys. B* **126**(2) (1977) 298.  
[http://dx.doi.org/10.1016/0550-3213\(77\)90384-4](http://dx.doi.org/10.1016/0550-3213(77)90384-4)
- [48] V.N. Gribov and L.N. Lipatov, *Sov. J. Nucl. Phys.* **15**(4) (1972) 438.
- [49] Y.L. Dokshitzer, *Sov. Phys. JETP* **46** (1977) 641.
- [50] D. Mason *et al.*, *Phys. Rev. Lett.* **99**(19) (2007) 192001.  
<http://dx.doi.org/10.1103/PhysRevLett.99.192001>
- [51] A. Cooper-Sarkar, *J. Phys. G: Nucl. Part. Phys. G* **39** (2012) 093001,  
<http://dx.doi.org/10.1088/0954-3899/39/9/093001>
- [52] S. Alekhin, K. Melnikov and F. Petriello, *Phys. Rev. D* **74**(5) (2006) 054033.  
<http://dx.doi.org/10.1103/PhysRevD.74.054033>
- [53] E.G. de Oliveira, A.D. Martin and M.G. Ryskin, *Eur. Phys. J. C* **72** (2012) 2069.  
<http://dx.doi.org/10.1140/epjc/s10052-012-2069-z>
- [54] S. Alekhin *et al.*, The PDF4LHC Working Group Interim Report, (2011),  
<https://arxiv.org/abs/1101.0536>
- [55] A. Buckley and M. Whalley, HepData reloaded: reinventing the HEP data archive (2010),  
<https://arxiv.org/abs/1006.0517> <http://hepdata.cedar.ac.uk>.
- [56] A.D. Martin *et al.*, *Eur. Phys. J. C* **63**(2) (2009) 189.  
<http://dx.doi.org/10.1140/epjc/s10052-009-1072-5>
- [57] J. Pumplin *et al.*, *J. High Energy Phys.* **0207** (2002) 012.  
<http://dx.doi.org/10.1088/1126-6708/2002/07/012>
- [58] G. Watt and R.S. Thorne, *J. High Energy Phys.* **1208** (2012) 052.  
[http://dx.doi.org/10.1007/JHEP08\(2012\)052](http://dx.doi.org/10.1007/JHEP08(2012)052)
- [59] M. Bengtsson, T. Sjöstrand and M. van Zijl, *Z. Phys. C* **32**(1) (1986) 67.  
<http://dx.doi.org/10.1007/BF01441353>
- [60] S. Gieseke, *J. High Energy Phys.* **0501** (2005) 058.  
<http://dx.doi.org/10.1088/1126-6708/2005/01/058>
- [61] Z. Bern *et al.*, The NLO multileg working group: Summary report, (2008) pp. 83,  
<https://arxiv.org/abs/0803.0494>
- [62] T. Kinoshita, *J. Math. Phys.* **3**(4) (1962) 650. <http://dx.doi.org/10.1063/1.1724268>
- [63] T.D. Lee and M. Nauenberg, *Phys. Rev.* **133**(6B) (1964) B1549.  
<http://dx.doi.org/10.1103/PhysRev.133.B1549>
- [64] S. Catani and M.H. Seymour, *Nucl. Phys. B* **485**(1-2) (1997) 291.  
[http://dx.doi.org/10.1016/S0550-3213\(96\)00589-5](http://dx.doi.org/10.1016/S0550-3213(96)00589-5)
- [65] S. Catani and M.H. Seymour, *Phys. Lett. B* **378**(1-4) (1996) 287.  
[http://dx.doi.org/10.1016/0370-2693\(96\)00425-X](http://dx.doi.org/10.1016/0370-2693(96)00425-X)
- [66] Z. Nagy, *Phys. Rev. D* **68**(9) (2003) 094002. <http://dx.doi.org/10.1103/PhysRevD.68.094002>
- [67] R. Frederix, T. Gehrmann and N. Greiner, *J. High Energy Phys.* **09** (2008) 122.  
<http://dx.doi.org/10.1088/1126-6708/2008/09/122>
- [68] D.A. Kosower, *Phys. Rev. D* **57**(9) (1998) 5410. <http://dx.doi.org/10.1103/PhysRevD.57.5410>
- [69] D.A. Kosower. *Phys. Rev. D* **71**(4) (2005) 045016.  
<http://dx.doi.org/10.1103/PhysRevD.71.045016>
- [70] A. Gehrmann-De Ridder, T. Gehrmann and E.W.N. Glover, *J. High Energy Phys.* **09** (2005) 056.  
<http://dx.doi.org/10.1088/1126-6708/2005/09/056>
- [71] A. Gehrmann-De Ridder *et al.*, *J. High Energy Phys.* **0712** (2007) 094.  
<http://dx.doi.org/10.1088/1126-6708/2007/12/094>
- [72] S. Weinzierl, *Phys. Rev. Lett.* **101**(16) (2008) 162001.



- <http://dx.doi.org/10.1103/PhysRevLett.101.162001>
- [73] G. Heinrich, *Int. J. Mod. Phys. A* **23**(10) (2008) 1457.  
<http://dx.doi.org/10.1142/S0217751X08040263>
- [74] R. Boughezal, K. Melnikov and F. Petriello, *Phys. Rev. D* **85**(3) (2012) 034025.  
<http://dx.doi.org/10.1103/PhysRevD.85.034025>
- [75] S. Catani and M. Grazzini, *Phys. Rev. Lett.* **98**(22) (2007) 222002.  
<http://dx.doi.org/10.1103/PhysRevLett.98.222002>
- [76] G. Gustafson and U. Pettersson, *Nucl. Phys. B* **306**(4) (1988) 746.  
[http://dx.doi.org/10.1016/0550-3213\(88\)90441-5](http://dx.doi.org/10.1016/0550-3213(88)90441-5)
- [77] A. Gehrmann-De Ridder and M. Ritzmann, *J. High Energy Phys.* **0907** (2009) 041.  
<http://dx.doi.org/10.1088/1126-6708/2009/07/041>
- [78] A. Gehrmann-De Ridder, M. Ritzmann and P. Skands, *Phys. Rev. D* **85**(1) (2012) 014013.  
<http://dx.doi.org/10.1103/PhysRevD.85.014013>
- [79] A.J. Larkoski and M.E. Peskin, *Phys. Rev. D* **81**(5) (2010) 054010.  
<http://dx.doi.org/10.1103/PhysRevD.81.054010>
- [80] W.T. Giele, D.A. Kosower and P.Z. Skands, *Phys. Rev. D* **84**(5) (2011) 054003.  
<http://dx.doi.org/10.1103/PhysRevD.84.054003>
- [81] J.J. Lopez-Villarejo and P. Skands, *J. High Energy Phys.* **1111** (2011) 150.  
[http://dx.doi.org/10.1007/JHEP11\(2011\)150](http://dx.doi.org/10.1007/JHEP11(2011)150)
- [82] A. Banfi, G.P. Salam and G. Zanderighi, *J. High Energy Phys.* **1006** (2010) 038.  
[http://dx.doi.org/10.1007/JHEP06\(2010\)038](http://dx.doi.org/10.1007/JHEP06(2010)038)
- [83] V. Khachatryan *et al.*, *Phys. Lett. B* **699**(1-2) (2011) 48.  
<http://dx.doi.org/10.1016/j.physletb.2011.03.060>
- [84] G. Aad *et al.*, *Eur. Phys. J. C* **72** (2012) 2211. <http://dx.doi.org/10.1140/epjc/s10052-012-2211-y>
- [85] K. Wraight and P. Skands, *Eur. Phys. J. C* **71** (2011) 1628.  
<http://dx.doi.org/10.1140/epjc/s10052-011-1628-z>
- [86] M. Cacciari, G.P. Salam and G. Soyez, *J. High Energy Phys.* **0804** (2008) 063.  
<http://dx.doi.org/10.1088/1126-6708/2008/04/063>
- [87] A. Abdesselam *et al.*, *Eur. Phys. J. C* **71** (2011) 1661.  
<http://dx.doi.org/10.1140/epjc/s10052-011-1661-y>
- [88] M. Cacciari, G.P. Salam and S. Sapeta, *J. High Energy Phys.* **1004** (2010) 065.  
[http://dx.doi.org/10.1007/JHEP04\(2010\)065](http://dx.doi.org/10.1007/JHEP04(2010)065)
- [89] G. Corcella *et al.*, *J. High Energy Phys.* **01** (2001) 010.  
<http://dx.doi.org/10.1088/1126-6708/2001/01/010>
- [90] T. Sjöstrand, S. Mrenna and P. Skands, *J. High Energy Phys.* **05** (2006) 026.  
<http://dx.doi.org/10.1088/1126-6708/2006/05/026>
- [91] T. Sjöstrand *et al.*, An Introduction to PYTHIA 8.2 (2014),  
<http://doi.org/10.1016/j.cpc.2015.01.024>
- [92] T. Gleisberg *et al.*, *J. High Energy Phys.* **02** (2009) 007.  
<http://dx.doi.org/10.1088/1126-6708/2009/02/007>
- [93] E. Boos *et al.*, Generic user process interface for event generators (2001),  
<https://arxiv.org/abs/hep-ph/0109068>
- [94] J. Alwall *et al.*, *Comput. Phys. Commun.* **176**(4) (2007) 300.  
<http://dx.doi.org/10.1016/j.cpc.2006.11.010>
- [95] A. Buckley *et al.*, Rivet user manual (2010), <https://arxiv.org/abs/1003.0694>
- [96] S. Agostinelli *et al.*, *Nucl. Instrum. Meth. A* **506**(3) (2003) 250.

- [http://dx.doi.org/10.1016/S0168-9002\(03\)01368-8](http://dx.doi.org/10.1016/S0168-9002(03)01368-8)
- [97] M. Dobbs and J.B. Hansen, *Comput. Phys. Commun.* **134**(1) (2001) 41.  
[http://dx.doi.org/10.1016/S0010-4655\(00\)00189-2](http://dx.doi.org/10.1016/S0010-4655(00)00189-2)
- [98] T. Sjöstrand, Monte Carlo Tools (2009), <https://arxiv.org/abs/0911.5286>
- [99] R. Kleiss, W.J. Stirling and S.D. Ellis, *Comput. Phys. Commun.* **40**(2-3) (1986) 359.  
[http://dx.doi.org/10.1016/0010-4655\(86\)90119-0](http://dx.doi.org/10.1016/0010-4655(86)90119-0)
- [100] G.P. Lepage, *J. Comput. Phys.* **27**(2) (1978) 192.  
[http://dx.doi.org/10.1016/0021-9991\(78\)90004-9](http://dx.doi.org/10.1016/0021-9991(78)90004-9)
- [101] G.P. Lepage, VEGAS – An adaptive multi-dimensional integration program, CLNS-80/447 (1980), <http://inspirehep.net/record/153221/>
- [102] P.D. Draggotis, A. van Hameren and R. Kleiss, *Phys. Lett. B* **483**(1-3) (2000) 124.  
[http://dx.doi.org/10.1016/S0370-2693\(00\)00532-3](http://dx.doi.org/10.1016/S0370-2693(00)00532-3)
- [103] G. Marchesini and B.R. Webber, *Nucl. Phys. B* **238**(1) (1984) 1.  
[http://dx.doi.org/10.1016/0550-3213\(84\)90463-2](http://dx.doi.org/10.1016/0550-3213(84)90463-2)
- [104] G. Marchesini and B.R. Webber, *Nucl. Phys. B* **310**(3-4) (1988) 461.  
[http://dx.doi.org/10.1016/0550-3213\(88\)90089-2](http://dx.doi.org/10.1016/0550-3213(88)90089-2)
- [105] S. Gieseke, P. Stephens and B. Webber, *J. High Energy Phys.* **12** (2003) 045.  
<http://dx.doi.org/10.1088/1126-6708/2003/12/045>
- [106] M. Bengtsson and T. Sjöstrand, *Nucl. Phys. B* **289** (1987) 810.  
[http://dx.doi.org/10.1016/0550-3213\(87\)90407-X](http://dx.doi.org/10.1016/0550-3213(87)90407-X)
- [107] L. Lönnblad, *Comput. Phys. Commun.* **71**(1-2) (1992) 15.  
[http://dx.doi.org/10.1016/0010-4655\(92\)90068-A](http://dx.doi.org/10.1016/0010-4655(92)90068-A)
- [108] Z. Nagy and D.E. Soper, *J. High Energy Phys.* **10** (2005) 024.  
<http://dx.doi.org/10.1088/1126-6708/2005/10/024>
- [109] S. Schumann and F. Krauss, *J. High Energy Phys.* **0803** (2008) 038.  
<http://dx.doi.org/10.1088/1126-6708/2008/03/038>
- [110] W.T. Giele, D.A. Kosower and P.Z. Skands, *Phys. Rev. D* **78**(1) (2008) 014026.  
<http://dx.doi.org/10.1103/PhysRevD.78.014026>
- [111] T. Sjöstrand and P.Z. Skands, *Eur. Phys. J. C* **39**(2) (2005) 129.  
<http://dx.doi.org/10.1140/epjc/s2004-02084-y>
- [112] N. Fischer *et al.*, *Eur. Phys. J. C* **74** (2014) 2831.  
<http://dx.doi.org/10.1140/epjc/s10052-014-2831-5>
- [113] J.C. Collins, *Nucl. Phys. B* **304** (1988) 794. [http://dx.doi.org/10.1016/0550-3213\(88\)90654-2](http://dx.doi.org/10.1016/0550-3213(88)90654-2)
- [114] I.G. Knowles, *Nucl. Phys. B* **310**(3-4) (1988) 571.  
[http://dx.doi.org/10.1016/0550-3213\(88\)90092-2](http://dx.doi.org/10.1016/0550-3213(88)90092-2)
- [115] P. Richardson, *J. High Energy Phys.* **11** (2001) 029.  
<http://dx.doi.org/10.1088/1126-6708/2001/11/029>
- [116] S. Catani, B.R. Webber and G. Marchesini, *Nucl. Phys. B* **349**(3) (1991) 635.  
[http://dx.doi.org/10.1016/0550-3213\(91\)90390-J](http://dx.doi.org/10.1016/0550-3213(91)90390-J)
- [117] M.A. Gigg and P. Richardson, Simulation of finite width effects in physics beyond the standard model (2008), <https://arxiv.org/abs/0805.3037>
- [118] M.H. Seymour, *Phys. Lett. B* **354**(3-4) (1995) 409.  
[http://dx.doi.org/10.1016/0370-2693\(95\)00699-L](http://dx.doi.org/10.1016/0370-2693(95)00699-L)
- [119] T. Stelzer and S. Willenbrock, *Phys. Lett. B* **374**(1-3) (1996) 169.  
[http://dx.doi.org/10.1016/0370-2693\(96\)00178-5](http://dx.doi.org/10.1016/0370-2693(96)00178-5)
- [120] S.J. Parke and Y. Shadmi, *Phys. Lett. B* **387**(1) (1996) 199.

- [http://dx.doi.org/10.1016/0370-2693\(96\)00998-7](http://dx.doi.org/10.1016/0370-2693(96)00998-7)
- [121] J.M. Smillie and B.R. Webber, *J. High Energy Phys.* **0510** (2005) 069.  
<http://dx.doi.org/10.1088/1126-6708/2005/10/069>
- [122] M.H. Seymour, *Nucl. Phys. B* **436**(3) (1995) 443.  
[http://dx.doi.org/10.1016/0550-3213\(94\)00554-R](http://dx.doi.org/10.1016/0550-3213(94)00554-R)
- [123] M.H. Seymour, *Comp. Phys. Commun.* **90**(1) (1995) 95.  
[http://dx.doi.org/10.1016/0010-4655\(95\)00064-M](http://dx.doi.org/10.1016/0010-4655(95)00064-M)
- [124] S. Catani *et al.*, *J. High Energy Phys.* **11** (2001) 063.  
<http://dx.doi.org/10.1088/1126-6708/2001/11/063>
- [125] L. Lönnblad, *J. High Energy Phys.* **05** (2002) 046.  
<http://dx.doi.org/10.1088/1126-6708/2002/05/046>
- [126] N. Lavesson and L. Lönnblad, *J. High Energy Phys.* **07** (2005) 054.  
<http://dx.doi.org/10.1088/1126-6708/2005/07/054>
- [127] M.L. Mangano *et al.*, *J. High Energy Phys.* **01** (2007) 013.  
<http://dx.doi.org/10.1088/1126-6708/2007/01/013>
- [128] S. Mrenna and P. Richardson, *J. High Energy Phys.* **05** (2004) 040.  
<http://dx.doi.org/10.1088/1126-6708/2004/05/040>
- [129] B. Cooper *et al.*, *Eur. Phys. J. C* **72** (2012) 2078.  
<http://dx.doi.org/10.1140/epjc/s10052-012-2078-y>
- [130] N. Lavesson and L. Lönnblad, *J. High Energy Phys.* **12** (2008) 070.  
<http://dx.doi.org/10.1088/1126-6708/2008/12/070>
- [131] S. Frixione and B.R. Webber, *J. High Energy Phys.* **06** (2002) 029.  
<http://dx.doi.org/10.1088/1126-6708/2002/06/029>
- [132] S. Frixione, P. Nason, and B.R. Webber, *J. High Energy Phys.* **08** (2003) 007.  
<http://dx.doi.org/10.1088/1126-6708/2003/08/007>
- [133] S. Frixione and B.R. Webber, The MC@NLO 3.4 event generator (2008),  
<https://arxiv.org/abs/0812.0770>
- [134] S. Frixione, P. Nason and C. Oleari, *J. High Energy Phys.* **11** (2007) 070.  
<http://dx.doi.org/10.1088/1126-6708/2007/11/070>
- [135] K. Hamilton and P. Nason, *J. High Energy Phys.* **06** (2010) 039.  
[http://dx.doi.org/10.1007/JHEP06\(2010\)039](http://dx.doi.org/10.1007/JHEP06(2010)039)
- [136] M. Bengtsson and T. Sjöstrand, *Phys. Lett. B* **185**(3-4) (1987) 435.  
[http://dx.doi.org/10.1016/0370-2693\(87\)91031-8](http://dx.doi.org/10.1016/0370-2693(87)91031-8)
- [137] S. Alioli *et al.*, *J. High Energy Phys.* **06** (2010) 043. [http://dx.doi.org/10.1007/JHEP06\(2010\)043](http://dx.doi.org/10.1007/JHEP06(2010)043)
- [138] L. Hartgring, E. Laenen and P. Skands, *J. High Energy Phys.* **1310** (2013) 127.  
[http://dx.doi.org/10.1007/JHEP10\(2013\)127](http://dx.doi.org/10.1007/JHEP10(2013)127)
- [139] P.Z. Skands, QCD for Collider Physics, 18th European School on High-Energy Physics (ESHEP), Raseborg, Finland, 2010, arXiv:1202.1629 (2011).
- [140] G.S. Bali and K. Schilling, *Phys. Rev. D* **46**(6) (1992) 2636.  
<http://dx.doi.org/10.1103/PhysRevD.46.2636>
- [141] D. Amati and G. Veneziano, *Phys. Lett. B* **83**(1) (1979) 87.  
[http://dx.doi.org/10.1016/0370-2693\(79\)90896-7](http://dx.doi.org/10.1016/0370-2693(79)90896-7)
- [142] S. Navin, Diffraction in Pythia (2010), <https://arxiv.org/abs/1005.3894>
- [143] X. Artru and G. Mennessier, *Nucl. Phys. B* **70**(1) (1974) 93.  
[http://dx.doi.org/10.1016/0550-3213\(74\)90360-5](http://dx.doi.org/10.1016/0550-3213(74)90360-5)
- [144] M. Travis *et al.*, *Sixteen Tons*, originally recorded for Folk Songs of the Hills (Capitol Records,

- 1946).
- [145] B. Andersson, G. Gustafson and T. Sjöstrand, *Nucl. Phys. B* **197**(1) (1982) 45.  
[http://dx.doi.org/10.1016/0550-3213\(82\)90153-5](http://dx.doi.org/10.1016/0550-3213(82)90153-5)
  - [146] B. Andersson, G. Gustafson and T. Sjöstrand, *Phys. Scripta* **32**(6) (1985) 574.  
<http://dx.doi.org/10.1088/0031-8949/32/6/003>
  - [147] P. Eden and G. Gustafson, *Z. Phys. C* **75**(1) (1997) 41. <http://dx.doi.org/10.1007/s002880050445>
  - [148] T. Sjöstrand and P.Z. Skands, *Nucl. Phys. B* **659**(1-2) (2003) 243.  
[http://dx.doi.org/10.1016/S0550-3213\(03\)00193-7](http://dx.doi.org/10.1016/S0550-3213(03)00193-7)
  - [149] T. Sjöstrand and P.Z. Skands, *J. High Energy Phys.* **03** (2004) 053.  
<http://dx.doi.org/10.1088/1126-6708/2004/03/053>
  - [150] B. Andersson, G. Gustafson and B. Söderberg, *Z. Phys. C* **20**(4) (1983) 317.  
<http://dx.doi.org/10.1007/BF01407824>
  - [151] M.G. Bowler, *Z. Phys. C* **11**(2) (1981) 169. <http://dx.doi.org/10.1007/BF01574001>
  - [152] K.G. Wilson, *Phys. Rev. D* **10**(8) (1974) 2445. <http://dx.doi.org/10.1103/PhysRevD.10.2445>
  - [153] G. Antchev *et al.*, *Phys. Rev. Lett.* **111**(1) (2013) 012001.  
<http://dx.doi.org/10.1103/PhysRevLett.111.012001>
  - [154] A. Donnachie and P.V. Landshoff, *Phys. Lett. B* **727**(4-5) (2013) 500.  
<http://dx.doi.org/10.1016/j.physletb.2013.10.068>
  - [155] V.A. Khoze *et al.*, *Eur. Phys. J. C* **69**(1) (2010) 85.  
<http://dx.doi.org/10.1140/epjc/s10052-010-1392-5>
  - [156] B. Blok *et al.*, *Phys. Rev. D* **83**(7) (2011) 071501.  
<http://dx.doi.org/10.1103/PhysRevD.83.071501>
  - [157] B. Blok *et al.*, *Eur. Phys. J. C* **72** (2012) 1963. <http://dx.doi.org/10.1140/epjc/s10052-012-1963-8>
  - [158] J.R. Gaunt and W.J. Stirling, Single and double perturbative splitting diagrams in double parton scattering (2012), <https://arxiv.org/abs/1202.3056>
  - [159] A.V. Manohar and W.J. Waalewijn, *Phys. Rev. D* **85**(11) (2012) 114009.  
<http://dx.doi.org/10.1103/PhysRevD.85.114009>
  - [160] T. Sjöstrand and M. van Zijl, *Phys. Rev. D* **36**(7) (1987) 2019.  
<http://dx.doi.org/10.1103/PhysRevD.36.2019>
  - [161] P. Skands, S. Carrazza and J. Rojo, *Eur. Phys. J. C* **74**(8) (2014) 3024.  
<http://dx.doi.org/10.1140/epjc/s10052-014-3024-y>
  - [162] J.M. Butterworth, J.R. Forshaw and M.H. Seymour, *Z. Phys. C* **72**(4) (1996) 637.  
<http://dx.doi.org/10.1007/s002880050286>
  - [163] M. Bähr *et al.*, Soft interactions in Herwig++ (2009), <https://arxiv.org/abs/0905.4671>
  - [164] M.G. Ryskin, A.D. Martin and V.A. Khoze, *Eur. Phys. J. C* **71** (2011) 1617.  
<http://dx.doi.org/10.1140/epjc/s10052-011-1617-2>
  - [165] H. Schulz and P.Z. Skands, *Eur. Phys. J. C* **71** (2011) 1644.  
<http://dx.doi.org/10.1140/epjc/s10052-011-1644-z>
  - [166] P.Z. Skands, *Phys. Rev. D* **82**(7) (2010) 074018. <http://dx.doi.org/10.1103/PhysRevD.82.074018>
  - [167] P.Z. Skands, Soft-QCD and UE spectra in pp collisions at very high CM energies (a Snowmass white paper) (2013), <https://arxiv.org/abs/1308.2813>
  - [168] R. Corke and T. Sjöstrand, *J. High Energy Phys.* **1105** (2011) 009.  
[http://dx.doi.org/10.1007/JHEP05\(2011\)009](http://dx.doi.org/10.1007/JHEP05(2011)009)
  - [169] G. Aad *et al.*, *Phys. Rev. D* **83**(11) (2011) 112001,  
<http://dx.doi.org/10.1103/PhysRevD.83.112001>
  - [170] A. Karneyeu *et al.*, *Eur. Phys. J. C* **74** (2014) 2714.

- <http://dx.doi.org/10.1140/epjc/s10052-014-2714-9>
- [171] D. Lombrana Gonzalez *et al.*, *Conf. Proc. C* **1205201** (2012) 505,  
<https://cds.cern.ch/record/1463291>
- [172] A. Buckley *et al.*, *Eur. Phys. J. C* **65** (2010) 331.  
<http://dx.doi.org/10.1140/epjc/s10052-009-1196-7>
- [173] P. Richardson and D. Winn, *Eur. Phys. J. C* **72** (2012) 2178.  
<http://dx.doi.org/10.1140/epjc/s10052-012-2178-8>
- [174] M. Ritzmann, D.A. Kosower and P. Skands, *Phys. Lett. B* **718**(4-5) (2013) 1345.  
<http://dx.doi.org/10.1016/j.physletb.2012.12.003>
- [175] P. Skands, B. Webber and J. Winter, *J. High Energy Phys.* **1207** (2012) 151.  
[http://dx.doi.org/10.1007/JHEP07\(2012\)151](http://dx.doi.org/10.1007/JHEP07(2012)151)
- [176] R. Field, *Acta Phys. Polon. B* **42** (2011) 2631. <http://dx.doi.org/10.5506/APhysPolB.42.2631>
- [177] L. Lönnblad and T. Sjöstrand, *Eur. Phys. J. C* **2** (1998) 165.  
<http://dx.doi.org/10.1007/s100520050131>
- [178] R. Corke and T. Sjöstrand, *J. High Energy Phys.* **01** (2009) 035.  
[http://dx.doi.org/10.1007/JHEP01\(2010\)035](http://dx.doi.org/10.1007/JHEP01(2010)035)
- [179] J. Rathsman, *Phys. Lett. B* **452**(3-4) (1999) 364.  
[http://dx.doi.org/10.1016/S0370-2693\(99\)00291-9](http://dx.doi.org/10.1016/S0370-2693(99)00291-9)
- [180] P.Z. Skands and D. Wicke, *Eur. Phys. J. C* **52**(1) (2007) 133.  
<http://dx.doi.org/10.1140/epjc/s10052-007-0352-1>
- [181] S. Gieseke, C. Rohr and A. Siodmok, *Eur. Phys. J. C* **72** (2012) 2225.  
<http://dx.doi.org/10.1140/epjc/s10052-012-2225-5>
- [182] K. Werner, I. Karpenko and T. Pierog, *Acta Phys. Polon. Supp.* **4** (2011) 629.  
<http://dx.doi.org/10.5506/APhysPolBSupp.4.629>
- [183] N. Ellis *et al.*, Proc. 2008 European School of High-Energy Physics (ESHEP), Herbeumont-sur-Semois, Belgium, (2009), CERN-2009-002 (2009).  
<http://dx.doi.org/10.5170/CERN-2009-002>
- [184] C. Grojean *et al.*, Proc. 2009 European School of High-Energy Physics (ESHEP), Bautzen, Germany, 2009 (2010).
- [185] N. Ellis *et al.*, 2007 European School of High-Energy Physics, Trest, Czech Republic, 2007, CERN-2008-007 (2008). <http://dx.doi.org/10.5170/CERN-2008-007>